Microsensor analysis of oxygen and sulfide turnover in hypersaline microbial mats

Dissertation
zur Erlangung des Grades eines
Doktors der Naturwissenschaften
-Dr. rer. nat.-

dem Fachbereich 2 (Biologie/Chemie) der
Universität Bremen
vorgelegt von

Andrea Wieland
aus Hannover

Bremen
Mai 1999

Die vorliegende Arbeit wurde in der Zeit von März 1996 bis Mai 1999 am Max-Planck-Institut für Marine Mikrobiologie in Bremen angefertigt.

1. Gutachter: Prof. Dr. Bo Barker Jørgensen
2. Gutachter: Prof. Dr. Friederike Koenig

Tag des Promotionskolloquiums: 21.6.1999

Preface

In this thesis oxygen and sulfide turnover in hypersaline microbial mats from Solar Lake (Sinai, Egypt) was investigated. The processes involved in oxygen and sulfide cycling were studied with microsensors, particularly their regulation by temperature and irradiance and the effect of these parameters on their interactions. The diffusional characteristics of the microbial mats were determined by application of NMR imaging.
The results of these studies are presented and discussed in the following chapters (2-4), followed by a summary of the thesis. A general introduction is presented in chapter 1.

This Ph.D. project was financially supported by the German Ministry of Education and Research (BMBF) as a part of the Red Sea Program on Marine Sciences (Project E: Microbial activities in marine interfaces controlling sediment-water fluxes), the Max-Planck-Society and the EU, which are gratefully acknowledged. Prof. Dr. Bo Barker Jørgensen is thanked for refereeing this thesis, for his support and his efforts on the ongoing of the project. Prof. Dr. Friederike Koenig is thanked for refereeing the thesis. My supervisor Michael Kühl is gratefully acknowledged for his support, his suggestions and all the time he took for me. The directors of the Max-Planck-Institute Bremen, Prof. Dr. Bo Barker Jørgensen and Prof. Dr. Friedrich Widdel, are thanked for their support at the institute. Yehuda Cohen is gratefully acknowledged for his support, his interest, his hospitality and for organizing all the Solar Lake field trips. I thank him and his group, Alon Zask, Sharon Avrahami, Avraham Fish, Naama Gazit Yaari, Pavel Sigalevich, Fikry Barghuthy, Gil Yaari, Eddy Cytryn for giving me a nice time in Israel. I really enjoyed each trip. Clivia Haese is thanked for taking good care of me in Eilat, her help and the nice time. The Interuniversity Institute in Eilat (Israel) is acknowledged for providing laboratory facilities and the Egyptian authorities for their permission to work at Solar Lake. Jakob Zopfi is thanked for the good time during common trips to Israel and for valuable discussions and comments. Gaby Eickert, Anja Eggers and Vera Hübner are thanked for all the microsensors and their technical assistance during field trips. I gratefully acknowledge all the help and valuable discussions with Eric Epping, Olivier Pringault, Ferran Garcia-Pichel, Oliver Kohls, Carsten Steuckart, Dirk de Beer and Peter Berg. Bettina König is thanked for her help with IDL and Bernd Stickfort for ordering the literature. The

microsensor group is thanked for the good atmosphere. Especially Gaby Eickert, Sijla Santegoeds, Stephanie Rink, Anja Eggers, Olivier Pringault, Ferran Garcia-Pichel, Jakob Zopfi and Anne Portwich are thanked for the nice time together. Finally, I want to thank my family and Michael for his patience and support.

Table of contents

Chapter 1

General Introduction

1.1 Microbial mats

Microbial mats are accretionary, cohesive microbial communities growing on solid surfaces, thereby often stabilizing unconsolidated sediments. These structured and coherent macroscopic accumulations of microorganisms often show a typical lamination pattern due to differences in pigmentation and cohesion of the distinct metabolic groups of microorganisms zonated within the mats. The mat-inhabiting microorganisms excrete considerable amounts of extracellular polysaccharides which form a polymer matrix in which the microorganisms are embedded, thereby contributing to a stabilization and formation of a cohesive structure (Pierson 1992). Microbial mats are the oldest structured and smallest ecosystems in the world (van Gemerden 1993; Karsten and Kühl 1996). Modern microbial mats are considered as recent analogues of lithified ancient microbial mats, preserved in the fossil record as stromatolites (Margulis et al. 1980; Walter et al. 1992). Studies of modern microbial mat communities may help to interpret the fossil record of ancient stromatolitic organisms and the chemical signatures left in stromatolites and may provide insight into these early stages of life, their environment and environmental changes in ancient atmospheres and oceans (Des Marais et al. 1992a; Castenholz 1994; Des Marais 1995).

Microbial mats are distributed all over the world and can be found in several environments, like marine sediments (supra-, inter- and subtidal), thermal springs, hypersaline lakes and lagoons, Antarctic lakes, deep sea hydrothermal vents, freshwater lakes and streams (overview of geographical distribution in Pierson 1992; Bauld 1981). The occurrence of well developed microbial mats seems to be restricted to environments where the prevailing conditions strongly reduce the survival of higher organisms and therefore the grazing pressure on the microorganisms (Cohen 1989; Pierson 1992), like e.g. in hypersaline environments (Krumbein et al. 1977; Bauld 1984; D`Amelio et al. 1989; Skyring and Bauld 1990; Des Marais et al. 1992b). Although some small grazers occur in hypersaline environments and thermal springs, they are not inhibiting the development of microbial mats (Farmer 1992). Cyanobacterial mats also develop in illuminated coastal sediments after removal of benthic fauna (Fenchel 1998).

Microbial mats are inhabited by diverse functional groups of microorganisms. Marine and hypersaline microbial mats generally consist of oxygenic and anoxygenic phototrophs, chemolithotrophic bacteria, aerobic and anaerobic heterotrophic bacteria, which show a typical zonation pattern within the mat (van Gemerden 1993). Cyanobacteria are often dominant phototrophs in these mats (Krumbein et al. 1977; Jørgensen et al. 1983; D`Amelio et al. 1989; Des Marais et al. 1992b), providing physical strength and growth substrates for diverse groups of mat-inhabiting organisms (van Gemerden 1993). Despite the occurence of high primary production, the yearly biomass accretion rate of hypersaline mats is low, due to high remineralization rates of organic matter by aerobic and anaerobic heterotrophic processes (Krumbein et al. 1977; Canfield and Des Marais 1993). The highest metabolic activity is confined to the uppermost millimeters of the mats, where the microorganisms closely interact, leading to the development of steep physico-chemical gradients (Revsbech et al. 1983; Des Marais 1995). Due to the close proximity of the microorganisms in these cohesive ecosystems, diffusion is the predominant mode of solute transport (van Gemerden 1993).

1.2 Oxygen and sulfur cycle in microbial mats

Important parameters for the metabolic activity and the vertical distribution of mat-inhabiting microorganisms are the distribution of oxygen and sulfide within the mat, which is strongly regulated by the natural light regime. Oxygenic photosynthesis by cyanobacteria and diatoms in the uppermost mat layer is the driving force of marine and hypersaline mats (van Gemerden 1993; Castenholz 1994). Cyanobacterial excretion and lysis products are respired by aerobic heterotrophic bacteria. Intense heterotrophic activity may create microenvironments around the cyanobacteria where oxygen becomes depleted and CO_2 is replenished, protecting the cyanobacteria from photooxidative stress (Marshall 1989). Other oxygen-consuming processes are associated with the phototrophic organisms, like respiration of organic carbon compounds ("dark respiration"), oxygenase activity of ribulose-1,5-bisphosphate carboxylase oxygenase (photorespiration) or pseudocyclic electron transport (Mehler reaction) (Beardall and Raven 1990). In hypersaline mats,

dissimilatory sulfate reduction is the dominant anaerobic process of carbon mineralization (Jørgensen et al. 1992; Canfield and Des Marais 1993). Fermentation by anaerobic heterotrophic microorganisms is tightly coupled to the terminal process of anaerobic decomposition via the production/consumption of fermentation products, i.e. low-molecular weight organic compounds and hydrogen (Jørgensen et al. 1992). The produced sulfide is aerobically oxidized by colorless sulfur bacteria (chemolithotrophs), which are therefore confined to the often very narrow oxygen-sulfide interface. In the light, anoxygenic phototrophic bacteria, which use sulfide as electron donor for photosynthetic carbon assimilation, have to compete with these organisms. The competition for reduced inorganic sulfur compounds between both groups is strongly regulated by the availability of oxygen and light (Jørgensen and Des Marais 1986). Low oxygen concentrations at the oxygen-sulfide interface can lead to incomplete sulfide oxidation by colorless sulfur bacteria, resulting in a coexistence of both processes in the mat (van Gemerden 1993; van den Ende et al. 1996). The beneficial and competitive interactions between these diverse functional groups of microorganisms finely regulate oxygen and sulfur cycling in microbial mats. A scheme of the various interactions between the mat-inhabiting microorganisms is given in Figure 1. The different groups of microorganisms occur in close association within the uppermost millimeters of the mat, showing a vertical zonation pattern which is often partly visible due to the pigmentation of dominant bacteria in the different layers. These layers do, however, not have well-defined boundaries, but rather show an overlap. The utilization and production of various intermediate sulfur compounds by the different groups of microorganisms (e.g. van Gemerden 1993; Cypionka 1994) and the involvement of physico-chemical processes, like e.g. chemical oxidation, polysulfide and iron sulfide formation, results in a complex oxygen and sulfur cycle within microbial mats.

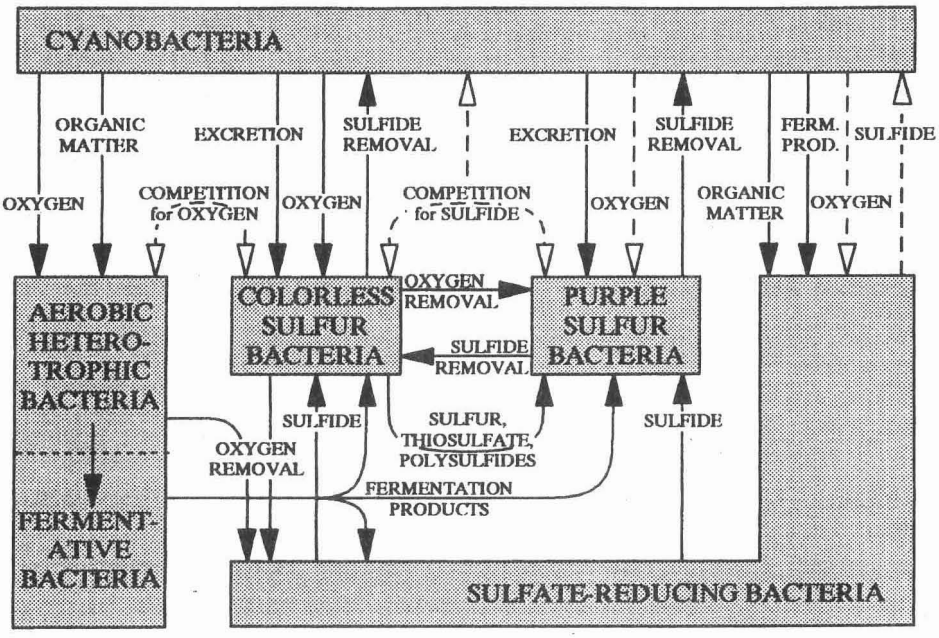

Figure 1: Scheme of the interactions between the different functional groups of microorganisms inhabiting microbial mats. Positive interactions are indicated by black arrows, negative by white arrows (from van den Ende and van Gemerden 1994).

The oxygen and sulfur cycle is strongly regulated by the natural light regime. Extreme variations of physico-chemical gradients occur in the mats between darkness and the exposure to bright sunlight at midday (Revsbech et al. 1983). Oxygenic photosynthesis during the day results in a pronounced build-up of oxygen supersaturation in the surface layer, shifting the oxygen-sulfide interface from the surface to greater depths within the mat. During the night, intense O_2 consumption results in oxygen depletion and only minor oxygen penetration, whereas sulfide accumulates and rises close to the mat surface (Revsbech et al. 1983). To thrive under these conditions requires physiological and behavioral adaptations of the different groups of mat-inhabiting microorganisms, like e.g. motility and metabolic versatility.

Mat-building cyanobacteria exhibit physiological flexibility and are able to switch to alternative modes of metabolism. Under dark anaerobic conditions, as it occurs in microbial mats during the night, some cyanobacteria are capable of fermentation and of

anaerobic respiration in the presence of elemental sulfur, resulting in the formation of sulfide (Oren and Shilo 1979; Heyer et al. 1989; Moezelaar et al. 1996). Anoxygenic photosynthesis in the presence of sulfide and light can be induced in several mat-building cyanobacteria (Cohen et al. 1975; Garlick et al. 1977; Cohen et al. 1986; de Wit and van Gemerden 1987b) and different adaptations to sulfide among cyanobacteria have been described (Cohen et al. 1986). This facultative anoxygenic phototrophy is advantageous especially in the early morning, when the cyanobacteria are exposed at sunrise to high sulfide levels that built up during the night. With the capability to remove sulfide, an inhibitor of oxygenic photosynthesis, and rapidly switch to oxygenic photosynthesis at low sulfide levels, cyanobacteria are well adapted to the pronounced diurnal fluctuations of sulfide and oxygen occurring in these ecosystems. The most versatile mode of adaptation to sulfide is represented by the cosmopolitan mat-building cyanobacteria *Microcoleus chthonoplastes*, since anoxygenic and partially inhibited oxygenic photosynthesis operate simultaneously in the presence of sulfide (Cohen et al. 1986; Jørgensen et al. 1986). The physiological flexibility of cyanobacteria to cope with the diurnal changes between aerobic-anaerobic conditions and periodical exposure to sulfide and oxygen, is a selective advantage and may be one reason for their pronounced abundance in these ecosystems. The drastic fluctuations in the photic zone seem to be selective environmental factors against both strict anaerobic and strict aerobic phototrophic organisms (Padan and Cohen 1982; Jørgensen et al. 1986). Anoxygenic mats exclusively formed by anoxygenic photosynthetic bacteria can be found in environments where both high temperatures and elevated sulfide concentrations prevail (Ward et al. 1989; Ward et al. 1992).

Many mat-building cyanobacteria are also able to migrate in response to light and can therefore position themselves at depths of optimal light intensity and avoid damaging high irradiances and excess exposure to UV (Castenholz 1982; Garcia-Pichel et al. 1994; Bebout and Garcia-Pichel 1995; Kruschel and Castenholz 1998). Some cyanobacterial migration may also be due to chemotaxis e.g. in response to sulfide (Castenholz 1982; Whale and Walsby 1984). Migration of other mat-inhabiting organisms e.g. in response to oxygen stress or depth zonation of the oxygen-sulfide interface include sulfate-reducing bacteria (Krekeler et al. 1998; Teske et al. 1998) and the colorless sulfur bacterium *Beggiatoa* sp. (e.g. Garcia-Pichel et al. 1994). The non-motile purple sulfur bacterium *Thiocapsa roseopersicina* is able to grow chemolithotrophically in the presence of oxygen, and is

therefore physiologically well adapted to the fluctuating oxygen-sulfide regimes in microbial mats (de Wit and van Gemerden 1987a; de Wit 1992).

The uppermost layers of microbial mats are densely populated by sulfate-reducing bacteria (Visscher et al. 1992; Teske et al. 1998). Since sulfate-reducing bacteria in these layers are exposed to pronounced oxygen fluctuations due to photosynthetic oxygen production during the day, they also seem to possess a high metabolic versatility and adaptive strategies to overcome unfavorable conditions during the day. These strategies include besides diurnal migration, facultative aerobic respiration and aggregate formation (Krekeler et al. 1998; Teske et al. 1998). Furthermore, significant sulfate reduction activity occurs in the upper well oxygenated zone of mats, where the produced sulfide does not accumulate due to rapid reoxidation (Canfield and Des Marais 1991; Fründ and Cohen 1992; Jørgensen 1994; Teske et al. 1998). It was suggested that sulfate reduction in this zone may be associated with the utilization of substrates excreted by the phototrophic community (Cohen 1984; Cohen et al. 1994).

Thus, the close proximity of the diverse functional groups of microorganisms within the mat enables several beneficial interactions between the organisms via substrate supply and consumption of metabolic products, but also requires adaptive strategies to cope with unfavorable conditions imposed by the dynamic and fluctuating microenvironment and to compete successfully for common substrates.

Microbial mats therefore represent ideal model systems to study biological dynamics and trophic interactions between microorganisms, as well as physiological and behavioral strategies of microorganisms to thrive in a highly dynamic ecosystem. Furthermore, due to the absence of bioturbation and the close association of primary producers with the heterotrophic community, microbial mats allow studies of biogeochemical processes, the coupling between various microbial processes involved in carbon, oxygen and sulfur cycling and their regulation on a microscale.

1.3 Regulation of oxygen and sulfur cycling by light and temperature

As described above, oxygen and sulfur cycling in microbial mats is strongly controlled by the diel light-dark cycle. Additional to these diel or short term variations, the light regime also changes on a seasonal scale. The particular prevailing light regime strongly influences the species composition, metabolic activity and vertical stratification of mat-constructing phototrophs (Skyring and Bauld 1990). Simultaneous with the changing light conditions, microbial mat communities generally experience covariations of temperature.

Light is strongly attenuated in densely populated microbial mats due to light scattering and absorption by phototrophic organisms. Selective absorbance of light by the differently pigmented mat-inhabiting phototrophs alters the spectral composition of light within the community (Jørgensen and Des Marais 1988; Kühl and Jørgensen 1992; Kühl et al. 1994). The depth of the photosynthetically active zone, the zonation of motile phototrophs and photosynthetic activity especially in deeper, light-limited parts of the mat therefore strongly depend on the intensity of the downwelling surface irradiance.

Photosynthesis generally increases with irradiance until photosynthesis gets saturated and approaches maximal photosynthesis. Photosynthesis remains then either constant with increasing irradiance or decreases due to photoinhibition. Photosynthesis at light-limiting conditions is controlled by the photochemical processes involved in photosynthesis. The initial increase of photosynthesis with irradiance therefore depends on the photosynthetic efficiency, i.e. light-harvesting and photosynthetic energy conversion efficiency, and is generally considered to be relatively insensitive to temperature on a short-term scale (Davison 1991; Henley 1993). Photosynthesis at light saturation is primarily limited by carbon metabolism, including enzymatic reactions of the Calvin cycle, diffusion and transport processes, and is therefore strongly regulated by temperature (Davison 1991; Henley 1993). The typical short-term response of light-saturated photosynthesis to increasing temperatures is a progressive increase up to an optimum temperature, and a rapid decline at temperatures above the optimum temperature (Javor and Castenholz 1984; Davison 1991; Blanchard et al. 1996). Variations of the light and temperature regime during a seasonal cycle, may lead to an acclimation and/or change in structure and composition of benthic phototrophic communities (Grant 1986; Blanchard et al. 1996;

Barranguet et al. 1998). Thus, temperature and light are major environmental factors controlling photosynthesis in benthic phototrophic communities (Cadée and Hegeman 1974; Rasmussen et al. 1983; Grant 1986; Canfield and Des Marais 1993; Barranguet et al. 1998).

The response of the phototrophic community to changing temperature and light conditions may have significant effects on different processes involved in oxygen and sulfur cycling in microbial mats, due to their dependence either on the supply of organic compounds and/or oxygen availability (1.2). Sulfate reduction in microbial mats increases with temperature (Skyring et al. 1983; Canfield and Des Marais 1991; Canfield and Des Marais 1993; Jørgensen 1994), and Q_{10} values of sulfate reduction of 2.0 to 2.4 were reported (Skyring et al. 1983; Jørgensen 1994). There seems to be no clear general effect of light on sulfate reduction rates (Canfield and Des Marais 1991; Fründ and Cohen 1992). A detailed study on the biogeochemistry of hypersaline mats showed that the major microbial processes involved in oxygen and sulfur cycling, i.e. oxygenic photosynthesis, sulfate reduction, oxygen consumption due to aerobic respiration and sulfide oxidation, significantly increased after a 10°C to 13°C temperature increase, and that primary production changed with temperature by a similar amount as the heterotrophic processes, indicating that hypersaline mats are closely coupled systems (Canfield and Des Marais 1993). It was suggested that carbon remineralization by aerobic and anaerobic processes alleviates CO_2 limitation at high photosynthetic rates (Canfield and Des Marais 1993; Teske et al. 1998), possibly further contributing to a complex regulation of oxygen and sulfur cycling in microbial mats. Although temperature and light are important environmental parameters controlling metabolic activities in benthic phototrophic communities, only little is known about the regulation of oxygen, sulfur and carbon cycling in microbial mats.

1.4 Solar Lake

Solar Lake is a small (140 by 50 m) and shallow (4-6 m deep) sea-marginal hypersaline lake on the Sinai coast, separated from the Red Sea by a gravel bar. Seawater seeps into the lake through the gravel bar and accumulates at the surface, where it is subjected to pronounced evaporation. Solar Lake is characterized by an exceptional limnological cycle, with an inverse thermal stratification during winter and holomixis during summer. A pycnocline establishes in autumn due to increasing water supply and decreasing solar radiation. Solar heating of the concentrated brine below the pycnocline leads to a simultaneous development of a thermocline. The salinity of the surface water increases towards summer due to increasing evaporation, which alleviates the density differences and subsequently results in overturn to holomixis in summer. Steep gradients of salinity, pH, oxygen, sulfide, and temperature occur during the stratification period of the lake, whereas during holomixis the water salinity, pH and temperature are constant throughout the water column (Cohen et al. 1977).

Distinct microbial mats cover the bottom of Solar Lake which were classified according to their general morphology, species composition and location (Krumbein et al. 1977; Jørgensen et al. 1983). Finely layered, compacted cyanobacterial mats up to 1 m thick occur in the shallow part of the lake. The cyanobacterial mats at increasing water depths, i.e. at the slope and bottom of the lake, are less structured. A flocculose cyanobacterial mat develops during winter stratification at the bottom of the lake at high sulfide concentrations, which is composed of filamentous cyanobacteria (mainly "*Oscillatoria limnetica*"), capable of performing anoxygenic photosynthesis (Cohen et al. 1975; Krumbein et al. 1977).

The mats in the shallow part of the lake were most intensively investigated. Depending on the season, the surface layer of these mats is dominated by unicellular cyanobacteria and diatoms, or by filamentous cyanobacteria (Krumbein et al. 1977). The mats are characterized by high concentrations of mostly autochthonous organic matter, high abundance of aerobic and anaerobic heterotrophic bacteria in the upper layers of the mat and an enrichment in polysulfides (Jørgensen and Cohen 1977; Krumbein et al. 1977; Cohen et al. 1980; Aizenshtat et al. 1984). Despite high primary productivity, the yearly

biomass accretion is low, due to high rates of carbon remineralization (Cohen et al. 1980). Several studies consider different aspects of oxygen and sulfur cycling in these mats, including determination of primary productivity, sulfate reduction activity, fine-scale distribution of oxygenic photosynthesis, oxygen, pH and sulfide, diurnal cycles of oxygen and sulfide microgradients, transition between anoxygenic and oxygenic photosynthesis, microbial composition and distribution (Jørgensen and Cohen 1977; Krumbein et al. 1977; Jørgensen et al. 1979; Jørgensen et al. 1983; Revsbech et al. 1983; Campbell and Golubic 1985; Jørgensen et al. 1986; Krekeler et al. 1998; Teske et al. 1998). However, little is known about the regulation of oxygen and sulfur cycling by environmental parameters, which may significantly influence the productivity of these mats.

1.5 Fine-scale measurements in microbial mats

Due to the close association of the diverse functional groups of microorganisms inhabiting microbial mats and the confinement of high microbial activity to the uppermost mat layers, techniques that allow measurements on a microscale have to be applied for the investigation of microbial mats. Microsensors are appropriate tools for the characterization of physico-chemical microenvironments within compact and complex ecosystems due to their small dimensions and concomitant high spatial resolution (Revsbech and Jørgensen 1986; Amann and Kühl 1998; Kühl and Revsbech 1999). Besides fine-scale microsensor measurements of concentration gradients of important solutes and metabolites like oxygen, hydrogen sulfide, pH, hydrogen, methane, carbon dioxide (Revsbech and Jørgensen 1986; Amann and Kühl 1998; Kühl and Revsbech 1999), it is also possible to determine the depth distribution of oxygenic gross photosynthesis at high spatial resolution (Revsbech and Jørgensen 1983). The simultaneous measurement of oxygenic gross photosynthesis and oxygen concentration profiles enables the estimation of oxygen consumption in distinct layers, i.e. in the photic and the aphotic zone of light incubated mats, using either computer simulations (Revsbech et al. 1986) or simple flux calculations (Jensen and Revsbech 1989; Kühl et al. 1996). An alternative approach to the application of microsensors for the determination of chemical gradients at high spatial resolution are

recently developed planar optodes which can be used to acquire 2-dimensional images of solute distribution in biological systems (Glud et al. 1998).

The steep chemical gradients within microbial mats are determined by intense microbial activity and solute diffusion. Diffusion in compact microbial ecosystems is hindered by the presence of impermeable particles and microbial cells, which also reduce the volume accessible for diffusion. From measured concentration profiles process rates and the depth zonation of processes can be estimated by application of diffusion-reaction models, which requires knowledge about the solute diffusivity within the system (e.g. Revsbech et al. 1986; Nielsen et al. 1990; Rasmussen and Jørgensen 1992; Epping and Jørgensen 1996; Berg et al. 1998).

1.6 Outline of this thesis

In this thesis, oxygen and sulfide cycling in hypersaline microbial mats was investigated with emphasis on regulatory effects of temperature and irradiance, which are important environmental parameters and determinants of metabolic activities in benthic phototrophic communities.

In the first study, the interactions of oxygen and sulfide producing/consuming processes and their regulation by temperature was investigated with microsensors in a Solar Lake microbial mat under dark and light conditions. The aim of this study was to investigate how temperature affects the major autotrophic and heterotrophic processes involved in oxygen and sulfide cycling, and hence in carbon cycling, and the balance between these processes. The results of this study are presented in chapter 2.

A detailed microsensor study on the temperature and irradiance regulation of oxygenic photosynthesis and oxygen consuming processes in a Solar Lake mat is presented in chapter 3. In this study, the effect of temperature on dark O_2 consumption and net photosynthesis at a saturating high surface irradiance, and on O_2 dynamics at the mat surface was investigated. Furthermore, the effect of increasing irradiance and temperature on oxygenic photosynthesis and oxygen consumption in distinct zones of the mat was studied.

In the third study, the diffusive properties of two structurally different Solar Lake microbial mats was investigated in two dimensions by application of non-invasive Nuclear Magnetic Resonance imaging. The aim of this study was to obtain information about solute diffusivity in microbial mats, which is an important factor for the quantification of biogeochemical processes in benthic ecosystems. The effect of the determined diffusive properties of the mat on the analysis of measured oxygen concentration microprofiles was estimated with a diffusion-reaction model. The results are presented in chapter 4.

1.7 References

Aizenshtat Z, Lipiner G, Cohen Y (1984). Biogeochemistry of carbon and sulfur cycle in the microbial mats of the Solar Lake (Sinai). In: Cohen Y, Castenholz RW, Halvorson HO (Ed.) Microbial mats: Stromatolites. Alan R Liss, New York, p 281-312

Amann R, Kühl M (1998). *In situ* methods for assessment of microorganisms and their activities. Curr Opin Microbiol 1:352-358

Barranguet C, Kromkamp J, Peene J (1998). Factors controlling primary production and photosynthetic characteristics of intertidal microphytobenthos. Mar Ecol Prog Ser 173:117-126

Bauld J (1981). Occurrence of benthic microbial mats in saline lakes. Hydrobiologia 81:87-111

Bauld J (1984). Microbial mats in marginal marine environments: Shark Bay, Western Australia, and Spencer Gulf, South Australia. In: Cohen Y, Castenholz RW, Halvorson HO (Ed.) Microbial mats: Stromatolites. Alan R Liss, New York, p 39-58

Beardall J, Raven JA (1990). Pathways and mechanisms of respiration in microalgae. Mar Microb Food Webs 4(1):7-30

Bebout BM, Garcia-Pichel F (1995). UV B-induced vertical migrations of cyanobacteria in a microbial mat. Appl Environ Microbiol 61(12):4215-4222

Berg P, Risgaard-Petersen N, Rysgaard S (1998). Interpretation of measured concentration profiles in sediment pore water. Limnol Oceanogr 43(7):1500-1510

Blanchard GF, Guarini J-M, Richard P, Gros P, Mornet F (1996). Quantifying the short-term temperature effect on light-saturated photosynthesis on intertidal microphytobenthos. Mar Ecol Prog Ser 134:309-313

Cadée GC, Hegeman J (1974). Primary production of the benthic microflora living on tidal flats in the Dutch Wadden Sea. Neth J Sea Res 8:260-291

Campbell SE, Golubic S (1985). Benthic cyanophytes (cyanobacteria) of Solar Lake (Sinai). Arch Hydrobiol Suppl (Algological Studies) 71:311-329

Canfield DE, Des Marais DJ (1991). Aerobic sulfate reduction in microbial mats. Science 251:1471-1473

Canfield DE, Des Marais DJ (1993). Biogeochemical cycles of carbon, sulfur, and free oxygen in a microbial mat. Geochim Cosmochim Acta 57:3971-3984

Castenholz RW (1982). Motility and taxes. In: Carr NG, Whitton BA (Ed.) The biology of cyanobacteria. Blackwell Scientific Publications, Oxford, p 413-440

Castenholz RW (1994). Microbial mat research: The recent past and new perspectives. In: Stal LJ, Caumette P (Ed.) Microbial Mats: Structure, Development and Environmental Significance. NATO ASI Series G Vol. 35. Springer, Berlin, p 3-18

Cohen Y (1984). Oxygenic photosynthesis, anoxygenic photosynthesis, and sulfate reduction in cyanobacterial mats. Curr Perspect Microb Ecol :435-441

Cohen Y (1989). Photosynthesis in cyanobacterial mats and its relation to the sulfur cycle: a model for microbial sulfur interactions. In: Cohen Y, Rosenberg E (Ed.) Microbial mats: Physiological ecology of benthic microbial communities. American Society for Microbiology, Washington DC, p 22-36

Cohen Y, Aizenshtat Z, Stoler A, Jørgensen BB (1980). The microbial geochemistry of Solar Lake, Sinai. In: Trudinger PA, Walter MR (Ed.) Biogeochemistry of ancient and modern environments. Springer, Berlin, p 167-172

Cohen Y, Helman Y, Sigalevich P (1994). Light-driven sulfate reduction and methane emission in hypersaline microbial mats. In: Stal LJ, Caumette P (Ed.) Microbial Mats: Structure, Development and Environmental Significance. NATO ASI Series G Vol. 35. Springer, Berlin, p 421-427

Cohen Y, Jørgensen BB, Revsbech NP, Poplawski R (1986). Adaptation to hydrogen sulfide of oxygenic and anoxygenic photosynthesis among cyanobacteria. Appl Environ Microbiol 51(2):398-407

Cohen Y, Krumbein WE, Goldberg M, Shilo M (1977). Solar Lake (Sinai). 1. Physical and chemical limnology. Limnol Oceanogr 22(4):597-608

Cohen Y, Padan E, Shilo M (1975). Facultative anoxygenic photosynthesis in the cyanobacterium *Oscillatoria limnetica*. J Bacteriol 123:855-861

Cypionka H (1994). Novel metabolic capacities of sulfate-reducing bacteria, and their activities in microbial mats. In: Stal LJ, Caumette P (Ed.) Microbial Mats:

Structure, Development and Environmental Significance. NATO ASI Series G Vol. 35. Springer, Berlin, p 367-376

D'Amelio ED, Cohen Y, Des Marais DJ (1989). Comparative functional ultrastructure of two hypersaline submerged cyanobacterial mats: Guerrero Negro, Baja California Sur, Mexico, and Solar Lake, Sinai, Egypt. In: Cohen Y, Rosenberg E (Ed.) Microbial mats: Physiological ecology of benthic microbial communities. American Society for Microbiology, Washington DC, p 97-113

Davison IR (1991). Environmental effects on algal photosynthesis: temperature. J Phycol 27:2-8

de Wit R (1992). Sulfide-containing environments. Encyclopedia of Microbiology 4:105-121

de Wit R, van Gemerden H (1987a). Chemolithotrophic growth of the phototrophic sulfur bacterium *Thiocapsa roseopersicina*. FEMS Microbiol Ecol 45:117-126

de Wit R, van Gemerden H (1987b). Oxidation of sulfide to thiosulfate by *Microcoleus chtonoplastes*. FEMS Microbiol Ecol 45:7-13

Des Marais DJ (1995). The biogeochemistry of hypersaline microbial mats. Adv Microb Ecol 14:251-274

Des Marais DJ, Bauld J, Palmisano AC, Summons RE, Ward DM (1992a). The biogeochemistry of carbon in modern microbial mats. In: Schopf JW, Klein C (Ed.) The proterozoic biosphere: a multidisciplinary study. Cambridge University Press, Cambridge, p 299-308

Des Marais DJ, D'Amelio ED, Farmer JD, Jørgensen BB, Palmisano AC, Pierson BK (1992b). Case study of a modern microbial mat-building community: the submerged cyanobacterial mats of Guerrero Negro, Baja California Sur, Mexico. In: Schopf JW, Klein C (Ed.) The proterozoic biosphere: a multidisciplinary study. Cambridge University Press, Cambridge, p 325-333

Epping EHG, Jørgensen BB (1996). Light-enhanced oxygen respiration in benthic phototrophic communities. Mar Ecol Prog Ser 139:193-203

Farmer JD (1992). Grazing and bioturbation in modern microbial mats. In: Schopf JW, Klein C (Ed.) The proterozoic biosphere: a multidisciplinary study. Cambridge University Press, Cambridge, p 295-297

Fenchel T (1998). Formation of laminated cyanobacterial mats in the absence of benthic fauna. Aquat Microb Ecol 14:235-240

Fründ C, Cohen Y (1992). Diurnal cycles of sulfate reduction under oxic conditions in cyanobacterial mats. Appl Environ Microbiol 58(1):70-77

Garcia-Pichel F, Mechling M, Castenholz RW (1994). Diel migrations of microorganisms within a benthic, hypersaline mat community. Appl Environ Microbiol 60(5):1 500-1511

Garlick S, Oren A, Padan E (1977). Occurence of facultative anoxygenic photosynthesis among filamentous and unicellular cyanobacteria. J Bacteriol 129(2):623-629

Glud RN, Santegoeds CM, de Beer D, Kohls O, Ramsing NB (1998). Oxygen dynamics at the base of a biofilm studied with planar optodes. Aquat Microb Ecol 14:223-233

Grant J (1986). Sensitivity of benthic community respiration and primary production to changes in temperature and light. Mar Biol 90:299-306

Henley WJ (1993). Measurement and interpretation of photosynthetic light-response curves in algae in the context of photoinhibition and diel changes. J Phycol 29:729-739

Heyer H, Stal L, Krumbein WE (1989). Simultaneous heterolactic and acetate fermentation in the marine cyanobacterium *Oscillatoria limosa* incubated anaerobically in the dark. Arch Microbiol 151:558-564

Javor BJ, Castenholz RW (1984). Productivity studies of microbial mats, Laguna Guerrero Negro, Mexico. In: Cohen Y, Castenholz RW, Halvorson HO (Ed.) Microbial mats: Stromatolites. Alan R Liss, New York, p 149-170

Jensen J, Revsbech NP (1989). Photosynthesis and respiration of a diatom biofilm cultured in a new gradient growth chamber. FEMS Microbiol Ecol 62:29-38

Jørgensen BB (1994). Sulfate reduction and thiosulfate transformations in a cyanobacterial mat during a diel oxygen cycle. FEMS Microbiol Ecol 13(4):303-312

Jørgensen BB, Cohen Y (1977). Solar Lake (Sinai). 5. The sulfur cycle of the benthic cyanobacterial mats. Limnol Oceanogr 22(4):657-666

Jørgensen BB, Cohen Y, Revsbech NP (1986). Transition from anoxygenic to oxygenic photosynthesis in a *Microcoleus chthonoplastes* cyanobacterial mat. Appl Environ Microbiol 51(2):408-417

Jørgensen BB, Des Marais DJ (1986). Competition for sulfide among colorless and purple sulfur bacteria in cyanobacterial mats. FEMS Microbiol Ecol 38:179-186

Jørgensen BB, Des Marais DJ (1988). Optical properties of benthic photosynthetic communities: Fiber-optic studies of cyanobacterial mats. Limnol Oceanogr 33(1):99-113

Jørgensen BB, Nelson DC, Ward DM (1992). Chemotrophy and decomposition in modern microbial mats. In: Schopf JW, Klein C (Ed.) The proterozoic biosphere: a multidisciplinary study. Cambridge University Press, Cambridge, p 287-293

Jørgensen BB, Revsbech NP, Blackburn TH, Cohen Y (1979). Diurnal cycle of oxygen and sulfide microgradients and microbial photosynthesis in a cyanobacterial mat sediment. Appl Environ Microbiol 38(1):46-58

Jørgensen BB, Revsbech NP, Cohen Y (1983). Photosynthesis and structure of benthic microbial mats: Microelectrode and SEM studies of four cyanobacterial communities. Limnol Oceanogr 28(6):1075-1093

Karsten U, Kühl M (1996). Die Mikrobenmatte-das kleinste Ökosystem der Welt. Biologie in unserer Zeit 26:16-26

Krekeler D, Teske A, Cypionka H (1998). Strategies of sulfate-reducing bacteria to escape oxygen stress in a cyanobacterial mat. FEMS Microbiol Ecol 25:89-96

Krumbein WE, Cohen Y, Shilo M (1977). Solar Lake (Sinai). 4. Stromatolitic cyanobacterial mats. Limnol Oceanogr 22(4):635-656

Kruschel C, Castenholz RW (1998). The effect of solar UV and visible irradiance on the vertical movements of cyanobacteria in microbial mats of hypersaline waters. FEMS Microbiol Ecol 27:53-72

Kühl M, Glud RN, Ploug H, Ramsing NB (1996). Microenvironmental control of photosynthesis and photosynthesis-coupled respiration in an epilithic cyanobacterial biofilm. J Phycol 32:799-812

Kühl M, Jørgensen BB (1992). Spectral light measurements in microbenthic phototrophic communities with a fiber-optic microprobe coupled to a sensitive diode array detector. Limnol Oceanogr 37(8):1813-1823

Kühl M, Lassen C, Jørgensen BB (1994). Optical properties of microbial mats: Light measurements with fiber-optic microprobes. In: Stal LJ, Caumette P (Ed.) Microbial Mats: Structure, Development and Environmental Significance. NATO ASI Series G Vol. 35. Springer, Berlin, p 149-166

Kühl M, Revsbech NP (1999). Microsensors for BBL studies. In: Boudreau BP, Jørgensen BB (Ed.) The benthic boundary layer. Oxford University Press, Oxford, in press

Margulis L, Barghoorn ES, Ashendorf D, Banarjee S, Chase D, Francis S, Giovannoni S, Stolz J (1980). The microbial community in the layered sediments at Laguna Figueroa, Baja California, Mexico: does it have precambrian analogues? Precambrian Res 11:93-123

Marshall KC (1989). Cyanobacterial-heterotrophic bacterial interaction. In: Cohen Y, Rosenberg E (Ed.) Microbial mats: Physiological ecology of benthic microbial communities. American Society for Microbiology, Washington DC, p 239-245

Moezelaar R, Bijvank SM, Stal LJ (1996). Fermentation and sulfur reduction in the mat-building cyanobacterium *Microcoleus chthonoplastes*. Appl Environ Microbiol 62(5):1752-1758

Nielsen LP, Christensen PB, Revsbech NP, Sørensen J (1990). Denitrification and oxygen respiration in biofilms studied with a microsensor for nitrous oxide and oxygen. Microb Ecol 19:63-72

Oren A, Shilo M (1979). Anaerobic heterotrophic dark metabolism in the cyanobacterium *Oscillatoria limnetica*: sulfur respiration and lactate fermentation. Arch Microbiol 122:77-84

Padan E, Cohen Y (1982). Anoxygenic photosynthesis. In: Carr NG, Whitton BA (Ed.) The biology of cyanobacteria. Blackwell Scientific Publications, Oxford, p 215-235

Pierson BK (1992). Introduction. In: Schopf JW, Klein C (Ed.) The proterozoic biosphere: a multidisciplinary study. Cambridge University Press, Cambridge, p 247-251

Rasmussen H, Jørgensen BB (1992). Microelectrode studies of seasonal oxygen uptake in a coastal sediment: role of molecular diffusion. Mar Ecol Prog Ser 81:289-303

Rasmussen MB, Henriksen K, Jensen A (1983). Possible causes of temporal fluctuations in primary production of the microphytobenthos in the Danish Wadden Sea. Mar Biol 73:109-114

Revsbech NP, Jørgensen BB (1983). Photosynthesis of benthic microflora measured with high spatial resolution by the oxygen microprofile method: Capabilities and limitations of the method. Limnol Oceanogr 28(4):749-756

Revsbech NP, Jørgensen BB (1986). Microelectrodes: Their use in microbial ecology. Adv Microb Ecol 9:293-352

Revsbech NP, Jørgensen BB, Blackburn TH, Cohen Y (1983). Microelectrode studies of the photosynthesis and O_2, H_2S, and pH profiles of a microbial mat. Limnol Oceanogr 28(6):1062-1074

Revsbech NP, Madsen B, Jørgensen BB (1986). Oxygen production and consumption in sediments determined at high spatial resolution by computer simulation of oxygen microelectrode data. Limnol Oceanogr 31(2):293-304

Skyring GW, Bauld J (1990). Microbial mats in australian coastal environments. Adv Microb Ecol 11:461-498

Skyring GW, Chambers LA, Bauld J (1983). Sulfate reduction in sediments colonized by cyanobacteria, Spencer Gulf, South Australia. Aust J Mar Freshw Res 34:359-374

Teske A, Ramsing NB, Habicht K, Fukui M, Küver J, Jørgensen BB, Cohen Y (1998). Sulfate-reducing bacteria and their activities in cyanobacterial mats of Solar Lake (Sinai, Egypt). Appl Environ Microbiol 64(8):2943-2951

van den Ende FP, Laverman AM, van Gemerden H (1996). Coexistence of aerobic chemotrophic and anaerobic phototrophic sulfur bacteria under oxygen limitation. FEMS Microbiol Ecol 19:141-151

van den Ende FP, van Gemerden H (1994). Relationships between functional groups of organisms in microbial mats. In: Stal LJ, Caumette P (Ed.) Microbial Mats: Structure, Development and Environmental Significance. NATO ASI Series G Vol. 35. Springer, Berlin, p 339-352

van Gemerden H (1993). Microbial mats: a joint venture. Mar Geol 113:3-25

Visscher PT, Prins RA, van Gemerden H (1992). Rates of sulfate reduction and thiosulfate consumption in a marine microbial mat. FEMS Microbiol Ecol 86:283-294

Walter MR, Bauld J, Des Marais DJ, Schopf JW (1992). A general comparison of microbial mats and microbial stromatolites: bridging the gap between the modern and the fossil. In: Schopf JW, Klein C (Ed.) The proterozoic biosphere: a multidisciplinary study. Cambridge University Press, Cambridge, p 335-338

Ward DM, Bauld J, Castenholz RW, Pierson BK (1992). Modern phototrophic microbial mats: anoxygenic, intermittently oxygenic/anoxygenic, thermal, eukaryotic, and terrestrial. In: Schopf JW, Klein C (Ed.) The proterozoic biosphere: a multidisciplinary study. Cambridge University Press, Cambridge, p 309-324

Ward DM, Weller R, Shiea J, Castenholz RW, Cohen Y (1989). Hot spring microbial mats: anoxygenic and oxygenic mats of possible evolutionary significance. In: Cohen Y, Rosenberg E (Ed.) Microbial mats: Physiological ecology of benthic microbial communities. American Society for Microbiology, Washington DC, p 3-15

Whale GF, Walsby AE (1984). Motility of the cyanobacterium *Microcoleus chthonoplastes* in mud. Br Phycol J 19:117-123

Chapter 2

Short term temperature effects on oxygen and sulfide cycling in a hypersaline cyanobacterial mat (Solar Lake, Egypt)

Andrea Wieland[1], Michael Kühl[2]

[1] Max-Planck-Institute for Marine Microbiology, Microsensor Research Group, Celsiusstr. 1, D-28359 Bremen, Germany

[2] Marine Biological Laboratory, University of Copenhagen Strandpromenaden 5, DK-3000 Helsingør, Denmark

Marine Ecology Progress Series, in press

ABSTRACT

We investigated short term temperature effects on oxygen and sulfide cycling with O_2, pH, and H_2S microsensors in a hypersaline cyanobacterial mat, incubated in darkness and at a downwelling irradiance, E_d (PAR), of 425 µmol photons m^{-2} s^{-1} in a laboratory. The incubation temperature was increased from 25°C to 40°C in 5°C intervals. Areal rates of gross and net photosynthesis, of O_2 consumption in the aphotic zone and of dark O_2 consumption were maximal at 30°C, i.e. close to the *in situ* temperature of the natural habitat. Areal rates of dark oxygen consumption showed only a minor temperature dependence as O_2 consumption was diffusion limited at all temperatures. Sulfide production increased strongly with temperature both in the dark and light incubated mat (Q_{10} = 1.8-3.2), and this led to saturation of sulfide oxidation and an increased sulfide efflux out of the dark incubated mat, which was maximal at 35°C. In the uppermost layer of the dark incubated mat, pH decreased due to aerobic respiration, sulfide oxidation and fermentation, and this decrease was enhanced with temperature. In the light incubated mat, the thickness of the photic zone decreased with temperature from 0.9 mm to 0.5 mm. Oxygen penetration and peak oxygen concentration decreased with temperature, whereas the upper sulfide boundary and thus the zone of sulfide oxidation rose closer to the mat surface in the light incubated mat. Areal rates of sulfide oxidation increased more than twofold from 25°C to 40°C in the light incubated mat. The relative contribution of sulfide oxidation to oxygen consumption in the aphotic zone increased significantly with temperature, indicating that at elevated temperatures incomplete sulfide oxidation occurred in the light incubated mat. Both the photosynthetically induced pH maximum and the overall pH of the mat decreased with increasing temperature due to enhanced heterotrophic activity, sulfide oxidation, and a changed depth distribution of these processes. Our data demonstrate a close coupling of oxygen and sulfur cycling in hypersaline microbial mats, which is strongly regulated by temperature.

INTRODUCTION

Microbial mats are benthic ecosystems where primary production, aerobic and anaerobic heterotrophic and chemolithotrophic processes occur in close association (van Gemerden 1993). In hypersaline environments, the elevated salinity excludes survival of most higher organisms and thus reduces grazing pressure and bioturbation leading to the development of thick and well laminated microbial mats. Such predominantly microbial systems are well suited to study the regulation and interaction of microbial processes involved in benthic carbon cycling. Furthermore, many microbial mat communities exhibit a striking similarity to Precambrian stromatolite communities in the fossil record (Schopf and Klein 1992). Biogeochemical and microbiological studies of recent microbial mats can, therefore, provide important information for interpreting the stable isotope signatures of carbon cycling left in the fossil record.

One of the best studied hypersaline environments is Solar Lake (Sinai, Egypt), a small lake characterized by an exceptional limnological cycle. During winter (and most of the year) the lake is stratified, with colder and less saline surface waters above the thermocline. Overturn to holomixis occurs in summer due to a salinity increase of the surface waters, caused by increasing evaporation towards summer (Por 1969; Cohen et al. 1977). During the stratification period, steep gradients of temperature, pH, redox potential, salinity, oxygen, and sulfide develop in the Solar Lake water column (Cohen et al. 1977). The bottom of Solar Lake is covered by well developed microbial mats (Krumbein et al. 1977; Jørgensen et al. 1983), with high concentrations of mostly autochthonous organic matter in the upper few cm of the shallow water mats (Krumbein et al. 1977; Aizenshtat et al. 1984). Although high primary production occurs in the uppermost millimeters of the mat, the yearly biomass accretion rate is relatively low, indicating high remineralization rates due to aerobic and anaerobic degradation (Krumbein et al. 1977). This indication is also supported by the high abundance of aerobic heterotrophs (Krumbein et al. 1977), anaerobic heterotrophs and, especially, of sulfate-reducing bacteria (Jørgensen and Cohen 1977) in the uppermost layer of the mat. Heterotrophic processes can supply CO_2 to the autotrophic community of the mat, alleviating the inorganic carbon limitation of photosynthesis (Canfield and Des Marais 1993; Teske et al. 1998), which is indicated by the enrichment in heavy carbon isotope (Schidlowski et al. 1984).

The physico-chemical conditions in microbial mats are characterized by pronounced fluctuations. Chemical gradients in the mat change drastically within a diel cycle (Revsbech et al. 1983). Solar radiation induces oxygenic photosynthesis in the mat, resulting in a pronounced build-up of oxygen supersaturation in the uppermost 1-3 mm thick surface layer above the sulfidic zone. During the night, sulfide accumulates and rises closer to the mat surface, with only minor oxygen penetration into the mat (Revsbech et al. 1983). Thus, the inhabiting microorganisms have to be physiologically flexible and fairly well adapted to the prevailing fluctuating conditions, as has already been demonstrated for the sulfate-reducing bacteria and cyanobacteria (Cohen et al. 1986; Jørgensen et al. 1986; Krekeler et al. 1997; Krekeler et al. 1998; Teske et al. 1998). Besides the light regime, also temperature changes on a diel basis (Revsbech et al. 1983). Temperature variations additionally occur throughout an annual cycle, due to the limnological cycle in the water column of the lake. Jørgensen et al. (1979) measured diel temperature variations at the mat surface both in winter and summer, ranging from 27°C - 33°C in summer (September) and from 22°C - 27°C in winter (March).

Temperature is an important environmental variable controlling benthic metabolic activities. Temperature effects on benthic primary production (e.g. Rasmussen et al. 1983; Grant 1986), aerobic respiration (Thamdrup et al. 1998) and sulfate reduction (e.g. Abdollahi and Nedwell 1979; Skyring 1987; Westrich and Berner 1988) have been investigated in marine sediments. Only little is known about the temperature regulation of carbon cycling in marine microbial mats and relatively few studies address the temperature regulation of metabolic processes in mats (Skyring et al. 1983; Javor and Castenholz 1984; Jørgensen 1994b). In a detailed study of the biogeochemistry of hypersaline mats, Canfield and Des Marais (1993) considered the major microbial processes (oxygenic photosynthesis, sulfate reduction, oxygen consumption due to aerobic respiration and sulfide oxidation). However, their measurements were limited to two different temperatures.

Whereas several microsensor studies of oxygen and sulfur cycling in hypersaline mats have been reported (e.g. Jørgensen et al. 1979; Jørgensen et al. 1983; Revsbech et al. 1983), we are not aware of studies, where the effect of temperature on oxygen and sulfide turnover, and their coupling to each other, has been addressed in detail. In this study, microsensor measurements in Solar Lake microbial mats were performed to investigate

short term temperature effects on the cycling of dissolved oxygen and sulfide in dark and light conditions. The goal was to gain detailed information on how temperature affects i) the major autotrophic and heterotrophic processes involved in carbon cycling, and ii) the balance between these processes in a hypersaline mat.

MATERIAL AND METHODS

Samples and experimental set-up. Microbial mat samples (approximately 30 cm x 25 cm x 4 cm) were collected by snorkeling in the shallow (0.4-0.5 m deep) eastern part of the hypersaline Solar Lake (Sinai, Egypt) in November 1996. The *in situ* temperature at the mat surface was 27.5°C and the salinity of the overlaying water was 105‰, as determined by a portable refractometer (Atago, S-28E, Japan). The mat sample was transferred within a few hours to the Interuniversity Institute in Eilat (Israel). During transport, the mat sample was kept moist in a plastic dish with only a thin film of Solar Lake water above the mat surface in order to avoid excess sulfide accumulation.

In the laboratory, a mat subsample (approximately 6 cm x 4 cm x 2.5 cm) was mounted in a flow chamber modified from Lorenzen et al. (1995). The subsample was embedded in agar (1.5% (w/v) in filtered Solar Lake water), leaving the mat surface flush with the surrounding agar surface. A submersible water pump (E-Heim, Germany) was connected with the flow chamber and generated a constant flow of filtered and aerated Solar Lake water over the mat surface. The temperature of the Solar Lake water reservoir was adjusted to ±0.5°C via a heat exchanging metal coil connected to a thermostat (Julabo, F32-HC, Germany). In the experimental set-up, the salinity was determined with a conductivity meter (WTW, LF 197, Germany), which was calibrated by readings with a refractometer.

The flow chamber was illuminated with a fiber-optic halogen light source (Schott, KL 1500, Germany), and the downwelling irradiance, E_d (PAR), at the mat surface was adjusted to 425 µmol photons m^{-2} s^{-1}, as determined by an underwater quantum irradiance meter (LiCor, LI-250, USA). For accurate determination of E_d (PAR), the quantum sensor was placed at the same distance from the light source and with the same amount of overlaying Solar Lake water as the microbial mat. Experimental light-dark shifts were

controlled by an electronical shutter (Vincent Ass., Uniblitz VS35S2TO, USA), that was inserted in the light path between the lamp and the mat sample.

Microsensors. Clark-type O_2 (Revsbech 1989) and H_2S (Jeroschewski et al. 1996; Kühl et al. 1998) microsensors, and glass pH microelectrodes (Revsbech and Jørgensen 1986) were used to measure the temperature dependent distribution of oxygen and sulfide in the light and dark incubated Solar Lake mat. The O_2 microsensor had a tip diameter of <10 µm, a stirring sensitivity of <2%, and a t_{90} response time of <0.5 s. The H_2S microsensor, which was coated with a black enamel paint to avoid light interference on the measuring signal (Kühl et al. 1998), had a tip diameter of <20 µm. The length of the pH-sensitive glass at the tip of the pH microelectrode was <100 µm, with a tip diameter of <15 µm.

Microsensor calibrations. The O_2 microsensor was linearly calibrated at each experimental temperature from readings of microsensor current in the anoxic part of the mat (0% oxygen) and in the overlaying air saturated Solar Lake brine (100% air saturation). Dissolved oxygen concentrations of air saturated brine at experimental temperatures and salinities were calculated according to Sherwood et al. (1991).

The glass pH microelectrodes were calibrated in standard buffer solutions (Mettler Toledo, Switzerland) at different temperatures. In one case (at 30°C), the pH microsensor was not calibrated at the measuring temperature. Therefore, the calibration slope obtained at 25°C was corrected for temperature, based on an average of the relative temperature dependent change of the calibration slope, as measured with 4 other pH microelectrodes. In the experimental set-up, the mV signals of the pH microelectrodes and the pH of the overlaying Solar Lake water, which was determined with a commercial pH meter (Mettler Toledo, MA 130, Switzerland) at 25°C, was used to correct for salinity (parallel shift of the calibration curve). For salinity corrections at elevated experimental temperatures (>25°C), the pH reading of the macroelectrode at 25°C was corrected for the temperature increase, assuming that the pH decreases 0.0114 pH units per 1°C temperature increase according to Grasshoff (1983).

Calibration of the H_2S microsensor was done in an Erlenmeyer flask closed with a silicon rubber stopper with holes for i) the microsensor, ii) a tube through which a constant flow of nitrogen gas was flushed into the flask, and iii) an inlet for addition of defined

volumes of Na_2S stock solution to the stirred anoxic buffer solution (200 mM phosphate buffer, pH 7). After each addition of Na_2S, a subsample was taken out and fixed in zinc acetate. The samples were stored dark and cold prior to the determination of total dissolved sulfide by the methylene blue method (Cline 1969). The H_2S concentration in the analyzed samples was calculated according to the equation (Jeroschewski et al. 1996)

$$[H_2S] = [S_{tot}] / \left(1 + \frac{K_1}{[H_3O^+]}\right) \quad (1)$$

where $[S_{tot}]$ is the total sulfide concentration, and K_1 is the first dissociation constant of the sulfide equilibrium, assuming a pK_1' of 7.05 (Kühl and Jørgensen 1992, and references therein). The slope of the H_2S calibration curve, determined by linear regression, was used to calculate the distribution of H_2S in the mat. Subsequently, the total sulfide distribution in the mat was calculated by use of eq. 1 with measured H_2S and pH values at corresponding depths. In the latter case, the pK_1' was corrected for temperature and salinity, as linearly extrapolated from the pK_1' measured in artificial Dead Sea brines and the pK_1' at 25°C in non-saline medium (Hershey et al. 1988). The slope of the H_2S calibration curve was corrected for temperature based on previously obtained data (C. Steuckart and A. Wieland, unpublished results). The slope decreased 5.6% at 30°C, 10.7% at 35°C and 13.1% at 40°C as compared to the slope of the calibration curve at 25°C. In the following, H_2S denotes dissolved hydrogen sulfide, whereas S_{tot} or sulfide denotes total sulfide, i.e. the sum of H_2S, HS^-, and S^{2-}.

Microprofile measurements. The H_2S and the pH microsensors were glued together, after orienting the tips of both microsensors as close as possible in the same horizontal plane under a microscope. The H_2S and the pH microsensors were fixed together with the O_2 microsensor (within an area of approximately 1 cm^2 of the mat surface) in a motor driven micromanipulator (Oriel, Encoder Mike, USA; Märzhäuser, MD4 modified, Germany). The O_2 and H_2S microsensors were connected to fast-responding picoamperemeters. The pH microelectrode was connected to a high impedance millivoltmeter. The microsensors were positioned on the mat surface by use of the motorized micromanipulator, while watching them through a dissection scope (Zeiss, SV6, Germany). The measuring signals were recorded with a strip chart recorder (Servogor, 124 plus, UK) and with a computer data acquisition system (National Instruments, Labview, USA) that also controlled the

micromanipulator. Profiles of O_2, pH and H_2S were measured with a vertical depth resolution of 100 µm. Microsensor measurements were started 1-3 h after changing the temperature conditions. Then several measurements were performed to ensure the establishment of a new steady state, which was normally reached within a few hours after the temperature change.

Gross photosynthesis measurements. Gross photosynthesis was measured with fast responding O_2 microelectrodes by means of the light-dark shift technique (Revsbech and Jørgensen 1983). Precisely defined light-dark shifts were realized with the electronical shutter (see above), which was triggered via the data acquisition software. A photodiode close to the shutter registered the moment of darkening. The initial rate of O_2 depletion was calculated automatically by the data acquisition software via linear regression on the acquired data points over the initial 1-2 seconds of darkening. Gross photosynthesis was recorded in steps of 100 µm vertical depth intervals. The distribution of the volumetric gross photosynthetic rates with depth is given as nmol O_2 cm^{-3} (porewater) s^{-1} (Revsbech et al. 1981). In the following, the photic zone refers to the zone in the mat where oxygenic photosynthesis could be detected by the light-dark shift technique. The aphotic zone refers to the oxic zone below the photic zone.

Calculations. Depth-integrated rates of gross photosynthesis, i.e. areal gross photosynthesis, were calculated from the porosity corrected volumetric rates in the photic zone. The mat porosity ϕ was assumed to be 0.9 (Jørgensen and Cohen 1977; Jørgensen et al. 1979). Areal rates of net photosynthesis and dark O_2 consumption were calculated from the linear O_2 gradient $\left(\frac{dC(z)}{dz}\right)$ in the diffusive boundary layer above the mat surface (Jørgensen and Revsbech 1985; Jensen and Revsbech 1989) according to Fick`s first law of (one-dimensional) diffusion:

$$J_0 = - D_0 * \left(\frac{dC(z)}{dz}\right) \quad (2)$$

where D_0 is the free solution molecular diffusion coefficient of O_2, and J_0 is the O_2 flux towards the mat surface (dark incubated mat) or towards the air saturated overlaying brine

(light incubated mat), respectively. Positive values of J_0 indicate a net O_2 import into the mat, whereas negative values of J_0 indicate a net O_2 export out of the mat.

The photosynthetically produced O_2 diffuses not only out of the mat into the overlaying brine, but also diffuses into the aphotic zone of the mat. This downward O_2 flux out of the photic zone, J_s, equals the areal O_2 consumption in the aphotic zone below (Jensen and Revsbech 1989; Kühl et al. 1996). J_s was calculated as:

$$J_s = - \phi \, D_s(z) * \left(\frac{dC(z)}{dz} \right) \quad (3)$$

where $\left(\frac{dC(z)}{dz} \right)$ is the O_2 concentration gradient at the lower boundary of the photic zone, i.e. the tangent to that point where the concavity of the O_2 profile changes direction. At lower incubation temperatures, this point was located slightly below the lower boundary of the photic zone. The sediment diffusion coefficient, D_s, was calculated from the free solution molecular diffusion coefficient, D_o, and the mat porosity, ϕ, according to Ullman and Aller (1982):

$$D_s = \phi^2 * D_o \quad (4)$$

The free solution diffusion coefficient of O_2 was taken from Broecker and Peng (1974) and corrected for temperature and salinity according to Li and Gregory (1974).

Net production and consumption zones of S_{tot} throughout the sulfidic zone of the mat were calculated by using a numerical procedure for the interpretation of measured steady state microprofiles (Berg et al. 1998). This procedure is based on a series of least square fits to the measured concentration profiles, assuming an increasing number of production and consumption zones. The fits are compared by statistical F-testing, so that the simplest production-consumption profile results, which reproduces the measured concentration profiles within the chosen statistical accuracy (more details in Berg et al. 1998). For this analysis, ϕ and D_s were estimated as for the calculation of J_s. The diffusion coefficient $D_o(S_{tot})$ was calculated from $D_o(O_2)$ assuming the same ratio between both diffusion coefficients as between the whole sediment diffusion coefficients (D_s) in the mat, where $D_s(S_{tot}) = 0.64 * D_s(O_2)$ (Jørgensen et al. 1979). Areal rates of net sulfide production-consumption were obtained by multiplying the calculated volumetric rates by the thickness of the reaction zones.

RESULTS

Mat structure and composition

The mat structure was compacted and finely layered with a smooth gelatinous ca. 1 mm thick brownish-orange surface layer. This surface layer was dominated by halotolerant unicellular cyanobacteria, most probably belonging to the *Halothece* cluster (Garcia-Pichel et al. 1998). A ca. 0.5 mm thick dark green band below the surface layer was dominated by filamentous cyanobacteria, mainly *Microcoleus chthonoplastes*. At 35°C, a macroscopic change of the mat surface was observed. The original brownish-orange color of the mat surface changed to greenish-white. After the experiment, and, thus, after measurements at 40°C, the mat sample was frozen in liquid nitrogen. Light microscopy on thawed samples revealed that the surface layer was now not only dominated by unicellular cyanobacteria, but also by filamentous cyanobacteria (mainly *Microcoleus chthonoplastes*) and *Chloroflexus*-type filamentous bacteria. Additionally, the whitish appearance of the surface layer was due to accumulation of elemental sulfur, mainly associated with small bacterial cells, resembling *Thiocapsa roseopersicina*, a non-motile, physiological versatile purple sulfur bacterium inhabiting microbial mats (de Wit and van Gemerden 1987).

Microprofiles of O_2, pH, S_{tot} and photosynthesis

In Figure 1 steady state O_2, pH and S_{tot} profiles in the dark and light (425 μmol photons m^{-2} s^{-1}) incubated Solar Lake mat are shown. Dark O_2 profiles were only slightly affected by changes in temperature, as O_2 was already at 25°C completely consumed in the uppermost 0.2 mm of the mat (Fig. 1, left panel). In the light incubated mat, O_2 penetration and maximal O_2 concentration were highest at 25°C as compared to the other incubation temperatures (see also Table 1). The oxic zone was 3.7 mm thick and the maximal pO_2 at 0.8 mm depth was >7 times air saturation. With increasing incubation temperature, O_2 penetration and peak O_2 concentration in the mat showed a decreasing trend (see also Table 1). The thickness of the photic zone decreased with temperature, while maximal volumetric rates of gross photosynthesis showed an increasing trend with temperature (Table 1).

Table 1: O_2 penetration, maximal O_2 concentration, the thickness of the photic zone, areal rates of gross photosynthesis, and maximal volumetric gross photosynthesis as a function of temperature.

Temperature	O_2 penetration	Maximal O_2 concentration	Photic zone	Gross photosynthesis	Maximal gross photosynthesis
(°C)	(mm)	(μM)	(mm)	(nmol O_2 cm^{-2} s^{-1})	(nmol O_2 cm^{-3} s^{-1})
25	3.7	1041 ± 8.74	0.9	0.22 ± 0.01	4.36 ± 1.01
30	2.6	967 ± 5.75	0.8	0.36 ± 0.01	7.13 ± 0.20
35	1.0	339 ± 14.25	0.6	0.30 ± 0.01	11.54 ± 0.36
40	1.2	400 ± 4.12	0.5	0.27 ± 0.01	10.40 ± 0.42

At 25°C, pH decreased strongly in the uppermost layer of the dark incubated mat due to aerobic respiration, fermentation and sulfide oxidation (Fig. 1, central panel). The pH dropped to a minimum value of 7.3 at 0.7-1.3 mm depth and then increased to pH 7.4. The pH decrease in the uppermost part of the mat became more pronounced with temperature, reaching a minimal pH of 7.0 at 40°C. The pH in the deeper parts of the mat also became more acidic with temperature and decreased approximately 0.4 pH units between 25°C and 40°C. In the light incubated mat, photosynthetic CO_2 fixation led to a broad maximum in pH (up to pH 9.5), indicating a predominance of photosynthesis at 25°C. Below this peak, pH strongly decreased due to aerobic respiration, fermentation and sulfide oxidation. The photosynthetically induced pH maximum decreased with temperature down to a peak pH of 8.2 at 40°C. Additionally, the zone below the pH maximum became more acidic with temperature.

Sulfide profiles, calculated from the measured pH and H_2S profiles, were strongly affected by temperature both in the dark and in the light incubated mat (Fig. 1, right panel). In the dark incubated mat, steep gradients of S_{tot} developed in response to the temperature increase. Maximal concentrations of 1552 μM of total sulfide, corresponding to 624 μM H_2S at the prevailing pH of 7.2 at that depth, were detected at 35°C in the dark incubated mat, as compared to 588 μM (216 μM H_2S, pH 7.4) at 25°C. In the dark, net sulfide production increased with temperature, and increasing amounts of sulfide diffused out of the mat at higher temperatures. The upper boundary of sulfide in the light incubated mat, i.e. the oxic-anoxic interphase, moved upwards when the temperature was increased. Also in the illuminated mat, steep sulfide gradients developed with increasing temperature as a result of enhanced sulfide production.

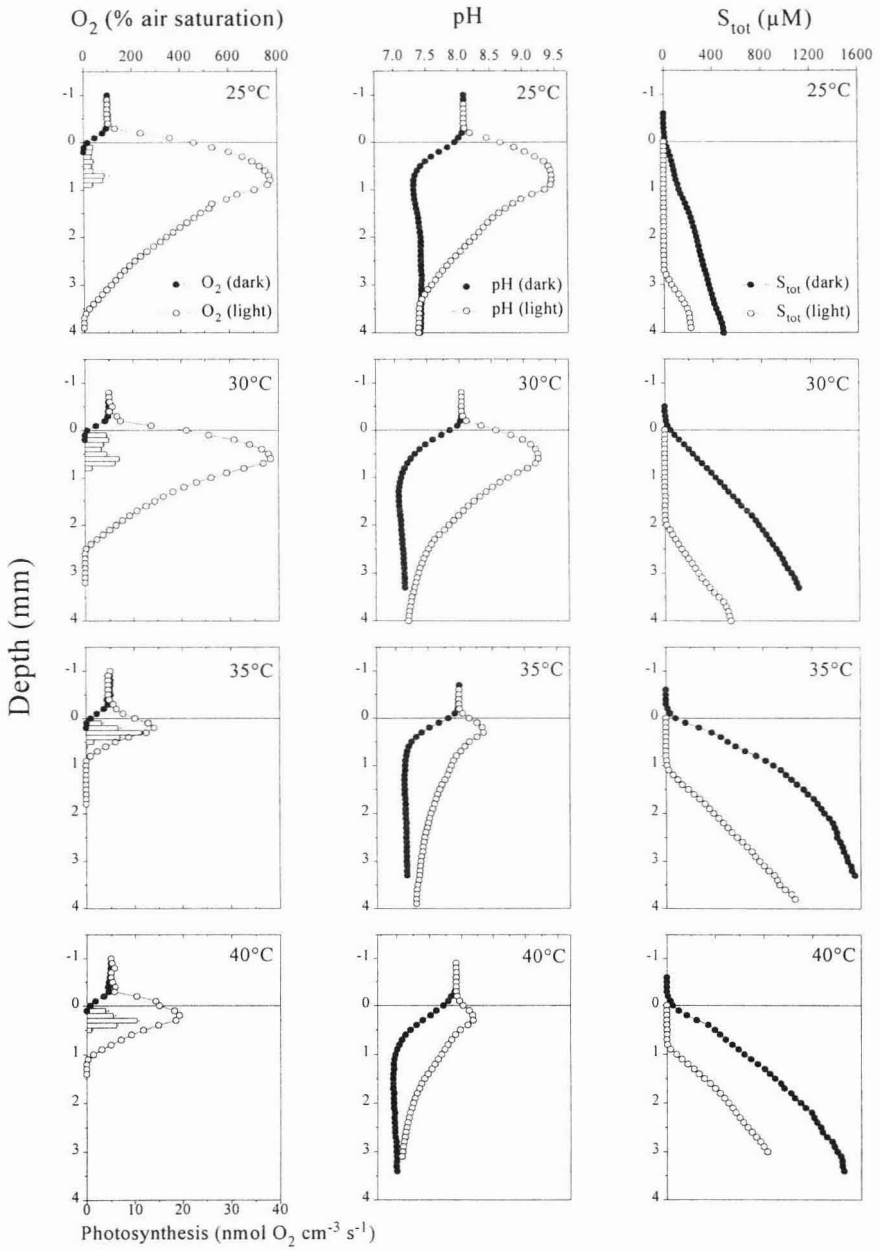

Figure 1. Average steady state concentration profiles (n = 2-3) of O_2, pH and S_{tot} as a function of temperature. S_{tot} refers to total sulfide. Bars represent average rates of volumetric gross photosynthesis, with standard deviation indicated by error bars (n = 3-7). Dark symbols indicate measurements in the dark incubated mat, open symbols indicate measurements in the light incubated mat (E_d (PAR) = 425 μmol photons m^{-2} s^{-1}).

Oxygen conversion

Figure 2 shows areal rates of gross and net photosynthesis, and dark O_2 consumption as a function of temperature. Net photosynthesis was affected most strongly by temperature and decreased significantly at temperatures above 30°C. Areal rates of dark O_2 consumption were much less influenced by increasing temperatures. Dark O_2 consumption, areal gross and net photosynthesis all exhibited a maximum at 30°C, and showed a decreasing trend with higher temperatures. The mismatch at 25°C and 30°C between gross and net photosynthesis has been observed and described previously in a similar microbial mat from a hypersaline lagoon in Spain (Epping and Kühl 1999). If rates of net photosynthesis are higher than apparent rates of gross photosynthesis, negative O_2 consumption rates would result. For this reason, the calculation of O_2 consumption rates in the light was neglected. Nevertheless, rates of net photosynthesis were minimal at 35°C indicating maximal O_2 consumption in the light. Furthermore, gross photosynthesis was minimal at 25°C with maximal O_2 penetration (Table 1), indicating minimal rates of O_2 consumption at 25°C.

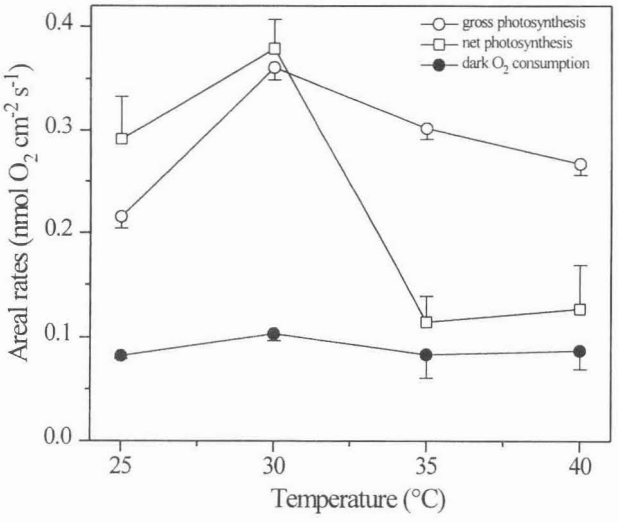

Figure 2. Areal rates (mean ± standard deviation) of gross photosynthesis (open circles), net photosynthesis (open squares), and dark O_2 consumption (closed circles), as calculated from O_2 profiles and volumetric gross photosynthetic rates shown in Fig. 1.

Sulfide conversion

The averaged S_{tot} profiles measured in the dark and in the light incubated mat (Fig. 1) were analyzed with a numerical procedure (Berg et al. 1998) and zones of net sulfide production (sulfate reduction) and net sulfide consumption (aerobic chemotrophic and chemical sulfide oxidation, anoxygenic phototrophic sulfide oxidation, sulfide precipitation by Fe^{2+} and polysulfide formation) were identified (Fig. 3). Rates of net sulfide production (positive values) and consumption (negative values) in the dark incubated mat at 25°C were low as compared to the higher incubation temperatures. In the uppermost part of the mat, a zone of net sulfide production was calculated. The lack of net sulfide oxidation in that zone led to a sulfide efflux out of the mat. Below this sulfide production zone, an apparently anaerobic net sulfide consumption zone was present. An increase of the experimental temperature caused an enhancement of sulfide production. Especially at 35°C and 40°C, zones of intense sulfide production developed close to the mat surface, and the efflux of sulfide increased with temperature (Fig. 3, left panel).

In the light, the upper boundary of sulfide and, therefore, the zone of sulfide oxidation moved upwards in the mat as a result of temperature increase, following roughly the decrease in O_2 penetration (Fig. 3, right panel). With increasing temperature, a zone of sulfide production developed just below the sulfide oxidation zone. The linear part of the sulfide gradients indicate zones, where no net sulfide production nor consumption occurred, i.e. zones where the gradients were solely determined by sulfide diffusion. Sulfide production in the light incubated mat was most probably underestimated at 35°C and 40°C, since the curvature of the sulfide profiles in the deeper zones, where sulfide concentration gradients became less steep were missed experimentally. The thickness of the zone where O_2 and S_{tot} coexisted decreased with temperature, from 1.2 mm at 25°C to a minimal thickness of 0.1 mm at 35°C.

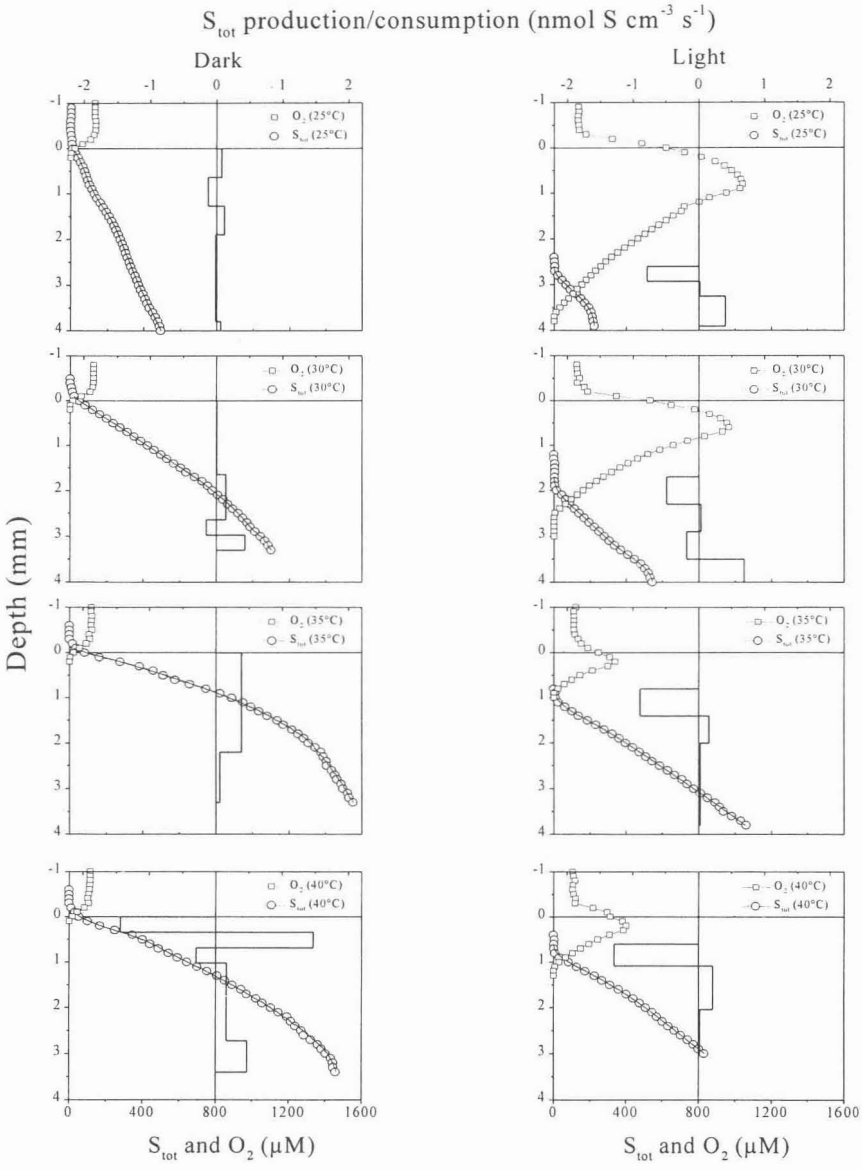

Figure 3. Production and consumption zones of S_{tot} (bars), and fitted profiles (line graph), as calculated by a numerical procedure (Berg et al. 1998) from measured steady state S_{tot} profiles (open circles). Zones of net S_{tot} production (consumption) are plotted as positive (negative) values. Oxygen profiles in the dark (left panel) and light (right panel) incubated mat are plotted as open squares.

Areal rates of O_2 consumption and net S_{tot} production, and the maximal possible O_2 fluxes through the diffusive boundary layer towards the mat surface (J_{max}) in the dark incubated mat are shown in Figure 4A. The calculation of J_{max} was based on the equation for the calculation of molecular diffusion fluxes, J, through the diffusive boundary layer from Jørgensen and Revsbech (1985):

$$J = D_0(O_2) * \Delta(O_2)/Z_\delta$$

where $D_0(O_2)$ is the molecular diffusion coefficient of O_2, Z_δ is the thickness of the effective diffusive boundary layer, and $\Delta(O_2)$ is the difference between the constant bulk water O_2 concentration and the O_2 concentration at the mat surface. For the calculation of J_{max}, the O_2 concentration at the mat surface was assumed to be zero and thus $\Delta(O_2)$ equaled the concentration of dissolved O_2 in the overlaying Solar Lake brine (100% air saturation). Z_δ was determined from measured dark O_2 microprofiles (Fig. 1) according to Jørgensen and Revsbech (1985).

Measured O_2 fluxes towards the dark incubated mat and calculated maximal O_2 fluxes, J_{max}, in the dark showed a similar temperature dependency. The differences between both rates was minimal at 30°C and maximal at 35°C, with J_{max} being 12% and 22% higher than the measured actual rates of dark O_2 consumption. Sulfide production in the dark increased from minimal rates of 0.024 nmol S_{tot} cm^{-2} s^{-1} at 25°C to maximal production rates of 0.111 nmol S_{tot} cm^{-2} s^{-1} at 40°C. The steepest, i.e. threefold, increase of areal S_{tot} production rates occurred between 30°C and 35°C, where also areal S_{tot} production rates started to exceed areal rates of dark O_2 consumption.

In Figure 4B areal rates of O_2 consumption in the aphotic zone J_s and of net sulfide oxidation at the upper sulfide boundary in the light incubated mat are shown. Taking not only net sulfide oxidation at the upper sulfide boundary into account, i.e. including also sulfide consumption zones in the deeper anoxic part of the mat, a measure of the total net sulfide production in the light incubated mat was obtained (dotted line). Areal rates of net sulfide production in the light incubated mat increased almost linearly with temperature, ranging from 0.026 nmol S_{tot} cm^{-2} s^{-1} at 25°C to 0.061 nmol S_{tot} cm^{-2} s^{-1} at 40°C. Net sulfide oxidation at the upper sulfide boundary showed a similar trend, with a 27% lower areal rate at 30°C, which is due to the zone of anaerobic sulfide consumption (Fig. 3). Oxygen consumption in the aphotic zone, J_s, expressed as the downward O_2 flux at the lower boundary of the photic zone in the light incubated mat, showed a similar, but more

pronounced, pattern of temperature response as compared with dark O_2 consumption. Maximal rates of J_s at 30°C amounted to 0.124 nmol O_2 cm^{-2} s^{-1}.

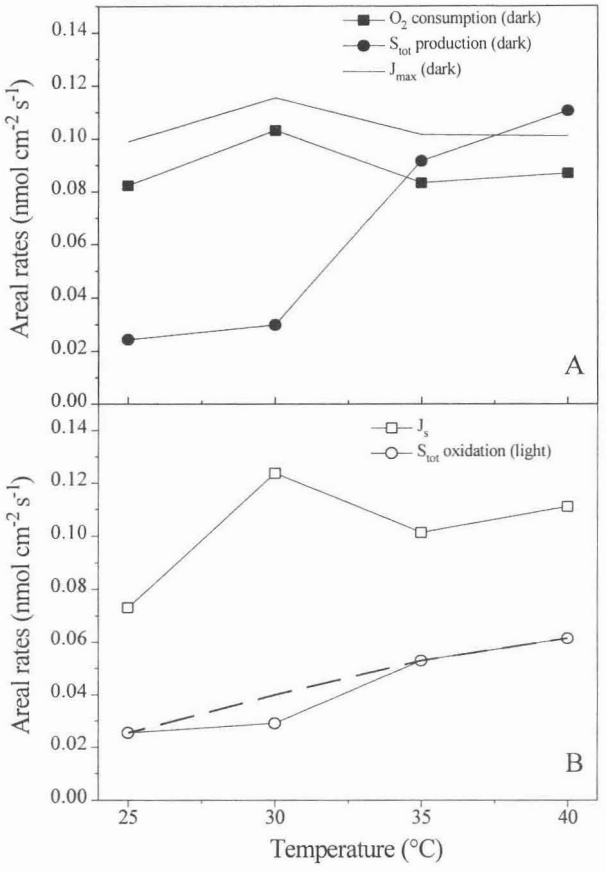

Figure 4. (A) Areal rates of O_2 consumption, net S_{tot} production, and of calculated maximal possible O_2 consumption (J_{max}, see text) in the dark incubated mat. (B) Areal rates of O_2 consumption in the aphotic zone J_s, net S_{tot} oxidation, and net S_{tot} production (dotted line, see text) in the light incubated mat.

The relative contribution of sulfide oxidation to the overall O_2 consumption in the aphotic zone of the light incubated mat is shown in Figure 5. From the sulfide oxidation rates at the upper sulfide boundary, the corresponding rates of O_2 consumption, which would be needed to oxidize all sulfide either to elemental sulfur, J_{S^o}, or sulfate, $J_{SO_4^{2-}}$, was

calculated and expressed relative to J_s, which was determined from the measured O_2 profiles. Calculations were based on the stoichiometry of the reactions (de Wit 1992):

$$H_2S + 0.5\ O_2 \rightarrow S^0 + H_2O$$

$$H_2S + 2\ O_2 \rightarrow SO_4^{2-} + 2\ H^+$$

Aerobic sulfide oxidation to elemental sulfur would have been possible at all incubation temperatures, accounting for minimal 12% (30°C) or maximal 28% of J_s (40°C). Complete sulfide oxidation to sulfate would not have been possible at elevated temperatures (35°C and 40°C), even if sulfide oxidation would have been the only O_2 consuming process in the aphotic zone. The drop of the relative contribution of sulfide oxidation to the total O_2 consumption in the aphotic zone at 30°C is due to the much stronger temperature-induced increase of J_s as compared to the increase of sulfide oxidation (Fig. 4). Even if complete sulfide oxidation to sulfate occurred at 30°C, still 53% of J_s would have been due to other O_2 dependent processes (e.g. heterotrophic respiration).

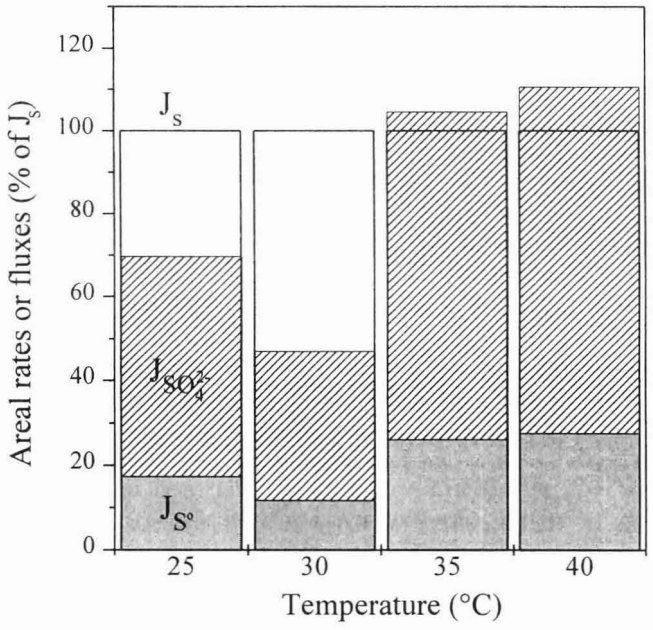

Figure 5. Areal O_2 consumption due to sulfide oxidation to elemental sulfur (J_{S^0}, solid bars) and to sulfate ($J_{SO_4^{2-}}$, hatched bars) relative to the overall areal O_2 consumption in the aphotic zone (J_s).

DISCUSSION

Our results show that increased temperature affected both reaction rates and the depth distribution of reaction zones for processes involved in O_2 and S_{tot} cycling in the microbial mat. Due to the numerous temperature dependent processes and their close coupling, direct and indirect temperature effects acted in concert and determined the temperature response of the microbial community.

Temperature effects on photosynthesis

Both the thickness of the photic zone and the volumetric rates of gross photosynthesis changed with temperature (Table 1, Fig. 1). The thickness of the photic zone decreased with temperature, whereas the individual volumetric rates generally increased, with the highest maximal volumetric gross photosynthetic rate detected at 35°C (Table 1). Indirect temperature effects on the rates of volumetric gross photosynthesis could have been due to the temperature response of the closely associated heterotrophic community, resulting in changes of chemical gradients. The temperature induced decrease of the pH maximum in the photic zone (Fig. 1) may have been of great significance for the regulation of photosynthesis. At a given concentration of inorganic carbon, high pH values cause a decrease of available CO_2 and vice versa. It was shown that the potential ^{14}C-assimilation in homogenized surface samples from the Danish Wadden Sea (tidal sandflat) increased with decreasing pH (Rasmussen et al. 1983). Furthermore, increased heterotrophic activity at higher temperatures could have enhanced the CO_2 supply for photosynthesis.

Temperature did not only affect volumetric gross photosynthesis rates and chemical gradients, but also the thickness of the photic zone. The most significant changes occurred between 30°C and 35°C, where also a macroscopic change of the mat surface was observed. The original brownish-orange color of the mat surface changed to a greenish-white appearance, most probably due to migration of filamentous cyanobacteria and the accumulation of elemental sulfur in the upper mat layers. The temperature-induced increase of the volumetric gross photosynthesis rates in the upper part of the mat surface could thus be explained by a direct temperature effect on photosynthesis or by an increased density of phototrophs in the surface layer caused by an upward migration of cyanobacteria.

Light dependent migration of filamentous cyanobacteria in microbial mats is well documented in the literature (Garcia-Pichel et al. 1994; Bebout and Garcia-Pichel 1995; Kruschel and Castenholz 1998). Our experiments were, however, conducted at constant light conditions and thus a light induced migration is unlikely. We cannot exclude, however, that the light field and vertical light distribution in the mat changed due to the observed changes of the mat surface. Increased light scattering in the surface layer at elevated temperatures due to the observed accumulation of elemental sulfur in combination with high absorption due to the pronounced abundance of filamentous cyanobacteria at the mat surface could have enhanced the light attenuation. The macroscopic change occurred at 35°C, where sulfide production increased strongly and steep sulfide gradients prevailed in the dark incubated mat, indicating an indirect temperature-induced migration due to enhanced sulfide production. Chemotaxis and also sulfide induced migration in benthic cyanobacterial systems was also suggested by Castenholz (1982) and Whale and Walsby (1984). Thus, the observed reduction of the photic zone was most likely caused by the migration of filamentous cyanobacteria.

Areal rates of oxygenic gross photosynthesis showed an optimum curve-like response to temperature, with a significant increase between 25°C and 30°C and a less steep decrease at increasing temperatures (Fig. 2). Maximal rates of gross photosynthesis were detected at 30°C, which was close to the *in situ* sampling temperature (27.5°C) and within the range of diel temperature variations in Solar Lake (Jørgensen et al. 1979). The optimum curve of gross photosynthesis in the Solar Lake mat differed from the typical response of photosynthesis to increasing temperatures, which is a progressive increase up to an optimum temperature, and a rapid decline at temperatures above the optimum temperature (Davison 1991). The most temperature sensitive processes of photosynthesis are the enzymatic reactions involved in CO_2 fixation, including the enzymes Ribulose-1,5-bisphosphate carboxylase oxygenase (Rubisco) and carbonic anhydrase (Davison 1991). Furthermore, temperature effects on diffusion processes, like e.g. diffusional supply of CO_2/HCO_3^- and nutrients, may also contribute to the temperature regulation of photosynthesis.

Net photosynthesis increased with temperature to an optimum at 30°C, and then decreased strongly at 35°C, with a slight increase again at 40°C. A similar optimum curve-like response of net photosynthesis has also been observed in other cyanobacterial mats

(Javor and Castenholz 1984). The different temperature responses of gross and net photosynthesis are due to temperature-induced changes of O_2 consumption in the light (see below). At 25°C and 30°C, net photosynthesis was higher than gross photosynthesis, and calculation of O_2 consumption would result in negative rates in the light. This mismatch was also observed and discussed by Epping and Kühl (1999). They suggested that if significant light-dependent hydrogen peroxide cycling occurs in microbial mats, this could lead to an underestimation of gross photosynthesis as determined by the light-dark shift technique. If the mismatch would be caused by an underestimation of gross photosynthetic rates due to H_2O_2 metabolism, and this metabolism would change with temperature, it should also have an effect on the temperature response curve of gross photosynthesis. However, further investigations are necessary to elucidate the mismatch between gross and net photosynthesis.

Temperature effects on O_2 consumption in the dark

Areal rates of dark O_2 consumption showed only minor temperature-induced changes, with a maximum at 30°C (Fig. 2). At the given diffusional O_2 supply through the diffusive boundary layer (DBL), intense O_2 consumption in the mat at 25°C limited O_2 penetration to the uppermost 0.2 mm. Due to the DBL mass transfer resistance, dark O_2 consumption of most shallow water sediments, microbial mats and other highly active microbial communities is limited and, therefore, regulated by the diffusional O_2 flux through the DBL (Jørgensen and Revsbech 1985; Jørgensen and Des Marais 1990; Kühl and Jørgensen 1992; Jørgensen 1994a). Enhanced O_2 supply due to a thinner DBL and an increased O_2 diffusion coefficient at increasing temperatures is partly counterbalanced by a lower O_2 solubility (Jørgensen and Revsbech 1985). Calculated rates of maximal possible dark O_2 consumption, J_{max}, (Fig. 4A) were significantly influenced by the effective DBL thickness, Z_δ, which was determined from the measured O_2 microprofiles. Z_δ was minimal at 30°C and then increased to a maximum at 40°C, where the mat surface topography became more rough. The difference between measured rates and calculated maximal possible rates of dark O_2 consumption was minimal at 30°C, with J_{max} being 12% higher than measured rates of dark O_2 consumption, thus indicating that dark O_2 consumption almost approached the limit of O_2 transport through the DBL.

Both heterotrophic aerobic respiration and oxidation of reduced inorganic compounds contributed to O_2 consumption in the dark incubated mat. Since no aerobic methane oxidation activity was detected in Solar Lake microbial mats (Conrad et al. 1995), it is unlikely that this process contributed significantly to O_2 consumption either in the dark or in the light incubated mat. Canfield and Des Marais (1993) estimated that most of the O_2 that diffuses into the mat (pond 5, Guerrero Negro, Baja California Sur, Mexico) at night is used for sulfide oxidation. In the Solar Lake mat, <60% of dark O_2 consumption at 25°C and 30°C would have been due to sulfide oxidation, assuming that all (net) produced sulfide was oxidized aerobically to sulfate within the mat. Aerobic sulfide oxidation occurred very close to the mat surface, since O_2 penetration at all temperatures was very low (0.1 to 0.2 mm depth, Fig. 1). This narrow zone of sulfide oxidation could be the reason that no net sulfide oxidation was calculated by the numerical procedure from Berg et al. (1998). Only at 40°C, a net sulfide consumption zone was calculated close to the mat surface (Fig. 3). This zone cannot only be attributed to aerobic sulfide oxidation since it also expands into the anoxic part of the mat, where e.g. polysulfide formation could have contributed to sulfide consumption.

With increasing temperature, the higher sulfide availability at the mat surface could have caused an O_2 limitation for sulfide oxidation, which is also indicated by the observed accumulation of elemental sulfur. Even if sulfide oxidation rates increased at elevated temperatures, the formation of sulfur could have led to a slight decrease in O_2 demand and thus, together with decreasing aerobic respiration, to a decrease of O_2 consumption (Fig. 2). Thamdrup et al. (1998) suggested that temperature effects on benthic O_2 uptake can largely be explained by the increased rates of anaerobic mineralisation and, thus, oxidation of reduced inorganic compounds at higher temperatures. Our data generally support this hypothesis, but sulfide production in the Solar Lake mat increased so strongly at elevated temperatures that sulfide oxidation became saturated and/or O_2 limited.

Temperature effects on O_2 consumption in the light

Oxygen consumption in the oxic zone of the light incubated mat, i.e. the difference between gross and net photosynthesis, was not calculated due to the observed mismatch between both rates (see above). However, it is indicated by the areal rates of gross photosynthesis and the pronounced decrease of net photosynthesis (Fig. 2) that O_2

consumption in the oxic zone was maximal at 35°C. Since O_2 consumption occurs both in the photic and the aphotic zone of the light incubated mat and O_2 consumption in the aphotic zone was maximal at 30°C (Fig. 4), O_2 consuming processes in the photic zone must have contributed to the indicated maximum at 35°C. Oxygen consumption in the photic zone can be related either to the phototrophic community or to the associated heterotrophic community. Photorespiration or consumption of produced glycolate could have contributed to O_2 consumption in the photic zone. It was shown in hot spring cyanobacterial mats, that glycolate represents a major fraction of excreted photosynthates (Bateson and Ward 1988). Although it is generally assumed that photorespiration is low in cyanobacteria, which have a DIC-concentrating mechanism (Aizawa and Miyachi 1986; Colman 1989), the role of photorespiration was so far not investigated under conditions that were observed in the Solar Lake microbial mat at lower temperatures, where high concentrations of dissolved O_2 (>7 times air saturation) occurred together with high pH (pH >9). High temperatures increase the potential for photorespiration (Davison 1991), but O_2 concentrations and pH, and thus probably also the O_2/CO_2 ratios, were much lower at 35°C and 40°C as compared to 25°C and 30°C, indicating less favorable conditions for photorespiration. Oxygen consumption in the photic zone at 35°C could also have been influenced by the observed changes of the surface layer.

In several systems, the excretion of organic compounds by primary producers and the subsequent uptake or turnover of these compounds by heterotrophic bacteria is indicated (e.g. Haack and McFeters 1982; Bateson and Ward 1988; Neely and Wetzel 1995; Malinsky-Rushansky and Legrand 1996). A close coupling of heterotrophic processes and photosynthesis was suggested for cyanobacterial mats (Canfield and Des Marais 1993; Teske et al. 1998) and epilithic cyanobacterial biofilms (Kühl et al. 1996). Zlotnik and Dubinsky (1989) suggested that significant excretion of dissolved organic carbon from phytoplankton occurs under conditions favorable for photosynthesis, i.e. when photosynthetic rates are high.

Both areal rates of gross photosynthesis (Fig. 2) and areal O_2 consumption in the aphotic zone J_s (Fig. 4) were maximal at 30°C and minimal at 25°C. Moreover, it is indicated that aerobic heterotrophic processes contributed significantly to J_s at 30°C (Fig. 5), possibly driven by a pronounced excretion of photosynthates at maximal rates of gross photosynthesis. However, J_s includes all biological and chemical O_2-consuming processes

(e.g. aerobic respiration and oxidation of reduced inorganic compounds) in the aphotic zone.

At higher temperatures, sulfide production increased and O_2 penetration decreased significantly pointing to an increasing contribution of sulfide oxidation to the overall O_2 consumption in the aphotic zone. Although sulfide can be oxidized both biologically and chemically, chemical sulfide oxidation is generally slower than biological oxidation of sulfide (e.g. Buisman et al. 1990). Revsbech et al. (1983) found that sulfide oxidation in the illuminated Solar Lake mat was primarily mediated biologically. An exact contribution of sulfide oxidation to O_2 consumption in the aphotic zone can, however, not be determined, since the O_2 demand for sulfide oxidation depends strongly on the oxidation product, on the microorganisms involved in sulfide oxidation, and also on the biological and chemical conversions of intermediate sulfide oxidation products. Furthermore, our microsensor measurements were not done in exactly the same point and a direct correlation of overlapping reaction zones of O_2 consumption and sulfide oxidation is critical. However, the measured O_2 and S_{tot} profiles showed clearly that i) sulfide oxidation, referred to as the S_{tot} consumption at the upper boundary of the profile, increased with temperature (Fig. 4), and ii) there was a pronounced change in O_2 availability for sulfide oxidation with temperature (Fig. 3). The O_2 availability can affect the types of sulfide oxidation products formed, as has been shown e.g. for *Thiobacillus thioparus* (van den Ende and van Gemerden 1993).

Different oxidation states of intermediate sulfide oxidation products do significantly influence the contribution of sulfide oxidation to O_2 consumption in the aphotic zone. Only at 25°C and 30°C, complete sulfide oxidation would have been possible, as estimated from J_s and calculated rates of sulfide oxidation (Fig. 5). At these temperatures, the zone of sulfide oxidation overlapped significantly with the aphotic zone (Fig. 3). It is thus likely that complete sulfide oxidation, or at least oxidation to highly oxidized intermediates, occurred at 25°C and 30°C. The situation changed drastically with increasing temperature. At higher temperatures complete sulfide oxidation would not have been possible, even if only sulfide oxidation contributed to J_s (Fig. 5). At 35°C, the thickness of the zone where O_2 and S_{tot} coexisted was minimal (0.1 mm, Fig. 3). Therefore, anoxic sulfide consumption by e.g. anoxygenic photosynthesis (see below) and polysulfide formation, cannot be excluded at 35°C, which could have led to a lower O_2 demand for sulfide oxidation. At

40°C, J_s increased again (Fig. 4), as a result of increasing sulfide oxidation and a slightly higher O_2 availability. Although the zone of sulfide oxidation was restricted to the aphotic zone, complete sulfide oxidation to sulfate was not possible, even if only sulfide oxidation would have contributed to O_2 consumption in the aphotic zone. Taking also O_2 consumption by aerobic respiration into account, it is probable that intermediate sulfide oxidation products with a low oxidation state accumulated due to incomplete sulfide oxidation.

Anoxygenic photosynthesis was not of major importance for sulfide oxidation, since O_2 penetrated deeper than the depth of the photic zone, and, besides at 35°C, O_2 and S_{tot} consumption zones overlapped. This points to a predominance of chemolithotrophic sulfide oxidation (Jørgensen and Des Marais 1986). However, incomplete aerobic sulfide oxidation under O_2 limitation could also support anoxygenic phototrophs via intermediate sulfide oxidation products (van den Ende et al. 1996), thus allowing for a coexistence of both processes. The latter is also indicated by the increased abundance of *Chloroflexus*-type filamentous bacteria in the surface layer, as observed by light microscopy after the experiments. Although we did not measure the vertical light distribution in the mat, enough light, especially near infrared light (Jørgensen et al. 1979), could have penetrated to the zone of sulfide oxidation at elevated temperatures. The use of intermediates is however not detectable with H_2S microelectrodes. Sulfide oxidation is also simplified if only sulfate and elemental sulfur as oxidation products are considered. Other possible intermediates like thiosulfate could also have been produced and further transformed via oxidation, reduction or disproportionation (e.g. Jørgensen 1990; Visscher et al. 1992; Jørgensen 1994b). Disproportionation reactions of different intermediates (e.g. thiosulfate, sulfite) can lead to additional sulfide production (Bak and Cypionka 1987; Bak and Pfennig 1987). Thus, our sulfide consumption rates may represent part of the actual rates of chemolithotrophic and anoxygenic phototrophic processes in the mat.

Temperature effects on pH microprofiles

The measured pH profiles are difficult to interpret in terms of specific chemical or biological processes. In the dark, pH decreased in the upper part of the mat. Since sulfide oxidation and heterotrophic respiration took place in the upper 0.2 mm of the dark incubated mat, the overall pH decrease with depth was probably also due to fermentation

processes by fermentative heterotrophic bacteria and/or cyanobacteria (Oren and Shilo 1979; Moezelaar et al. 1996; Nold and Ward 1996). Fermentation increased with temperature as indicated from the decreasing pH in the upper part of the dark incubated mat. Accumulation of fermentation products under dark anaerobic conditions was shown in hot spring cyanobacterial mats (Anderson et al. 1987). Such fermentation products could serve as substrates for sulfate-reducing bacteria (Moezelaar et al. 1996). Furthermore, fermentative production of H_2 could support sulfate reduction in the dark (Skyring et al. 1988).

The pH maximum in the photic zone represents the balance between the photosynthetically induced pH increase due to CO_2 fixation and heterotrophic activity, which tends to decrease the pH. The pH decrease in the aphotic zone was caused by aerobic respiration and sulfide oxidation. The chemical gradients and thus the depth distribution of these processes changed significantly with temperature (Fig. 3), contributing to the observed temperature-enhanced pH decrease in the aphotic zone and to the decrease of the photosynthesis-induced pH maximum.

Temperature effects on sulfide production

Sulfide production increased with temperature, both in the dark and light incubated mat (Fig. 3 and 4). The Q_{10} of sulfide production was determined according to Isaksen and Jørgensen (1996). In the temperature range of 25°C-35°C (30°C-40°C) a Q_{10} of 1.82 (1.78) in the light and a Q_{10} of 3.16 (3.05) in the dark incubated mat was calculated. Generally, reported Q_{10} values of sulfate reduction in cyanobacterial mats and saltmarsh sediments are in the range of 2.0 to 3.5 (Abdollahi and Nedwell 1979; Skyring et al. 1983; Jørgensen 1994b). In other hypersaline mats, a 10°C temperature increase caused a two- to four-fold enhancement of sulfate reduction both during the day and night (Canfield and Des Marais 1991; Canfield and Des Marais 1993).

Our sulfide production rates represent net rates of sulfide production, which, together with sulfide consumption rates, represent a measure of net sulfide cycling in the mat. Actual rates of sulfate reduction may have been higher at all conditions. High rates of sulfate reduction have been measured in the uppermost few cm in Solar Lake mats, and it was found that 50% of the total daily areal sulfate reduction occurred in the uppermost 5 mm and 90% in the uppermost 3 cm of the mat, respectively (Jørgensen and Cohen

1977). Furthermore, several studies indicate that sulfate reduction also occurs in the well oxygenated zone of light incubated hypersaline mats, where the produced sulfide is rapidly reoxidized (Canfield and Des Marais 1991; Fründ and Cohen 1992; Jørgensen 1994b; Teske et al. 1998). These processes are not included in our net sulfide production rates, which could be one reason for the different Q_{10} values of sulfide production in the dark and light incubated mat.

The most pronounced increase of sulfide production in the dark incubated mat occurred between 30°C and 35°C (Fig. 4), and a zone of high sulfide production developed in the upper layer of the mat (Fig. 3). This significant increase could have been due to both a higher temperature optimum of the sulfate-reducing bacterial community and possibly an increased availability of electron donors. Thus, sulfate reduction became of increasing importance for the mineralisation of organic matter at elevated temperatures. A stronger temperature dependency of sulfate reduction than aerobic respiration and an increased role of anaerobic mineralisation at increasing temperatures was also suggested by Thamdrup et al. (1998) in a study of suspended marine sediments.

The measured S_{tot} profiles did not always exhibit a clear spatial separation of sulfide production and consumption zones, and sometimes several zones were calculated by the numerical procedure (Fig. 3). Especially at 40°C in the dark incubated mat, zones of high sulfide production and consumption were calculated close to the mat surface and it is difficult to estimate if these zones are only due to biological sulfide production/consumption processes or if various chemical processes like polysulfide formation via reactions between sulfide and elemental sulfur took place. Also the occurrence of zones of anaerobic sulfide consumption under several conditions (Fig. 3) is difficult to interpret. Besides chemical reactions, these zones could also result from changes of physical parameters in the mat, like the porosity and the diffusion coefficient D_s, which were assumed to be constant.

Conclusions

Temperature had a complex effect on processes involved in O_2 and sulfide cycling in the Solar Lake cyanobacterial mat. Most of the involved microbial processes are not only directly regulated by temperature, but also depend on the availability of various substrates, either supplied by closely associated microbial activities or by diffusional transport. These are also temperature dependent and therefore contributed indirectly to the temperature response of e.g. photosynthesis and O_2 consumption. In the Solar Lake mat, sulfide conversion processes became of increasing importance for the O_2 turnover at elevated temperatures. Thus, when temperature was increased above *in situ* environmental temperatures, the sulfur cycle strongly influenced the aerobic community and its metabolism, and became a major controlling factor of carbon turnover in the microbial mat.

ACKNOWLEDGEMENTS

This study was supported by the Red Sea Program on Marine Sciences, Project E: Microbial activities in marine interfaces controlling sediment-water fluxes, financed by the German Ministry for Research and Development (BMBF). We thank Gaby Eickert, Anja Eggers and Vera Hübner for the construction of the microsensors, and Gaby Eickert for technical assistance in Eilat. We acknowledge the fruitful discussions with Carsten Steuckart, Ferran Garcia-Pichel and Peter Berg. The Interuniversity Institute in Eilat (Israel) is thanked for providing laboratory facilities, and especially Yehuda Cohen is thanked for his hospitality and for neverending enthusiasm and efforts to arrange the Solar Lake field trips. The Egyptian authorities are thanked for their allowance to work at Solar Lake.

REFERENCES

Abdollahi H, Nedwell DB (1979). Seasonal temperature as a factor influencing bacterial sulfate reduction in a saltmarsh sediment. Microb Ecol 5:73-79

Aizawa K, Miyachi S (1986). Carbonic anhydrase and CO_2 concentrating mechanisms in microalgae and cyanobacteria. FEMS Microbiol Rev 39:215-233

Aizenshtat Z, Lipiner G, Cohen Y (1984). Biogeochemistry of carbon and sulfur cycle in the microbial mats of the Solar Lake (Sinai). In: Cohen Y, Castenholz RW, Halvorson HO (Ed.) Microbial mats: Stromatolites. Alan R Liss, New York, p 281-312

Anderson KL, Tayne TA, Ward DM (1987). Formation and fate of fermentation products in hot spring cyanobacterial mats. Appl Environ Microbiol 53(10):2343-2352

Bak F, Cypionka H (1987). A novel type of energy metabolism involving fermentation of inorganic sulphur compounds. Nature 326:891-892

Bak F, Pfennig N (1987). Chemolithotrophic growth of *Desulfovibrio sulfodismutans* sp. nov. by disproportionation of inorganic sulfur compounds. Arch Microbiol 147:184-189

Bateson MM, Ward DM (1988). Photoexcretion and fate of glycolate in a hot spring cyanobacterial mat. Appl Environ Microbiol 54(7):1738-1743

Bebout BM, Garcia-Pichel F (1995). UV B-induced vertical migrations of cyanobacteria in a microbial mat. Appl Environ Microbiol 61(12):4215-4222

Berg P, Risgaard-Petersen N, Rysgaard S (1998). Interpretation of measured concentration profiles in sediment pore water. Limnol Oceanogr 43(7):1500-1510

Broecker WS, Peng T-H (1974). Gas exchange rates between air and sea. Tellus 26:21-35

Buisman C, Ijspeert P, Janssen A, Lettinga G (1990). Kinetics of chemical and biological sulphide oxidation in aqueous solutions. Wat Res 24(5):667-671

Canfield DE, Des Marais DJ (1991). Aerobic sulfate reduction in microbial mats. Science 251:1471-1473

Canfield DE, Des Marais DJ (1993). Biogeochemical cycles of carbon, sulfur, and free oxygen in a microbial mat. Geochim Cosmochim Acta 57:3971-3984

Castenholz RW (1982). Motility and taxes. In: Carr NG, Whitton BA (Ed.) The biology of cyanobacteria. Blackwell Scientific Publications, Oxford, p 413-440

Cline JD (1969). Spectrophotometric determination of hydrogen sulfide in natural waters. Limnol Oceanogr 14:454-458

Cohen Y, Jørgensen BB, Revsbech NP, Poplawski R (1986). Adaptation to hydrogen sulfide of oxygenic and anoxygenic photosynthesis among cyanobacteria. Appl Environ Microbiol 51(2):398-407

Cohen Y, Krumbein WE, Goldberg M, Shilo M (1977). Solar Lake (Sinai). 1. Physical and chemical limnology. Limnol Oceanogr 22(4):597-608

Colman B (1989). Photosynthetic carbon assimilation and the suppression of photorespiration in the cyanobacteria. Aquat Bot 34:211-231

Conrad R, Frenzel P, Cohen Y (1995). Methane emission from hypersaline microbial mats: lack of aerobic methane oxidation activity. FEMS Microbiol Ecol 16:297-306

Davison IR (1991). Environmental effects on algal photosynthesis: temperature. J Phycol 27:2-8

de Wit R (1992). Sulfide-containing environments. Encyclopedia of Microbiology 4:105-121

de Wit R, van Gemerden H (1987). Chemolithotrophic growth of the phototrophic sulfur bacterium *Thiocapsa roseopersicina*. FEMS Microbiol Ecol 45:117-126

Epping EHG, Kühl M (1999). Short-term effects of temperature and irradiance on photosynthesis and oxygen consumption in a microbial mat. submitted to J Phycol

Fründ C, Cohen Y (1992). Diurnal cycles of sulfate reduction under oxic conditions in cyanobacterial mats. Appl Environ Microbiol 58(1):70-77

Garcia-Pichel F, Mechling M, Castenholz RW (1994). Diel migrations of microorganisms within a benthic, hypersaline mat community. Appl Environ Microbiol 60(5):1500-1511

Garcia-Pichel F, Nübel U, Muyzer G (1998). The phylogeny of unicellular, extremely halotolerant cyanobacteria. Arch Microbiol 169:469-482

Grant J (1986). Sensitivity of benthic community respiration and primary production to changes in temperature and light. Mar Biol 90:299-306

Grasshoff K (1983). Determination of pH. In: Grasshoff K, Ehrhardt M, Kremling K (Ed.) Methods of Seawater Analysis. Verlag Chemie, Weinheim, p 85-97

Haack TK, McFeters GA (1982). Nutritional relationship among microorganisms in an epilithic biofilm community. Microb Ecol 8:115-126

Hershey JP, Plese T, Millero FJ (1988). The pK_1^* for the dissociation of H_2S in various ionic media. Geochim Cosmochim Acta 52:2047-2051

Isaksen MF, Jørgensen BB (1996). Adaptation of psychrophilic and psychrotrophic sulfate-reducing bacteria to permanently cold marine environments. Appl Environ Microbiol 62(2):408-414

Javor BJ, Castenholz RW (1984). Productivity studies of microbial mats, Laguna Guerrero Negro, Mexico. In: Cohen Y, Castenholz RW, Halvorson HO (Ed.) Microbial mats: Stromatolites. Alan R Liss, New York, p 149-170

Jensen J, Revsbech NP (1989). Photosynthesis and respiration of a diatom biofilm cultured in a new gradient growth chamber. FEMS Microbiol Ecol 62:29-38

Jeroschewski P, Steuckart C, Kühl M (1996). An amperometric microsensor for the determination of H_2S in aquatic environments. Anal Chem 68:4351-4357

Jørgensen BB (1990). A thiosulfate shunt in the sulfur cycle of marine sediments. Science 249:152-154

Jørgensen BB (1994a). Diffusion processes and boundary layers in microbial mats. In: Stal LJ, Caumette P (Ed.) Microbial Mats: Structure, Development and Environmental Significance, NATO ASI Series G Vol. 35. Springer, Berlin, p 243-253

Jørgensen BB (1994b). Sulfate reduction and thiosulfate transformations in a cyanobacterial mat during a diel oxygen cycle. FEMS Microbiol Ecol 13(4):303-312

Jørgensen BB, Cohen Y (1977). Solar Lake (Sinai). 5. The sulfur cycle of the benthic cyanobacterial mats. Limnol Oceanogr 22(4):657-666

Jørgensen BB, Cohen Y, Revsbech NP (1986). Transition from anoxygenic to oxygenic photosynthesis in a *Microcoleus chthonoplastes* cyanobacterial mat. Appl Environ Microbiol 51(2):408-417

Jørgensen BB, Des Marais DJ (1986). Competition for sulfide among colorless and purple sulfur bacteria in cyanobacterial mats. FEMS Microbiol Ecol 38:179-186

Jørgensen BB, Des Marais DJ (1990). The diffusive boundary layer of sediments: oxygen microgradients over a microbial mat. Limnol Oceanogr 35(6):1343-1355

Jørgensen BB, Revsbech NP (1985). Diffusive boundary layers and the oxygen uptake of sediments and detritus. Limnol Oceanogr 30(1):111-122

Jørgensen BB, Revsbech NP, Blackburn TH, Cohen Y (1979). Diurnal cycle of oxygen and sulfide microgradients and microbial photosynthesis in a cyanobacterial mat sediment. Appl Environ Microbiol 38(1):46-58

Jørgensen BB, Revsbech NP, Cohen Y (1983). Photosynthesis and structure of benthic microbial mats: Microelectrode and SEM studies of four cyanobacterial communities. Limnol Oceanogr 28(6):1075-1093

Krekeler D, Sigalevich P, Teske A, Cypionka H, Cohen Y (1997). A sulfate-reducing bacterium from the oxic layer of a microbial mat from Solar Lake (Sinai), *Desulfovibrio oxyclinae* sp. nov. Arch Microbiol 167:369-375

Krekeler D, Teske A, Cypionka H (1998). Strategies of sulfate-reducing bacteria to escape oxygen stress in a cyanobacterial mat. FEMS Microbiol Ecol 25:89-96

Krumbein WE, Cohen Y, Shilo M (1977). Solar Lake (Sinai). 4. Stromatolitic cyanobacterial mats. Limnol Oceanogr 22(4):635-656

Kruschel C, Castenholz RW (1998). The effect of solar UV and visible irradiance on the vertical movements of cyanobacteria in microbial mats of hypersaline waters. FEMS Microbiol Ecol 27:53-72

Kühl M, Glud RN, Ploug H, Ramsing NB (1996). Microenvironmental control of photosynthesis and photosynthesis-coupled respiration in an epilithic cyanobacterial biofilm. J Phycol 32:799-812

Kühl M, Jørgensen BB (1992). Microsensor measurements of sulfate reduction and sulfide oxidation in compact microbial communities of aerobic biofilms. Appl Environ Microbiol 58(4):1164-1174

Kühl M, Steuckart C, Eickert G, Jeroschewski P (1998). A H_2S microsensor for profiling biofilms and sediments: application in an acidic lake sediment. Aquat Microb Ecol 15:201-209

Li Y-H, Gregory S (1974). Diffusion of ions in sea water and in deep-sea sediments. Geochim Cosmochim Acta 38:703-714

Lorenzen J, Glud RN, Revsbech NP (1995). Impact of microsensor-caused changes in diffusive boundary layer thickness on O_2 profiles and photosynthetic rates in benthic communities of microorganisms. Mar Ecol Prog Ser 119:237-241

Malinsky-Rushansky NZ, Legrand C (1996). Excretion of dissolved organic carbon by phytoplankton of different sizes and subsequent bacterial uptake. Mar Ecol Prog Ser 132:249-255

Moezelaar R, Bijvank SM, Stal LJ (1996). Fermentation and sulfur reduction in the mat-building cyanobacterium *Microcoleus chthonoplastes*. Appl Environ Microbiol 62(5):1752-1758

Neely RK, Wetzel RG (1995). Simultaneous use of ^{14}C and ^{3}H to determine autotrophic production and bacterial protein production in periphyton. Microb Ecol 30:227-237

Nold SC, Ward DM (1996). Photosynthate partitioning and fermentation in hot spring microbial mat communities. Appl Environ Microbiol 62(12):4598-4607

Oren A, Shilo M (1979). Anaerobic heterotrophic dark metabolism in the cyanobacterium *Oscillatoria limnetica*: sulfur respiration and lactate fermentation. Arch Microbiol 122:77-84

Por FD (1969). Limnology of the heliothermal Solar Lake on the coast of Sinai (Gulf of Elat). Intern Ver Theor Angew Limnol Verh 17:1031-1034

Rasmussen MB, Henriksen K, Jensen A (1983). Possible causes of temporal fluctuations in primary production of the microphytobenthos in the Danish Wadden Sea. Mar Biol 73:109-114

Revsbech NP (1989). An oxygen microelectrode with a guard cathode. Limnol Oceanogr 34:474-478

Revsbech NP, Jørgensen BB (1983). Photosynthesis of benthic microflora measured with high spatial resolution by the oxygen microprofile method: Capabilities and limitations of the method. Limnol Oceanogr 28(4):749-756

Revsbech NP, Jørgensen BB (1986). Microelectrodes: Their use in microbial ecology. Adv Microb Ecol 9:293-352

Revsbech NP, Jørgensen BB, Blackburn TH, Cohen Y (1983). Microelectrode studies of the photosynthesis and O_2, H_2S, and pH profiles of a microbial mat. Limnol Oceanogr 28(6):1062-1074

Revsbech NP, Jørgensen BB, Brix O (1981). Primary production of microalgae in sediments measured by oxygen microprofile, $H^{14}CO_3^-$ fixation, and oxygen exchange methods. Limnol Oceanogr 26(4):717-730

Schidlowski M, Matzigkeit U, Krumbein WE (1984). Superheavy organic carbon from hypersaline microbial mats. Naturwissenschaften 71:303-308

Schopf JW, Klein C (1992). The proterozoic biosphere: a multidisciplinary study. Cambridge University Press, Cambridge.

Sherwood JE, Stagnitti F, Kokkinn MJ, Williams WD (1991). Dissolved oxygen concentrations in hypersaline waters. Limnol Oceanogr 36(2):235-250

Skyring GW (1987). Sulfate reduction in coastal ecosystems. Geomicrobiol J 5:295-374

Skyring GW, Chambers LA, Bauld J (1983). Sulfate reduction in sediments colonized by cyanobacteria, Spencer Gulf, South Australia. Aust J Mar Freshw Res 34:359-374

Skyring GW, Lynch RM, Smith GD (1988). Acetylene reduction and hydrogen metabolism by a cyanobacterial/sulfate-reducing bacterial mat ecosystem. Geomicrobiol J 6:25-31

Teske A, Ramsing NB, Habicht K, Fukui M, Küver J, Jørgensen BB, Cohen Y (1998). Sulfate-reducing bacteria and their activities in cyanobacterial mats of Solar Lake (Sinai, Egypt). Appl Environ Microbiol 64(8):2943-2951

Thamdrup B, Hansen JW, Jørgensen BB (1998). Temperature dependence of aerobic respiration in a coastal sediment. FEMS Microbiol Ecol 25:189-200

Ullman WJ, Aller RC (1982). Diffusion coefficients in nearshore marine sediments. Limnol Oceanogr 27(3):552-556

van den Ende FP, Laverman AM, van Gemerden H (1996). Coexistence of aerobic chemotrophic and anaerobic phototrophic sulfur bacteria under oxygen limitation. FEMS Microbiol Ecol 19:141-151

van den Ende FP, van Gemerden H (1993). Sulfide oxidation under oxygen limitation by a *Thiobacillus thioparus* isolated from a marine microbial mat. FEMS Microbiol Ecol 13:69-78

van Gemerden H (1993). Microbial mats: a joint venture. Mar Geol 113:3-25

Visscher PT, Prins RA, van Gemerden H (1992). Rates of sulfate reduction and thiosulfate consumption in a marine microbial mat. FEMS Microbiol Ecol 86:283-294

Westrich JT, Berner RA (1988). The effect of temperature on rates of sulfate reduction in marine sediments. Geomicrobiol J 6:99-117

Whale GF, Walsby AE (1984). Motility of the cyanobacterium *Microcoleus chthonoplastes* in mud. Br Phycol J 19:117-123

Zlotnik I, Dubinsky Z (1989). The effect of light and temperature on DOC excretion by phytoplankton. Limnol Oceanogr 34(5):831-839

Chapter 3

Irradiance and temperature regulation of oxygenic photosynthesis and O_2 consumption in a hypersaline cyanobacterial mat (Solar Lake, Egypt)

Andrea Wieland[1], Michael Kühl[2]

[1] Max-Planck-Institute for Marine Microbiology, Microsensor Research Group
Celsiusstr. 1, D-28359 Bremen, Germany
[2] Marine Biological Laboratory, University of Copenhagen
Strandpromenaden 5, DK-3000 Helsingør, Denmark

submitted to Marine Biology

ABSTRACT

Short term effects of temperature and irradiance on oxygenic photosynthesis and O_2 consumption in a hypersaline cyanobacterial mat were investigated with O_2 microsensors in a laboratory. The effect of temperature on O_2 fluxes across the mat-water interface was studied in the dark and at a saturating high surface irradiance (2162 μmol photons m^{-2} s^{-1}) in the temperature range from 15°C to 45°C. Areal rates of dark O_2 consumption increased almost linearly with temperature. The apparent activation energy of 18 kJ mol^{-1} and the corresponding Q_{10} value (25°C-35°C) of 1.3 indicated a relative low temperature dependence of dark O_2 consumption due to mass transfer limitations imposed by the diffusive boundary layer at all temperatures. Areal rates of net photosynthesis increased with temperature up to 40°C and exhibited a Q_{10} value (20°C-30°C) of 2.8. Both O_2 dynamics and rates of gross photosynthesis at the mat surface increased with temperature up to 40°C, with the most pronounced increase of gross photosynthesis at the mat surface between 25°C and 35°C (Q_{10} of 3.1). In another mat sample, measurements at increasing surface irradiances (0-2319 μmol photons m^{-2} s^{-1}) were performed at 25°C, 33°C (the *in situ* temperature) and 40°C. At all temperatures, areal rates of gross photosynthesis saturated with no significant reduction due to photoinhibition at high irradiances. The initial slope and the onset of saturation (E_k = 148-185 μmol photons m^{-2} s^{-1}) estimated from P vs. E_d curves showed no clear trend with temperature, while maximal photosynthesis increased with temperature. Gross photosynthesis was stimulated by temperature at each irradiance except at the lowest irradiance of 54 μmol photons m^{-2} s^{-1}, where oxygenic gross photosynthesis and also the thickness of the photic zone was significantly reduced at 40°C. The compensation irradiance increased with temperature, from 32 μmol photons m^{-2} s^{-1} at 25°C to 77 μmol photons m^{-2} s^{-1} at 40°C, due to increased rates of O_2 consumption relative to gross photosynthesis. Areal rates of O_2 consumption in the illuminated mat were higher than dark O_2 consumption at corresponding temperatures, due to an increasing O_2 consumption in the photic zone with increasing irradiance. Both light and temperature enhanced the internal O_2 cycling within hypersaline cyanobacterial mats.

INTRODUCTION

Temperature and light are major environmental factors controlling benthic primary productivity (Cadée and Hegeman 1974; Rasmussen et al. 1983; Grant 1986; Canfield and Des Marais 1993; Barranguet et al. 1998). Benthic phototrophic communities often experience fluctuating environmental conditions, e.g. variation of the light regime as well as temperature changes, both on a daily and on a seasonal scale. During a seasonal cycle, the benthic community may acclimate and/or undergo a change in structure and composition due to such environmental fluctuations (Grant 1986; Blanchard et al. 1996; Barranguet et al. 1998).

In microbial mats photosynthesis and heterotrophic processes occur in close association within a few millimeter thick microbial community (van Gemerden 1993). If environmental conditions, like elevated salinities or temperature, preclude survival of higher organisms and, consequently, reduce the grazing pressure on the microbes, thick laminated microbial mats develop, which are characterized by high microbial population densities and steep physico-chemical gradients (Stal and Caumette 1994). This process can also be artificially induced in normal coastal sediments by removal of higher trophic levels (Fenchel 1998). Due to the absence of bioturbation and their compacted microbial composition, microbial mats are ideal model systems to study the regulation and interaction of various autotrophic and heterotrophic processes.

The required spatial resolution and sensitivity to study microbial processes on a microscale can be obtained by the application of microsensors (Revsbech and Jørgensen 1986; Amann and Kühl 1998). With the so-called light-dark shift technique the distribution of oxygenic gross photosynthesis can be determined at high spatial resolution (Revsbech and Jørgensen 1983). From depth-integrated rates of gross photosynthesis and oxygen fluxes, determined from steady state oxygen microprofiles, oxygen consumption in the light can be estimated for distinct layers of the community, i.e. in the photic and aphotic parts of the oxic zone (Jensen and Revsbech 1989; Kühl et al. 1996).

A stimulation of oxygen consumption in the light has been demonstrated in biofilms and microbial mats (Kuenen et al. 1986; Jensen and Revsbech 1989; Neely and Wetzel 1995; Epping and Jørgensen 1996; Kühl et al. 1996) and a close coupling between oxygen and inorganic carbon producing/consuming processes and, therefore, between autotrophic and

heterotrophic microbes was suggested (Canfield and Des Marais 1993; Kühl et al. 1996). The response of photosynthesis to light and temperature may thus also affect various heterotrophic processes in microbial mats and vice versa. Photosynthesis is strongly regulated by light, and the effect of temperature on photosynthesis seems also dependent on the light level (Davison 1991). Thus, in the natural habitat several environmental parameters vary simultaneously and determine a complex regulation of phototrophic and oxygen consuming processes.

Solar Lake is a small hypersaline lake situated at the coast of Sinai (Egypt). The lake has a characteristic limnological cycle causing pronounced variations of environmental conditions (Cohen et al. 1977). The cyanobacterial mats covering the bottom of the lake (Krumbein et al. 1977; Jørgensen et al. 1983) are characterized by steep chemical gradients as a result of the high activity of phototrophic and heterotrophic processes within the mats (Revsbech et al. 1983). Cyanobacterial mats in the shallow part of the lake are subjected to diel temperature variations (Jørgensen et al. 1979; Revsbech et al. 1983). As already indicated in earlier studies of hypersaline microbial mats from different localities (Canfield and Des Marais 1993; Epping and Kühl 1999), the oxygen metabolism in the mat may be significantly regulated by both temperature and irradiance.

The aim of the present study was to obtain detailed information about the regulation of oxygenic photosynthesis and O_2 consuming processes by temperature and irradiance. We studied the short term response of oxygenic photosynthesis and O_2 consumption to varying light and temperature conditions in a Solar Lake cyanobacterial mat by use of O_2 microsensors under controlled laboratory conditions. In another study, we also investigated the interactions of O_2 and H_2S producing/consuming processes in microbial mats and how these are regulated by temperature under dark and light conditions (Wieland and Kühl 1999).

MATERIAL AND METHODS

Samples. Microbial mats were collected in the shallow eastern part of the hypersaline Solar Lake (Sinai, Egypt) at an approximate water depth of 0.4-0.5 m in June 1997. The mat samples (3-4 cm thick) were taken by Plexiglas corers with an inner diameter of

5.0-5.6 cm. The *in situ* temperature was 33°C and the salinity at the sampling site was 114‰, as determined by a refractometer (Atago, Japan). Maximal irradiances at noon reached ~2300 µmol photons m^{-2} s^{-1} (Eilat, Israel). The mat samples in the cores were transported to the Interuniversity Institute in Eilat within a few hours after sampling, where measurements were performed under controlled laboratory conditions.

Experimental set-up. Mat subsamples (approximately 2.5 cm x 2.5 cm x 2 cm) were immobilized (1.5% agar (w/v) in filtered Solar Lake water) and mounted in a flow chamber modified from Lorenzen et al. (1995). The flow chamber was connected to a submersible water pump (E-Heim, Germany), which created a constant flow of aerated and filtered Solar Lake water over the mat surface. Experimental temperatures of the water reservoir were adjusted to ±0.5°C with a heat exchanging metal coil connected to a thermostat (Julabo, Germany). The mat surface was illuminated with a fiber-optic halogen light source (Schott KL 1500, Germany). Neutral density filters (Oriel, USA) were inserted in the collimated light beam to adjust the downwelling surface irradiance, E_d (PAR). For quantification of E_d (PAR) with an underwater quantum irradiance meter (LiCor, USA), the flow chamber was replaced by the underwater quantum sensor, which was submerged in Solar Lake water and placed at the same position and distance as the mat sample relative to the light source.

Microsensor measurements. Microprofiles of O_2 and gross photosynthesis were measured with Clark-type O_2 microelectrodes (Revsbech 1989). The O_2 microelectrodes had outer tip diameters of <10 µm, stirring sensitivities of <2% and t_{90} response times of <0.5 s. The O_2 microelectrodes were connected to a fast responding, miniaturized picoamperemeter (MasCom GmbH, Germany) plugged onto the prolonged shaft of the microelectrodes and mounted on a motor driven micromanipulator (Oriel, USA; Märzhäuser, Germany). The microsensors were positioned on the mat surface by use of the micromanipulator, while watching the mat surface and the tip of the microelectrode through a dissection microscope (Zeiss, Germany). The measuring signals were recorded on a strip chart recorder (Servogor, UK) and on a computer data acquisition system (National Instruments, Labview, USA), that also controlled the micromanipulator. Linear calibration of the O_2 microelectrode from readings in the aerated overlaying Solar Lake water (100% air

saturation) and in the anoxic part of the mat (0% oxygen) was done with every measured profile. Dissolved O_2 concentrations in aerated Solar Lake brine at experimental temperatures and salinities were calculated according to Sherwood et al. (1991). Steady state O_2 microprofiles were measured in steps of 100 µm vertical depth intervals.

Gross photosynthesis was measured by means of the light-dark shift technique (Revsbech and Jørgensen 1983). The mat surface was darkened by closing an electronical shutter (Vincent Ass., Uniblitz, USA), which was fixed in the light beam and triggered by the data acquisition software. A photodiode close to the shutter registered the moment of darkening. The rate of O_2 depletion after darkening of the mat was calculated automatically via linear regression over the initial 1-2 s by the software. Gross photosynthesis profiles were recorded with 100 µm vertical depth resolution. Since volumetric gross photosynthetic rates determined with the light-dark shift technique are given as nmol O_2 cm^{-3} (porewater) s^{-1} (Revsbech et al. 1981), measured rates of volumetric gross photosynthesis were corrected for porosity, which was assumed to be 0.9 (Jørgensen and Cohen 1977; Jørgensen et al. 1979). The zone where gross photosynthesis was measurable with the light-dark shift technique is in the following referred to as the photic zone. The aphotic zone represents the oxic zone below the photic zone.

Experimental light-dark cycles at increasing temperatures were performed on the mat surface at a downwelling irradiance of 2162 µmol photons m^{-2} s^{-1}. The O_2 microelectrode was positioned on the mat surface and after reaching O_2 steady state levels in the dark (light), the light was turned on (off).

Calculations. Diffusive fluxes of O_2 across the mat-water interface J_0 were calculated from steady state O_2 profiles using Fick's first law of (one-dimensional) diffusion:

$$J_0 = - D_0 * \left(\frac{dC(z)}{dz} \right) \quad (1)$$

where D_0 is the free solution molecular diffusion coefficient of O_2, and $\left(\frac{dC(z)}{dz} \right)$ is the linear O_2 concentration gradient in the diffusive boundary layer above the mat surface, where transport of solutes is dominated by molecular diffusion (Jørgensen and Revsbech 1985). A positive flux indicates a net O_2 uptake, while a negative flux indicates a net O_2 export out of the mat. In the dark incubated mat, J_0 is a measure of O_2 consumption rate per

unit area of the microbial mat, R_{dark}. In the light incubated mat, $-J_o$ is a measure of areal rates of net photosynthesis, P_n. If O_2 consumption is higher than gross photosynthesis, this leads to a net O_2 uptake in the light and P_n is, therefore, negative. Areal rates of net photosynthesis in the photic zone, $P_{n,phot}$, were calculated as the total O_2 flux out of the photic zone (Jensen and Revsbech 1989; Kühl et al. 1996; Epping and Kühl 1999):

$$P_{n,phot} = J_s - J_o \quad (2)$$

The downward O_2 flux, J_s, at the lower boundary of the photic zone, which is also a measure of O_2 consumption in the aphotic zone, R_{aphot}, was calculated by:

$$J_s = - \phi * D_s * \left(\frac{dC(z)}{dz} \right) \quad (3)$$

The porosity, ϕ, of the mat was assumed to be 0.9 (see above). The sediment diffusion coefficient, D_s, was calculated from the mat porosity and the free solution molecular diffusion coefficient, D_o, according to Ullman and Aller (1982):

$$D_s = \phi^2 * D_o \quad (4)$$

The free solution molecular diffusion coefficient of O_2 was taken from Broecker and Peng (1974) and corrected for temperature and salinity (Li and Gregory 1974).

Areal rates of total O_2 consumption in the light, R_{light}, and of O_2 consumption in the photic zone, R_{phot}, were calculated by (Kühl et al. 1996):

$$R_{light} = P_g - P_n \quad (5)$$

and

$$R_{phot} = P_g - P_{n,phot} \quad (6)$$

where P_g is the areal rate of gross photosynthesis, calculated by integration of the porosity corrected volumetric gross photosynthesis rates over the depth of the photic zone. Volumetric rates of O_2 consumption in the photic zone were calculated by dividing calculated areal rates of R_{phot} (eq. 6) by the thickness of the photic zone.

Photosynthesis versus irradiance curves (P vs. E_d curves) were obtained by fitting areal rates of gross photosynthesis at increasing irradiances to an exponential function (Webb et al. 1974) using the solver routine of Excel 5.0 (Microsoft):

$$P = P_m [1-\exp(-\alpha E_d/P_m)] \quad (7)$$

where P_m is the maximal photosynthetic rate at light saturation, and α is the initial slope of the P vs. E_d curve.

The effect of temperature on process rates was quantified by calculating the apparent activation energy, E_a, and the corresponding Q_{10} according to Isaksen and Jørgensen (1996). E_a was determined from the slope of an Arrhenius plot, i.e. ln(k) versus $(R*T)^{-1}$, based on the integrated form of the Arrhenius equation:

$$\ln(k) = \ln(A) + (-E_a*(R*T)^{-1}) \quad (8)$$

where k is the process rate, A is the Arrhenius constant, R is the gas constant (8.3144 J K^{-1} mol^{-1}) and T is the absolute temperature (°K). Q_{10}, which is the factor of process rate increase by a 10°C temperature increase, was calculated by:

$$Q_{10} = \exp [E_a *10 \text{ K} * (R*T*(T + 10 \text{ K}))^{-1}] \quad (9)$$

RESULTS

The microbial mat had a gelatinous structure with a 1-2 mm thick yellow-brownish surface layer composed of diatoms (*Navicula* sp., *Nitzschia* sp.) and unicellular cyanobacteria, belonging to the *Halothece* cluster (Garcia-Pichel et al. 1998). The surface layer was followed by a dense ca. 0.5-1 mm thick green layer of filamentous cyanobacteria (mainly *Microcoleus chthonoplastes*). At higher experimental temperatures, the mat topography became rough, probably due to migration and aggregation of microbes in the surface layer of the mat.

Oxygen fluxes and O_2 dynamics as a function of temperature

In the dark incubated mat, O_2 penetration and O_2 concentration at the mat surface decreased gradually from 15°C to 35°C. At further increasing temperatures, the O_2 concentration at the mat surface slightly increased again (Fig. 1). In the light incubated mat (E_d (PAR): 2162 µmol photons m^{-2} s^{-1}), O_2 penetration decreased from 3.8 mm at 15°C to 2.1 mm at 35°C, and increased again at 40°C and 45°C to 2.2 mm (profiles not shown).

Areal rates of dark O_2 consumption, R_{dark}, increased almost linearly with temperature from 0.042 (± 0.001) nmol O_2 cm^{-2} s^{-1} at 15°C to 0.084 (± 0.004) nmol O_2 cm^{-2} s^{-1} at 45°C (Fig. 2A). The apparent activation energy of R_{dark}, as determined from the linear slope of an Arrhenius plot of these data, amounted to 18 kJ mol^{-1} (Fig. 2B) and is a measure of the

temperature response of all O_2 consuming processes in the mat. In the light incubated mat (E_d (PAR): 2162 µmol photons m^{-2} s^{-1}), areal rates of net photosynthesis, P_n, increased between 15°C and 40°C from 0.044 (± 0.004) to 0.264 (± 0.008) nmol O_2 cm^{-2} s^{-1}, and then decreased at 45°C to 0.245 (± 0.016) nmol O_2 cm^{-2} s^{-1} (Fig. 2A). The apparent activation energy, calculated in the temperature range from 15°C-30°C, amounted to 77 kJ mol^{-1} (Fig. 2B). From the activation energies, we calculated Q_{10} values of 1.3 (25°C-35°C) and 2.8 (20°C-30°C) for areal dark O_2 consumption and net photosynthesis, respectively.

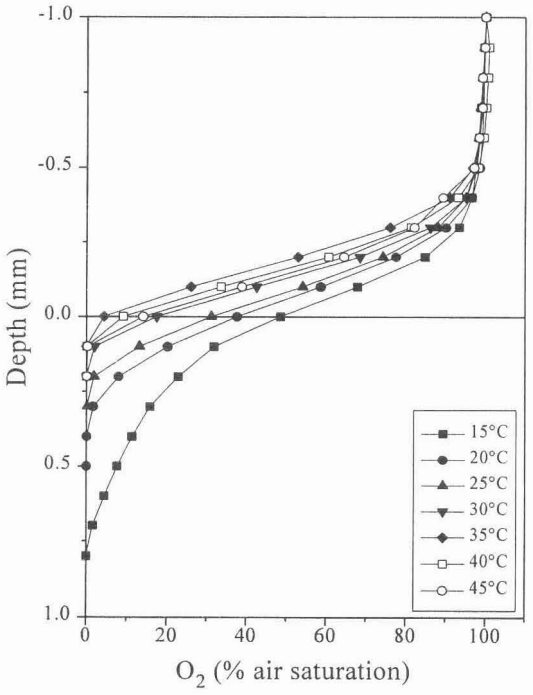

Figure 1. Averaged steady state O_2 concentration profiles (n = 3) measured in a dark incubated mat at increasing temperatures (indicated in graph). Note that the 100% air saturation value translates into decreasing amounts of absolute O_2 concentration with increasing temperature.

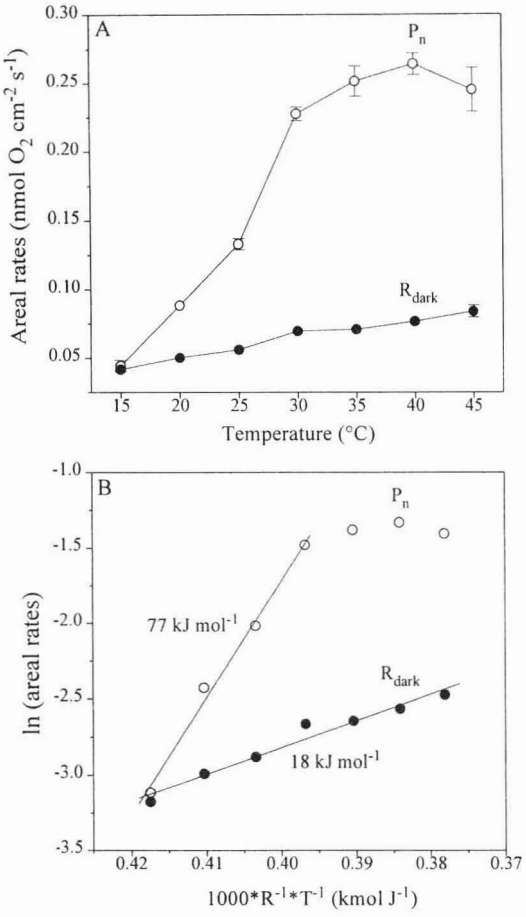

Figure 2. (A) Areal rates of dark O_2 consumption, R_{dark}, and of net photosynthesis, P_n, at increasing temperatures. Symbol and error bars indicate mean ± standard deviation (n = 2-3). (B) Arrhenius plot of the rates shown in (A).

Both the steady state O_2 levels and the O_2 dynamic on the mat surface changed with increasing temperature (Fig. 3). The O_2 steady state concentration in the light increased from 283 µM at 15°C to 596 µM at 40°C, whereas the O_2 steady state concentration in the dark decreased from 93 µM at 15°C to 10 µM at 40°C.

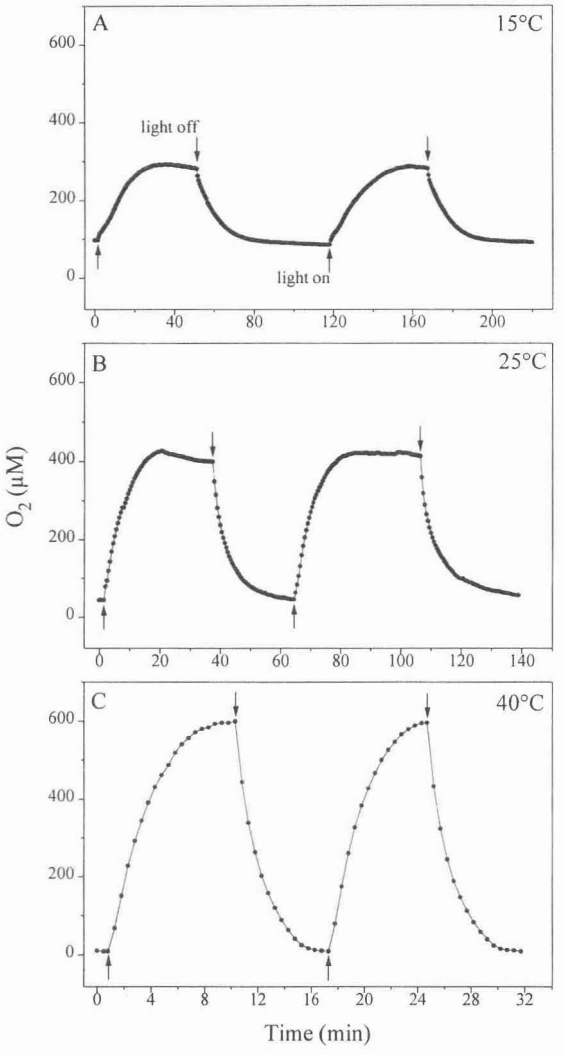

Figure 3. Oxygen dynamics at the mat surface during experimental light-dark cycles (E_d (PAR): 2162 µmol photons m^{-2} s^{-1}) at 15°C (A), 25°C (B) and 40°C (C). Note different time scales.

The initial rate of O_2 depletion after darkening, i.e. the gross photosynthesis at the mat surface, increased with temperature up to 40°C and then decreased at 45°C (Fig. 4A). An apparent activation energy of 86 kJ mol^{-1} in the temperature range from 15°C to 35°C was calculated (Fig. 4B), yielding a Q_{10} of 3.1 (25°C-35°C).

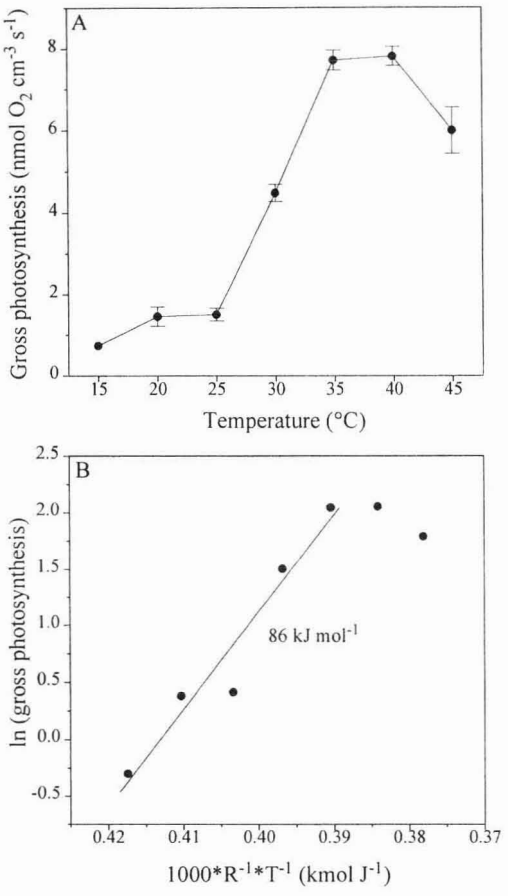

Figure 4. (A) The initial rate of O_2 depletion after darkening, i.e. gross photosynthesis, as determined on the mat surface from experimental light-dark cycles at increasing temperatures (calculated from data in Fig. 3). Symbols and error bars indicate mean ± standard deviation (n = 2-3). (B) Arrhenius plot of the rates shown in (A).

Microprofiles of O_2 and gross photosynthesis

Depth profiles of dissolved O_2 and gross photosynthesis as a function of increasing downwelling irradiance and temperature, were measured in another mat subsample (Fig. 5). At all experimental temperatures, O_2 penetration increased with increasing irradiance. Oxygen concentrations within the mat increased with irradiance up to a maximal O_2 concentration at 626 µmol photons m^{-2} s^{-1} at each experimental temperature.

Oxygen penetration in the dark decreased with increasing temperature from 0.5 mm at 25°C to 0.2 mm at 40°C. A temperature-induced decrease of O_2 penetration was also found in the illuminated mat. At low irradiances, i.e. 54 and 119 µmol photons m^{-2} s^{-1}, both O_2 penetration and peak O_2 concentration decreased with temperature. At 54 µmol photons m^{-2} s^{-1}, a gradual transition from a net O_2 export (25°C) towards a net O_2 import (40°C) across the mat-water interface was observed. Peak O_2 concentrations at high irradiances, i.e. 626, 1000 and 2319 µmol photons m^{-2} s^{-1}, were maximal at 25°C and minimal at 33°C at each irradiance. The thickness of the aphotic zone decreased at each light condition with increasing temperature.

The vertical zonation of gross photosynthetic activity changed with increasing irradiance and exhibited two to three distinct zones of high activity at saturating irradiances. At low irradiances, the thickness of the photic zone was constant at 25°C (1.7 mm) and 33°C (1.5 mm), whereas at 40°C it increased significantly from 0.7 mm to 1.6 mm between 54 and 119 µmol photons m^{-2} s^{-1}. At each temperature, an additional subsurface peak of photosynthesis was found at 626 µmol photons m^{-2} s^{-1}. This peak moved deeper into the mat at higher irradiance (Fig. 5, 6C).

At each temperature, the volumetric gross photosynthesis rate at the mat surface increased with irradiance up to 626 µmol photons m^{-2} s^{-1}, and decreased at higher irradiances (Fig. 6A). The averaged volumetric gross photosynthesis rate in the upper 0.1-0.7 mm of the mat showed a similar trend at 33°C and 40°C (Fig. 6B). At 25°C, the averaged gross photosynthesis rate did not decrease, but approached saturation at high irradiances.

Photosynthesis versus irradiance at 3 experimental temperatures

At each temperature, areal rates of gross photosynthesis, P_g, increased with irradiance up to 626 µmol photons m^{-2} s^{-1} (Fig. 7, left panel). The initial slope of the P vs. E_d curve, α, and the onset of saturation at irradiance $E_k = P_m/\alpha$ showed no clear trend with temperature (α = 0.0022, 0.0031, and 0.0026; E_k = 175, 148, and 185 µmol photons m^{-2} s^{-1} at 25°C, 33°C, and 40°C, respectively). The maximal photosynthetic rate at light saturation, P_m (eq. 7), increased from 0.38 nmol O_2 cm^{-2} s^{-1} at 25°C to 0.48 nmol O_2 cm^{-2} s^{-1} at 40°C. An increase of P_g with temperature was found at each irradiance except at 54 µmol photons m^{-2} s^{-1}, where P_g first increased between 25°C and 33°C, and then decreased again at 40°C.

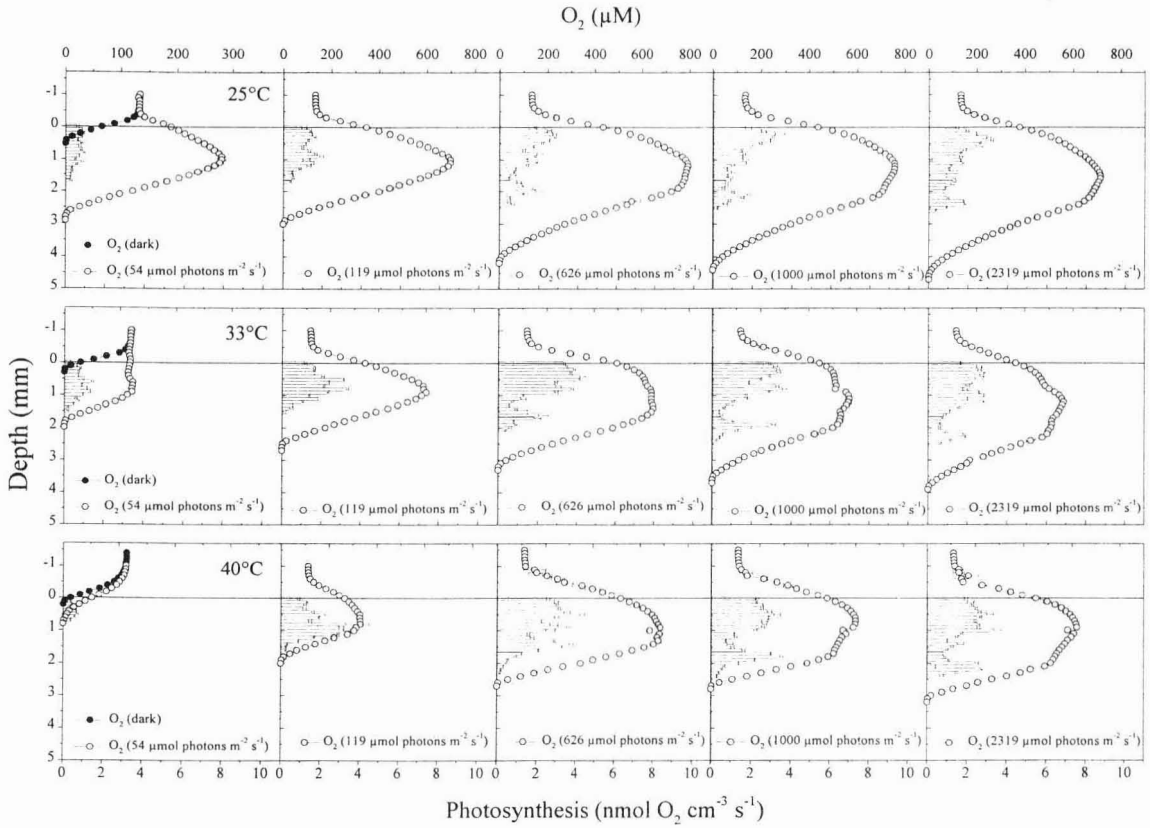

Figure 5. Averaged depth profiles of O_2 concentration and gross photosynthesis as a function of increasing downwelling irradiance at 25°C (upper panel), 33°C (central panel), and 40°C (lower panel). Note the different O_2 concentration scales. Standard deviation of gross photosynthesis at each depth is indicated by error bars (n = 2-5). Error bars were only included in the averaged O_2 profiles (n = 2-3) if the standard deviation was higher than the O_2 concentration range that is comprised by the symbol.

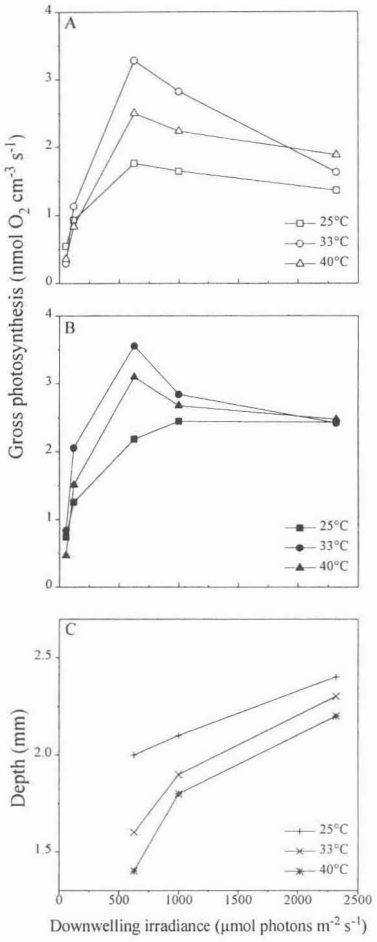

Figure 6. (A) Volumetric gross photosynthesis rate at the mat surface, (B) the averaged volumetric gross photosynthesis rate in the upper 0.1-0.7 mm of the mat, and (C) the depth of the maximal volumetric gross photosynthesis rate of the subsurface photosynthesis peak vs. downwelling irradiance at 25°C, 33°C and 40°C (see text for more details).

Areal rates of net photosynthesis, P_n, and of net photosynthesis in the photic zone, $P_{n,phot}$, increased with irradiance up to 626 µmol photons m^{-2} s^{-1} at each temperature and then either decreased (25°C and 33°C) or further increased with increasing irradiance (40°C). The compensation irradiance, E_c, where O_2 production (P_g) is balanced by O_2 consumption (R_{light}), i.e. $P_n = 0$, increased with temperature from 32 µmol photons m^{-2} s^{-1} at 25°C to 53 µmol photons m^{-2} s^{-1} at 33°C and to 77 µmol photons m^{-2} s^{-1} at 40°C.

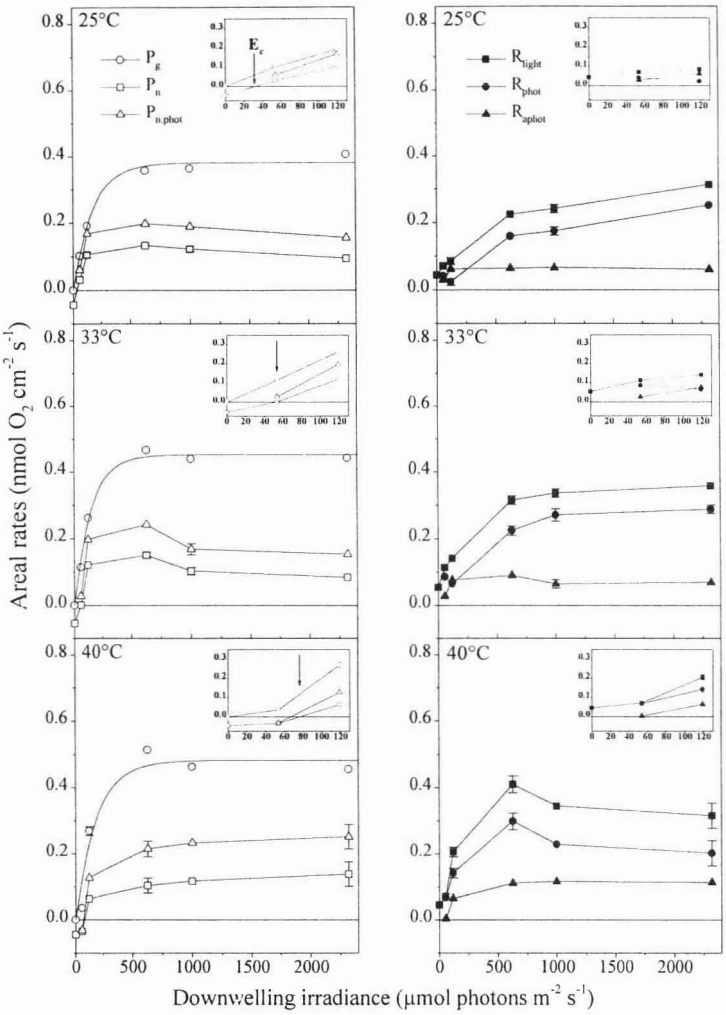

Figure 7. Areal rates of gross photosynthesis, P_g, net photosynthesis, P_n, net photosynthesis in the photic zone, $P_{n,phot}$ (left panel), and areal rates of total O_2 consumption, R_{light}, O_2 consumption in the photic zone, R_{phot}, and in the aphotic zone, R_{aphot}, (right panel) vs. downwelling irradiance at 25°C, 33°C and 40°C. Areal rates of gross photosynthesis were fitted (solid line) to an exponential function (Webb et al. 1974). Areal rates at irradiances below 120 µmol photons m^{-2} s^{-1} are shown in more detail within the graph insets.

Oxygen consumption versus irradiance at 3 experimental temperatures

Areal rates of total O_2 consumption in the mat, R_{light}, increased at each temperature with irradiance up to 626 µmol photons m^{-2} s^{-1} (Fig. 7, right panel). At higher irradiances, R_{light} increased further (25°C) or approached saturation (33°C), while at 40°C R_{light} decreased at

irradiances above 626 µmol photons m^{-2} s^{-1}. Areal rates of O_2 consumption in the photic zone, R_{phot}, showed in general a similar trend, but decreased between 54 and 119 µmol photons m^{-2} s^{-1} at 25°C and 33°C. Rates of O_2 consumption in the aphotic zone, R_{aphot}, initially increased with irradiance at each temperature, but were almost invariant at high irradiances as compared to R_{light} and R_{phot}. At high irradiances, R_{phot} was always higher than R_{aphot} and thus mainly contributed to R_{light}.

At each temperature, both R_{light} and R_{phot} increased with P_g until gross photosynthesis was saturated (Fig. 8). R_{aphot} showed a less pronounced correlation with gross photosynthesis.

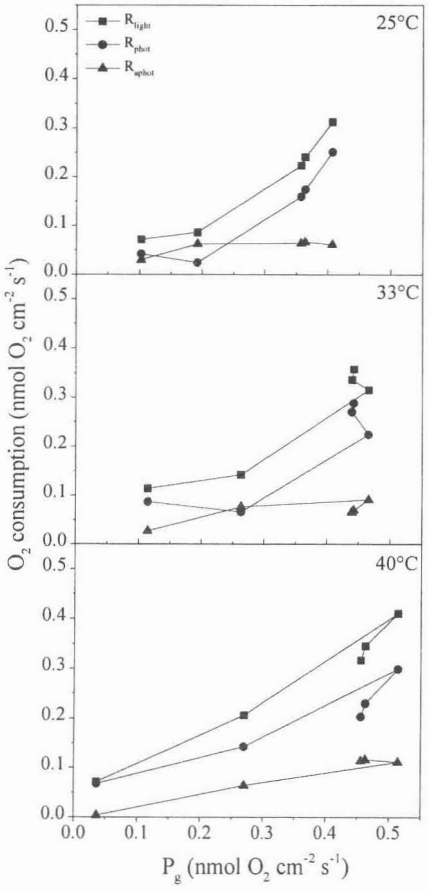

Figure 8. Areal rates of O_2 consumption in the photic zone, R_{phot}, in the aphotic zone, R_{aphot}, and total O_2 consumption in the light incubated mat, R_{light}, vs. areal rates of gross photosynthesis, P_g, at 25°C, 33°C and 40°C. At each temperature, the succession of the symbols indicates the rates at increasing irradiances.

Effect of temperature and irradiance on O_2 turnover

Areal rates of dark O_2 consumption, R_{dark}, showed no clear trend with temperature (Fig. 9A). At all irradiances, R_{light} was higher than R_{dark} at corresponding temperatures.

At 54 µmol photons m^{-2} s^{-1} (Fig. 9B), temperature had a significant effect on the balance between photosynthesis and O_2 consumption. Both gross photosynthesis, P_g, and total O_2 consumption, R_{light}, increased with temperature from 25°C to 33°C and then decreased again at 40°C. Net photosynthesis, P_n, decreased with temperature. At 25°C, R_{light} amounted to 70% of P_g, whereas at 33°C photosynthetic O_2 production was almost balanced by O_2 consumption (99% of P_g). At 40°C, O_2 consumption exceeded photosynthetic O_2 production (197% of P_g), leading to an import of O_2 across the mat-water interface, which almost equaled the O_2 supply by photosynthesis (97% of P_g). Relative to P_g, R_{phot} strongly increased with temperature from 41% at 25°C to 187% at 40°C. Both absolute and relative rates of R_{aphot} and P_n decreased with temperature.

At 119 and 626 µmol photons m^{-2} s^{-1} (Fig. 9 C, D), P_g as well as R_{phot} and R_{light} increased with temperature. At 25°C, 55-37% of the photosynthetically produced O_2 diffused out of the mat, whereas the remaining 45-63% were consumed within the mat. At higher temperatures, the relative O_2 export across the mat-water interface, P_n, decreased with temperature due to increased O_2 consumption within the mat. Relative to P_g, R_{aphot} decreased (119 µmol photons m^{-2} s^{-1}) or increased (626 µmol photons m^{-2} s^{-1}) with temperature.

At 1000 and 2319 µmol photons m^{-2} s^{-1} (Fig. 9 E, F), similar trends were observed. However, the percentage of the produced O_2 which was consumed within the mat decreased at 40°C. R_{aphot} increased between 33°C and 40°C. Although P_g was highest at 40°C, R_{phot} decreased so strong that even the increased rates of R_{aphot} could not compensate for the decrease, and thus the relative O_2 consumption within the mat decreased, resulting in an increased O_2 export across the mat-water interface, i.e. an increase of net photosynthesis.

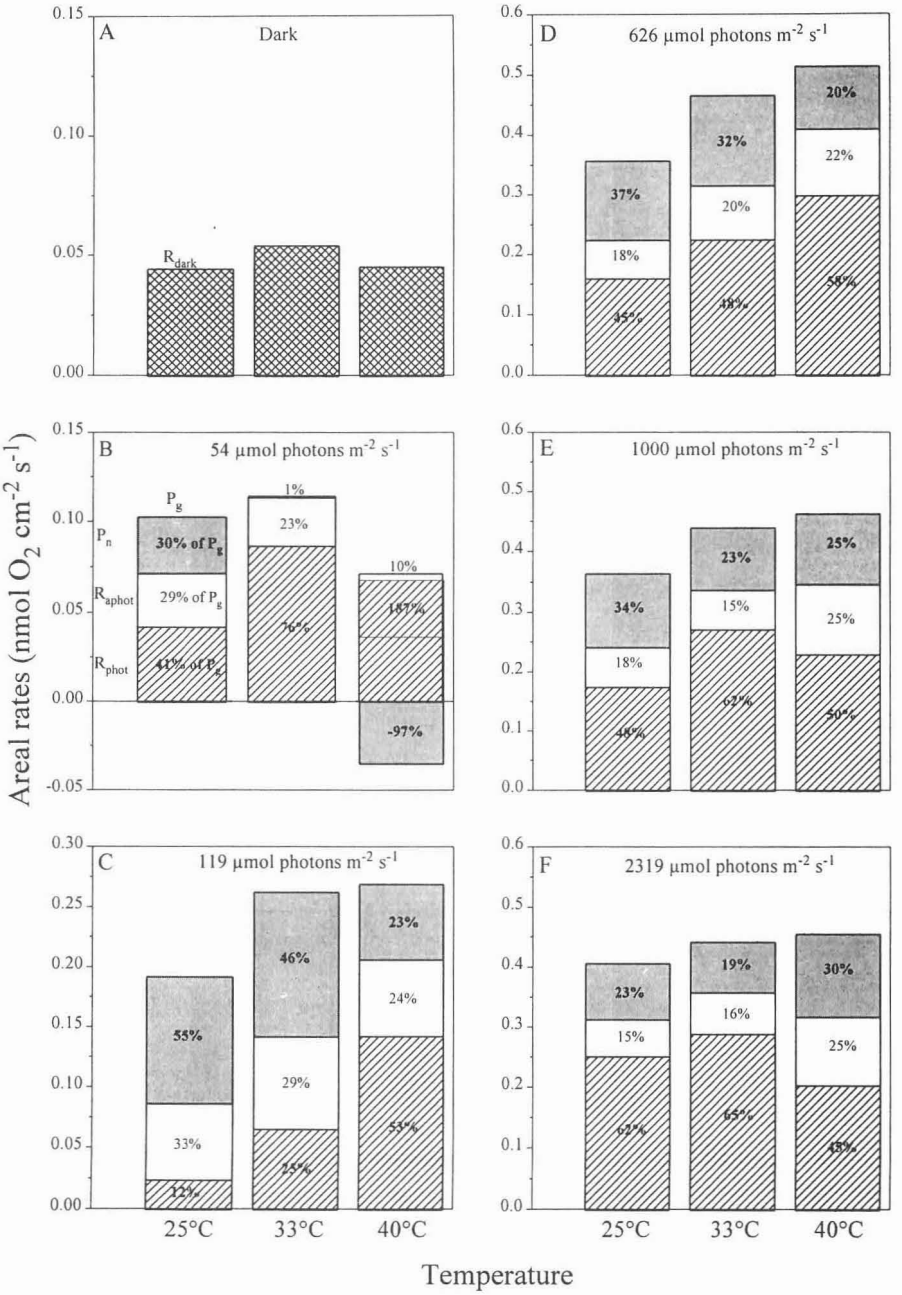

Figure 9. Areal rates of dark O_2 consumption (R_{dark}) vs. temperature (A), and areal rates of gross and net photosynthesis (P_g, P_n) and of O_2 consumption in the photic and in the aphotic zone (R_{phot}, R_{aphot}) vs. temperature at 54 (B), 119 (C), 626 (D), 1000 (E), and 2319 µmol photons m^{-2} s^{-1} (F), respectively. Total O_2 consumption, R_{light}, is represented by the sum of R_{phot} and R_{aphot}. Areal rates of P_n, R_{phot} and R_{aphot} are also expressed relative to P_g (numbers in the corresponding zones of the columns). Note the different scales.

DISCUSSION

Temperature and diffusive boundary layer effects on O_2 fluxes

Our data showed a temperature-induced increase of the O_2 dynamics on the mat surface and of the fluxes across the mat-water interface. In highly active communities, the diffusive boundary layer (DBL) poses a mass-transfer resistance and thus limits the O_2 flux across the solid-water interface (Jørgensen and Revsbech 1985; Jørgensen and Des Marais 1990; Kühl and Jørgensen 1992a; Kühl et al. 1996). The thickness of the DBL is influenced by the hydrodynamic conditions (e.g. flow velocity) and the roughness (topography) of the mat (Jørgensen and Revsbech 1985; Jørgensen and Des Marais 1990).

Temperature increases the diffusive O_2 transport through the DBL, since the diffusion coefficient of O_2 increases, and theoretically the DBL thickness decreases with temperature (Jørgensen and Revsbech 1985). This is, however, partly counterbalanced by a decreased O_2 solubility at higher temperature. Thus, the effect of temperature on the O_2 exchange across the mat-water interface is not only determined by temperature-induced changes of biological activity, but also by temperature effects on the physical parameters influencing the O_2 flux across the mat-water interface.

The presence of a microsensor above the mat induces a local compression of the DBL (Glud et al. 1994). This effect is most pronounced for smooth surface topographies and seems to be alleviated in heterogeneous phototrophic mats (Lorenzen et al. 1995). The same authors conclude that the microsensor induced DBL compression can be treated as being equivalent to measuring at a higher local flow velocity, as long as the microsensor is kept near to the mat surface for long enough periods to allow for steady state conditions to establish. The exact mechanism behind the DBL compression and whether it has a temperature dependent component, e.g. due to changes in fluid viscosity and density, awaits further investigation.

In the dark incubated mat, the O_2 flux towards the mat surface, i.e. dark O_2 consumption R_{dark}, was enhanced by increasing temperatures (Fig. 2), which amounted to an increase of 102% between 15°C and 45°C. The O_2 diffusion coefficient increased by 99% and the O_2 solubility decreased by 27%. Theoretically, the effective thickness of the DBL, Z_δ, should decrease by 24% between 15°C and 45°C, as estimated by the equation for the calculation

of Z_δ for flow over a flat plate (Jørgensen and Revsbech 1985; Vogel 1989):

$$Z_\delta = 5\sqrt{\frac{x\mu}{U\rho}} \qquad (10)$$

where x is the distance from the leading edge of the plate, U is the flow velocity, μ is the dynamic viscosity and ρ is the density of the liquid. The theoretical decrease of Z_δ with temperature was calculated from eq. 10, using Z_δ determined from the measured O_2 profile at 15°C (280 μm) with the temperature dependent changes of μ and ρ (Riley and Skirrow 1975; Millero and Poisson 1981).

With these values, we would expect an increase of the O_2 flux by 91% between 15°C and 45°C, as estimated from the equation (Jørgensen and Revsbech 1985):

$$J = D * (\Delta O_2)/Z_\delta \qquad (11)$$

where ΔO_2 is the difference between the O_2 concentration in the bulk water and at the mat surface, which was determined from the dark O_2 profile at 15°C.

However, we cannot differentiate clearly between the contribution of temperature-induced changes of biological activity and of physical parameters to the measured changes of R_{dark}. In our data, Z_δ showed an increasing trend with temperature, as determined from measured dark O_2 profiles, with a slope of increase of 76 μm (27%) per 30°C temperature increase. This points to a temperature dependent change in surface roughness, e.g. due to migration of microbes, which leads to a thicker DBL.

We found a relatively low Q_{10} value of 1.3 for dark O_2 consumption. At elevated temperatures, enhanced O_2 consumption reduced O_2 penetration to the uppermost 0.1-0.2 mm of the mat (Fig. 1). Since Z_δ increased slightly with temperature, the total O_2 consumption of the mat was apparently limited by the diffusive O_2 supply through the DBL. The low temperature dependence of R_{dark} can thus be explained by the constraints on mass transfer imposed by the DBL at all experimental temperatures. A similar mechanism was postulated by Thamdrup et al. (1998).

R_{dark} includes both O_2 consumption due to aerobic heterotrophic respiration and due to oxidation of reduced inorganic compounds like sulfide. Temperature stimulates both

processes directly, and sulfide oxidation could have been further enhanced by an increased sulfide flux towards the mat surface, as sulfate reduction in hypersaline mats is known to increase with temperature (Skyring et al. 1983; Canfield and Des Marais 1991; Canfield and Des Marais 1993; Jørgensen 1994). In another study, we quantified the temperature-induced increase of net sulfide production/consumption rates in a Solar Lake mat sampled during the winter period (November 1996) (Wieland and Kühl 1999). In that mat, a significant stimulation of both sulfate reduction and sulfide oxidation was observed with increasing temperature, and an increasing amount of O_2 consumption at elevated temperature was due to sulfide oxidation. However, both structure and microbial composition of the surface layer differed from the mat investigated in the present study and we can only speculate on the role of sulfide in the present study.

The temperature-induced changes of net photosynthesis, P_n, represent the combined effect of temperature on the mass transfer resistance imposed by the DBL, and on gross photosynthesis and O_2 consumption within the mat. Net photosynthesis at 2162 µmol photons m^{-2} s^{-1} increased with temperature and reached an optimum at 40°C (Fig. 2A). Thus, net photosynthetic activity was highest in the temperature range around the observed *in situ* temperature. We calculated a Q_{10} of 2.8 for P_n in the temperature range from 20°C to 30°C, which is within the range of reported values for light saturated photosynthesis (Davison 1991). Temperature had also a significant effect on the O_2 dynamics on the mat surface as measured by experimental light-dark shifts (Fig. 3). This increase in O_2 dynamics can be explained by increasing gross photosynthetic activity as well as by increasing O_2 consumption. The temperature-enhanced rates of gross photosynthesis at the mat surface, with a Q_{10} of 3.1 (25°C-35°C), indicate that light-saturated gross photosynthesis was regulated by temperature sensitive processes involved in carbon assimilation. The decrease of gross photosynthesis at the mat surface at 45°C was probably due to the combined inhibitory effect of high irradiance and temperature, which may have also led to the decrease of net photosynthesis (Fig. 2, see also above).

Regulation of photosynthesis by irradiance and temperature

In microbial mats and other densely populated phototrophic communities, light is strongly attenuated due to scattering and absorption by phototrophic organisms resulting in a steep light gradient within the mat. The spectral composition of light is changing within the

community due to selective absorbance of light qualities by various photosynthetic pigments (Jørgensen and Des Marais 1988; Kühl and Jørgensen 1992b; Lassen et al. 1992; Kühl et al. 1994). Light scattering can cause locally increased light intensities near the mat surface (e.g. Jørgensen and Des Marais 1988). Increasing surface irradiance increases light penetration and activates photosynthesis in deeper, light-limited parts of the mat, resulting in a deepening of the photic zone. However, many cyanobacteria are able to migrate within the mat and can thus position themselves at depths where favorable conditions prevail (Castenholz et al. 1991; Garcia-Pichel et al. 1994; Kruschel and Castenholz 1998), i.e. upward migration towards the mat surface at low irradiances and downward migration at high inhibitory irradiances. Furthermore, the zonation and activity of aerobic heterotrophic organisms may also influence the photosynthetic response, e.g. by alleviating inorganic carbon limitation at high photosynthetic rates (Canfield and Des Marais 1993; Kühl et al. 1996). The P vs. E_d curve thus represents the depth-integrated response of the phototrophic community to increasing irradiances, including migration events, light intensity induced changes of photosynthetic activity, increases in the thickness of the photic zone and changes of photosynthetic activity in response to varying chemical gradients and heterotrophic activities.

The initial slope, α, of the P vs. E_d curve is determined by light-harvesting efficiency and photosynthetic energy conversion efficiency (Henley 1993). α can be affected by temperature, since both temperature independent (photochemical reactions, light absorption, excitation energy transfer) and temperature sensitive processes (photophosphorylation, electron transport, plastoquinone diffusion) are associated with photosynthesis (Raven and Geider 1988; Davison 1991). Above a certain irradiance, E_k, photosynthesis starts to saturate and approaches a maximal photosynthesis rate, P_m. Light-saturated photosynthesis is primarily limited by carbon metabolism, including enzymatic reactions, diffusion and transport processes, and is thus inherently sensitive to temperature (Davison 1991; Henley 1993).

In the Solar Lake mat, maximal photosynthesis at light saturation, P_m, increased with temperature (Fig. 7), indicating that temperature stimulated processes involved in carbon assimilation. The initial slope of the P vs. E_d curves and E_k did not show a clear trend with temperature. The temperature optimum of light-saturated photosynthesis was apparently around or at 40°C (Fig. 9), i.e. slightly above the *in situ* temperature. Rasmussen et al.

(1983) found that *in situ* temperatures were below the experimental optimum temperature for potential photosynthesis in a coastal sediment.

No significant reduction of gross photosynthesis occurred at high irradiances above 626 µmol photons m^{-2} s^{-1} (Fig. 7). The phototrophic community thus seemed to be high light adapted. Revsbech et al. (1983) did not detect an overall photoinhibition, i.e. reduction of gross photosynthesis, in a Solar Lake mat with 1670 µmol photons m^{-2} s^{-1} of sunlight. In our study, volumetric gross photosynthetic rates at the mat surface decreased at high irradiances (Fig. 6), indicating a partial photoinhibition of the phototrophic community in the surface layer of the mat (see also Kühl et al. 1997). If this reduction was caused only by photoinhibition can, however, not be judged since motile phototrophs can avoid photoinhibitory conditions by downward migration into the mat (Bebout and Garcia-Pichel 1995). Migration can be implied by the increasing depth, where the maximal volumetric gross photosynthesis rate of the subsurface photosynthesis peak occurred at high irradiances (Fig. 6). The reduced rates in the surface layer were apparently compensated by the broadening of the photic zone and increasing rates in deeper layers due to increased light penetration.

Except at 54 µmol photons m^{-2} s^{-1}, P_g was stimulated by increasing temperatures at each light condition (Fig. 9), indicating that gross photosynthesis was also sensitive to temperature at subsaturating irradiances. At 54 µmol photons m^{-2} s^{-1}, P_g and the thickness of the photic zone strongly decreased at 40°C (Figs. 5 and 9), possibly since cyanobacteria switched to an alternative mode of metabolism. Oxygen was almost completely consumed within the photic zone of the mat and the oxic-anoxic interface was close to the lower boundary of the photic zone (Fig. 5). Temperature-enhanced sulfide production (Skyring et al. 1983; Canfield and Des Marais 1991; Canfield and Des Marais 1993; Jørgensen 1994; Wieland and Kühl 1999) could have led to a penetration of sulfide into the cyanobacterial layer of the mat at 40°C. Thus, the reduction of the (oxygenic) photic zone and probably also the reduction of gross photosynthesis could have been due to cyanobacterial anoxygenic photosynthesis (Garlick et al. 1977; Cohen et al. 1986; Jørgensen et al. 1986; de Wit and van Gemerden 1987) or sulfide-inhibition of oxygenic photosynthesis driven by an increased sulfide availability at elevated temperatures. We can also not exclude that some oxygenic gross photosynthesis occurred in the apparent anoxic layer, where

photosynthetically produced O_2 was immediately consumed and, therefore, not measurable with O_2 microelectrodes (see also Castenholz et al. 1991).

Net photosynthesis and the total O_2 flux out of the photic zone showed, except at 40°C, a decreasing trend at irradiances above 626 µmol photons m^{-2} s^{-1} (Fig. 7), indicating an increasing internal O_2 cycling within the mat (see also below). At the compensation irradiance, E_c, gross photosynthesis is balanced by O_2 consumption and thus no net O_2 exchange occurs across the mat-water interface. The compensation irradiance increased with temperature, as O_2 consumption was strongly increased relative to gross photosynthesis. Consequently, higher irradiances were required to turn the mat into a net autotrophic community at elevated temperatures. Increasing compensation irradiances with temperature were also found for the brown alga *Laminaria saccharina* (Davison 1991), and for a temperate hypersaline microbial mat from the Ebro Delta, Spain (Epping and Kühl 1999).

Regulation of oxygen consumption by irradiance and temperature

Total O_2 consumption in the mat increased with irradiance. Only at 40°C did R_{light} decrease at irradiances above 626 µmol photons m^{-2} s^{-1} (Fig. 7). In the light, O_2 consumption occurs both in the photic and in the aphotic zone of the mat. In the aphotic zone of the mat, O_2 was consumed by aerobic respiration and sulfide oxidation. Oxygen consumption in the aphotic zone, R_{aphot}, did not significantly change with irradiance (Fig. 7) and was apparently not directly controlled by photosynthesis (Fig. 8). At 40°C, R_{aphot} was controlled at low irradiances by the rates of O_2 consumption in the photic zone and since the latter were controlled by photosynthesis, R_{aphot} also showed an indirect initial increase with gross photosynthesis (Fig. 8). Enhanced aerobic sulfide oxidation due to temperature-enhanced sulfide production could have caused the significant reduction of the aphotic zone observed at 40°C (see also Wieland and Kühl 1999).

In the photic zone, both heterotrophic and phototrophic microorganisms can participate in O_2 consumption. Oxygen consuming processes associated with the phototrophic organisms include pseudocyclic electron transport (Mehler reaction), respiration and photorespiration. In the Mehler reaction, O_2 instead of $NADP^+$ is the terminal electron acceptor for (non-cyclic) photosynthetic electron transport, leading to the formation of hydrogen peroxide (Beardall and Raven 1990). In cyanobacteria, O_2 consumption due to

the Mehler reaction can increase significantly at high irradiances, where carbon assimilation gets saturated and thus $NADP^+$ gets limited relative to the rate of non-cyclic photosynthetic electron transport (Kana 1992). An increased O_2 consumption due to the Mehler reaction can also occur during e.g. active transport of dissolved inorganic carbon (Miller et al. 1988). However, only if the produced H_2O_2 is not or at least not completely detoxified by catalase, a net O_2 consumption due to the Mehler reaction would occur (Beardall and Raven 1990). Since catalase activity is inhibited by light (Butow et al. 1994), it seems likely that O_2 consumption due to the Mehler reaction could have occurred in the light incubated mat at high irradiances.

Photorespiration, i.e. O_2 consumption due to the oxygenase activity of ribulose-1,5-bisphosphate carboxylase oxygenase (Beardall and Raven 1990), is thought to be suppressed in cyanobacteria due to their efficient inorganic carbon concentrating mechanisms (Colman 1989). Some marine diatoms can also use bicarbonate (which is converted to CO_2) as an inorganic carbon source for photosynthesis (Korb et al. 1997), but photorespiration was indicated in diatom-dominated freshwater biofilms (Glud et al. 1992) and in an artificially grown diatom biofilm (Jensen and Revsbech 1989). Thus, photorespiration in the Solar Lake microbial mat cannot be completely excluded, especially under conditions where high O_2 concentrations prevailed in the mat (Fig. 5).

Photosynthates released during photosynthesis by the phototrophic community can serve as substrates for heterotrophic bacteria and therefore stimulate aerobic respiration. In a hot spring cyanobacterial mat, the production and excretion of photosynthates, mainly glycolate, was shown by Bateson and Ward (1988). An uptake and utilization of excreted photosynthates by heterotrophs is also indicated in other communities (Haack and McFeters 1982; Bateson and Ward 1988; Neely and Wetzel 1995). Furthermore, a close coupling of photosynthesis and heterotrophic respiration was suggested for a hypersaline microbial mat (Canfield and Des Marais 1993) and for an epilithic cyanobacterial biofilm (Kühl et al. 1996). Thus, increasing gross photosynthesis could have led to an increasing release of photosynthate, stimulating aerobic respiration in the photic zone of the Solar Lake mat.

Oxygen consumption in the photic zone of the mat, R_{phot}, generally increased with irradiance and temperature (Figs. 7 and 9) and was mainly controlled by gross photosynthesis (Fig. 8). However, some additional factors seem to have controlled O_2

consumption in the photic zone at low and high irradiances. R_{phot} (in % of P_g) and volumetric rates of O_2 consumption in the photic zone decreased at each incubation temperature between 54 and 119 µmol photons m^{-2} s^{-1} (Table 1, Fig. 9). Thus, at 54 µmol photons m^{-2} s^{-1}, R_{phot} must have been stimulated by other processes than gross photosynthesis; especially at 40°C, where R_{phot} amounted to 187 % of P_g (Fig. 9 B).

Table 1: Volumetric rates of O_2 consumption in the photic zone R_{phot} at experimental irradiances and temperatures

E_d (PAR) µmol photons m^{-2} s^{-1}	R_{phot} (25°C) nmol O_2 cm^{-3} s^{-1}	R_{phot} (33°C) nmol O_2 cm^{-3} s^{-1}	R_{phot} (40°C) nmol O_2 cm^{-3} s^{-1}
54	0.25	0.58	0.97
119	0.14	0.44	0.89
626	0.67	1.07	1.30
1000	0.70	1.13	0.96
2319	0.97	1.15	0.85

Due to the limited O_2 penetration during darkness, cyanobacteria must have switched to an alternative mode of metabolism than aerobic respiration and/or may have migrated towards the mat surface. Fermentation under dark anaerobic conditions was demonstrated in several cyanobacteria (Oren and Shilo 1979; Heyer et al. 1989; Moezelaar et al. 1996) and in hot spring mats (Nold and Ward 1996). Hence, accumulated fermentation products could have stimulated heterotrophic respiration at 54 µmol photons m^{-2} s^{-1}. Since this effect was restricted to R_{phot}, and the thickness of the photic zone did not increase as E_d (PAR) was increased from 54 to 119 µmol photons m^{-2} s^{-1} at 25°C and 33°C, we speculate that cyanobacteria migrated towards the mat surface during darkness and remained there at low irradiances. Accumulated fermentation products within this zone may have fueled aerobic respiration when the light was turned on and photosynthesis led to a sufficient O_2 supply.

Also at high irradiance, some additional temperature sensitive processes must have influenced O_2 consumption in the photic zone. At 33°C, R_{phot} increased slightly further at high irradiances although photosynthesis was saturated. At 40°C, R_{phot} decreased at irradiances above 626 µmol photons m^{-2} s^{-1} (Fig. 8). Furthermore, R_{phot} decreased at 40°C as compared to the lower temperatures, which was independent of gross photosynthesis, since P_g increased with temperature (Fig. 9 E, F). This excludes a deleterious effect of the

combination of elevated temperatures and irradiances, since the phototrophic population should have then also been affected. Regulating mechanisms, like e.g. the release of photosynthates, may have changed at high irradiances in response to temperature, but presently we cannot clearly point to a certain mechanism.

Summary/Conclusions

In summary, O_2 consumption in the photic zone was coupled to photosynthesis and contributed significantly to the total O_2 consumption of the microbial mat in the light. Such a coupling can be explained via several possible mechanisms, like photorespiration, the Mehler reaction and the turnover of excreted photosynthates. At moderate irradiances, temperature clearly increased the percentage of the photosynthetically produced O_2 which was consumed within the mat. Thus, elevated temperatures increase the light requirement to turn the mat into a net autotrophic community, as estimated from the O_2 budget. We can, however, not exclude that photosynthetic CO_2 fixation and thus net primary production was underestimated due to the possibility of anoxygenic photosynthesis. Although we suggest that temperature was the main direct factor that stimulated O_2 consumption, elevated temperatures could have also led to an increased release of photosynthates, additionally stimulating O_2 consumption in the photic zone. The response of photosynthesis demonstrates an adaptation of the phototrophic community to high irradiances and an apparent optimum temperature of photosynthesis slightly above the *in situ* temperature.

Dark O_2 consumption in hypersaline mats is strongly regulated by the mass transfer constraints imposed by the diffusive boundary layer. Temperature-enhanced sulfate reduction can indirectly lead to a significant enhancement of dark O_2 consumption and O_2 consumption in the aphotic zone of the illuminated mat due to increased sulfide oxidation. In the light the mass transfer constraints on oxygen availability are alleviated and we have shown a pronounced coupling of O_2 production and consumption within the photic zone of the illuminated mat. This coupling is stimulated by irradiance as well as by temperature.

Based on our findings on O_2 turnover, we speculate that the carbon turnover is characterized by a similar close coupling between autotrophs and heterotrophs, which is affected significantly by irradiance and temperature. Such a mechanism has important

implications for the way photosynthesis rates are estimated. Traditionally, O_2 consumption in dark incubations is assumed representative for O_2 consumption in the light, and gross O_2 production is estimated by summing net O_2 production in the light with dark O_2 consumption (Geider and Osborne 1992). The use of this approach would significantly underestimate gross photosynthesis in microbial mats, where light stimulated O_2 consumption takes place. Such an underestimation would be even more pronounced at elevated temperature and/or high irradiance.

ACKNOWLEDGEMENTS

We acknowledge the financial support by the Max-Planck-Society and the Red Sea Program on Marine Sciences, Project E: Microbial activities in marine interfaces controlling sediment-water fluxes, financed by the German Ministry for Research and Development (BMBF). M.K. acknowledges the support by the Danish Natural Science Research Council. We thank Gaby Eickert, Anja Eggers and Vera Hübner for the construction of the microsensors. The Interuniversity Institute in Eilat (Israel) is thanked for providing laboratory facilities. Yehuda Cohen is thanked for his hospitality, inspiration, and for arranging the logistics of the Solar Lake field trip. The Egyptian authorities are thanked for their allowance to work at Solar Lake.

REFERENCES

Amann R, Kühl M (1998). *In situ* methods for assessment of microorganisms and their activities. Curr Opin Microbiol 1:352-358

Barranguet C, Kromkamp J, Peene J (1998). Factors controlling primary production and photosynthetic characteristics of intertidal microphytobenthos. Mar Ecol Prog Ser 173:117-126

Bateson MM, Ward DM (1988). Photoexcretion and fate of glycolate in a hot spring cyanobacterial mat. Appl Environ Microbiol 54:1738-1743

Beardall J, Raven JA (1990). Pathways and mechanisms of respiration in microalgae. Mar Microb Food Webs 4(1):7-30

Bebout BM, Garcia-Pichel F (1995). UV B-induced vertical migrations of cyanobacteria in a microbial mat. Appl Environ Microbiol 61(12):4215-4222

Blanchard GF, Guarini J-M, Richard P, Gros P, Mornet F (1996). Quantifying the short-term temperature effect on light-saturated photosynthesis on intertidal microphytobenthos. Mar Ecol Prog Ser 134:309-313

Broecker WS, Peng T-H (1974). Gas exchange rates between air and sea. Tellus 26:21-35

Butow B, Wynne D, Tel-Or E (1994). Response of catalase activity to environmental stress in the freshwater dinoflagellate *Peridinium gatunense*. J Phycol 30:17-22

Cadée GC, Hegeman J (1974). Primary production of the benthic microflora living on tidal flats in the Dutch Wadden Sea. Neth J Sea Res 8:260-291

Canfield DE, Des Marais DJ (1991). Aerobic sulfate reduction in microbial mats. Science 251:1471-1473

Canfield DE, Des Marais DJ (1993). Biogeochemical cycles of carbon, sulfur, and free oxygen in a microbial mat. Geochim Cosmochim Acta 57:3971-3984

Castenholz RW, Jørgensen BB, D'Amelio ED, Bauld J (1991). Photosynthetic and behavioral versatility of the cyanobacterium *Oscillatoria boryana* in a sulfide-rich microbial mat. FEMS Microbiol Ecol 86:43-58

Cohen Y, Jørgensen BB, Revsbech NP, Poplawski R (1986). Adaptation to hydrogen sulfide of oxygenic and anoxygenic photosynthesis among cyanobacteria. Appl Environ Microbiol 51(2):398-407

Cohen Y, Krumbein WE, Goldberg M, Shilo M (1977). Solar Lake (Sinai). 1. Physical and chemical limnology. Limnol Oceanogr 22(4):597-608

Colman B (1989). Photosynthetic carbon assimilation and the suppression of photorespiration in the cyanobacteria. Aquat Bot 34:211-231

Davison IR (1991). Environmental effects on algal photosynthesis: temperature. J Phycol 27:2-8

de Wit R, van Gemerden H (1987). Oxidation of sulfide to thiosulfate by *Microcoleus chtonoplastes*. FEMS Microbiol Ecol 45:7-13

Epping EHG, Jørgensen BB (1996). Light-enhanced oxygen respiration in benthic phototrophic communities. Mar Ecol Prog Ser 139:193-203

Epping EHG, Kühl M (1999). Short-term effects of temperature and irradiance on photosynthesis and oxygen consumption in a microbial mat. submitted to J Phycol

Fenchel T (1998). Formation of laminated cyanobacterial mats in the absence of benthic fauna. Aquat Microb Ecol 14:235-240

Garcia-Pichel F, Mechling M, Castenholz RW (1994). Diel migrations of microorganisms within a benthic, hypersaline mat community. Appl Environ Microbiol 60(5):1500-1511

Garcia-Pichel F, Nübel U, Muyzer G (1998). The phylogeny of unicellular, extremely halotolerant cyanobacteria. Arch Microbiol 169:469-482

Garlick S, Oren A, Padan E (1977). Occurence of facultative anoxygenic photosynthesis among filamentous and unicellular cyanobacteria. J Bacteriol 129(2):623-629

Geider RJ, Osborne BA (1992). Algal photosynthesis: the measurement of algal gas exchange. Chapman and Hall, New York.

Glud RN, Gundersen JK, Revsbech NP, Jørgensen BB (1994). Effects on the benthic diffusive boundary layer imposed by microelectrodes. Limnol Oceanogr 39:462-467

Glud RN, Ramsing NB, Revsbech NP (1992). Photosynthesis and photosynthesis-coupled respiration in natural biofilms quantified with oxygen microsensors. J Phycol 28:51-60

Grant J (1986). Sensitivity of benthic community respiration and primary production to changes in temperature and light. Mar Biol 90:299-306

Haack TK, McFeters GA (1982). Nutritional relationships among microorganisms in an epilithic biofilm community. Microb Ecol 8:115-126

Henley WJ (1993). Measurement and interpretation of photosynthetic light-response curves in algae in the context of photoinhibition and diel changes. J Phycol 29:729-739

Heyer H, Stal L, Krumbein WE (1989). Simultaneous heterolactic and acetate fermentation in the marine cyanobacterium *Oscillatoria limosa* incubated anaerobically in the dark. Arch Microbiol 151:558-564

Isaksen MF, Jørgensen BB (1996). Adaptation of psychrophilic and psychrotrophic sulfate-reducing bacteria to permanently cold marine environments. Appl Environ Microbiol 62(2):408-414

Jensen J, Revsbech NP (1989). Photosynthesis and respiration of a diatom biofilm cultured in a new gradient growth chamber. FEMS Microbiol Ecol 62:29-38

Jørgensen BB (1994). Sulfate reduction and thiosulfate transformations in a cyanobacterial mat during a diel oxygen cycle. FEMS Microbiol Ecol 13(4):303-312

Jørgensen BB, Cohen Y (1977). Solar Lake (Sinai). 5. The sulfur cycle of the benthic cyanobacterial mats. Limnol Oceanogr 22(4):657-666

Jørgensen BB, Cohen Y, Revsbech NP (1986). Transition from anoxygenic to oxygenic photosynthesis in a *Microcoleus chthonoplastes* cyanobacterial mat. Appl Environ Microbiol 51(2):408-417

Jørgensen BB, Des Marais DJ (1988). Optical properties of benthic photosynthetic communities: Fiber-optic studies of cyanobacterial mats. Limnol Oceanogr 33(1):99-113

Jørgensen BB, Des Marais DJ (1990). The diffusive boundary layer of sediments: oxygen microgradients over a microbial mat. Limnol Oceanogr 35(6):1343-1355

Jørgensen BB, Revsbech NP (1985). Diffusive boundary layers and the oxygen uptake of sediments and detritus. Limnol Oceanogr 30(1):111-122

Jørgensen BB, Revsbech NP, Blackburn TH, Cohen Y (1979). Diurnal cycle of oxygen and sulfide microgradients and microbial photosynthesis in a cyanobacterial mat sediment. Appl Environ Microbiol 38(1):46-58

Jørgensen BB, Revsbech NP, Cohen Y (1983). Photosynthesis and structure of benthic microbial mats: Microelectrode and SEM studies of four cyanobacterial communities. Limnol Oceanogr 28(6):1075-1093

Kana TM (1992). Relationship between photosynthetic oxygen cycling and carbon assimilation in *Synechococcus* WH7803 (Cyanophyta). J Phycol 28:304-308

Korb RE, Saville PJ, Johnston AM, Raven JA (1997). Sources of inorganic carbon for photosynthesis by three species of marine diatom. J Phycol 33:433-440

Krumbein WE, Cohen Y, Shilo M (1977). Solar Lake (Sinai). 4. Stromatolitic cyanobacterial mats. Limnol Oceanogr 22(4):635-656

Kruschel C, Castenholz RW (1998). The effect of solar UV and visible irradiance on the vertical movements of cyanobacteria in microbial mats of hypersaline waters. FEMS Microbiol Ecol 27:53-72

Kuenen JG, Jørgensen BB, Revsbech NP (1986). Oxygen microprofiles of trickling filter biofilms. Wat Res 20(12):1589-1598

Kühl M, Glud RN, Ploug H, Ramsing NB (1996). Microenvironmental control of photosynthesis and photosynthesis-coupled respiration in an epilithic cyanobacterial biofilm. J Phycol 32:799-812

Kühl M, Jørgensen BB (1992a). Microsensor measurements of sulfate reduction and sulfide oxidation in compact microbial communities of aerobic biofilms. Appl Environ Microbiol 58(4):1164-1174

Kühl M, Jørgensen BB (1992b). Spectral light measurements in microbenthic phototrophic communities with a fiber-optic microprobe coupled to a sensitive diode array detector. Limnol Oceanogr 37(8):1813-1823

Kühl M, Lassen C, Jørgensen BB (1994). Optical properties of microbial mats: Light measurements with fiber-optic microprobes. In: Stal LJ, Caumette P (Ed.) Microbial Mats: Structure, Development and Environmental Significance. NATO ASI Series G Vol. 35. Springer, Berlin, p 149-166

Kühl M, Lassen C, Revsbech NP (1997). A simple light meter for measurements of PAR (400 to 700 nm) with fiber-optic microprobes: application for P vs E_0 (PAR) measurements in a microbial mat. Aquat Microb Ecol 13:197-207

Lassen C, Ploug H, Jørgensen BB (1992). Microalgal photosynthesis and spectral scalar irradiance in coastal marine sediments of Limfjorden, Denmark. Limnol Oceanogr 37(4):760-772

Li Y-H, Gregory S (1974). Diffusion of ions in sea water and in deep-sea sediments. Geochim Cosmochim Acta 38:703-714

Lorenzen J, Glud RN, Revsbech NP (1995). Impact of microsensor-caused changes in diffusive boundary layer thickness on O_2 profiles and photosynthetic rates in benthic communities of microorganisms. Mar Ecol Prog Ser 119:237-241

Miller AG, Espie GS, Canvin DT (1988). Active transport of inorganic carbon increases the rate of O_2 photoreduction by the cyanobacterium *Synechococcus* UTEX 625. Plant Physiol 88:6-9

Millero FJ, Poisson A (1981). International one-atmosphere equation of state of seawater. Deep Sea Res 28:625-629

Moezelaar R, Bijvank SM, Stal LJ (1996). Fermentation and sulfur reduction in the mat-building cyanobacterium *Microcoleus chthonoplastes*. Appl Environ Microbiol 62(5):1752-1758

Neely RK, Wetzel RG (1995). Simultaneous use of ^{14}C and ^{3}H to determine autotrophic production and bacterial protein production in periphyton. Microb Ecol 30:227-237

Nold SC, Ward DM (1996). Photosynthate partitioning and fermentation in hot spring microbial mat communities. Appl Environ Microbiol 62(12):4598-4607

Oren A, Shilo M (1979). Anaerobic heterotrophic dark metabolism in the cyanobacterium *Oscillatoria limnetica*: sulfur respiration and lactate fermentation. Arch Microbiol 122:77-84

Rasmussen MB, Henriksen K, Jensen A (1983). Possible causes of temporal fluctuations in primary production of the microphytobenthos in the Danish Wadden Sea. Mar Biol 73:109-114

Raven JA, Geider RJ (1988). Temperature and algal growth. New Phytol 110:441-461

Revsbech NP (1989). An oxygen microelectrode with a guard cathode. Limnol Oceanogr 34:474-478

Revsbech NP, Jørgensen BB (1983). Photosynthesis of benthic microflora measured with high spatial resolution by the oxygen microprofile method: Capabilities and limitations of the method. Limnol Oceanogr 28(4):749-756

Revsbech NP, Jørgensen BB (1986). Microelectrodes: Their use in microbial ecology. Adv Microb Ecol 9:293-352

Revsbech NP, Jørgensen BB, Blackburn TH, Cohen Y (1983). Microelectrode studies of the photosynthesis and O_2, H_2S, and pH profiles of a microbial mat. Limnol Oceanogr 28(6):1062-1074

Revsbech NP, Jørgensen BB, Brix O (1981). Primary production of microalgae in sediments measured by oxygen microprofile, $H^{14}CO_3^-$ fixation, and oxygen exchange methods. Limnol Oceanogr 26(4):717-730

Riley JP, Skirrow G (1975). Chemical Oceanography. Academic Press, London, p 338

Sherwood JE, Stagnitti F, Kokkinn MJ, Williams WD (1991). Dissolved oxygen concentrations in hypersaline waters. Limnol Oceanogr 36(2):235-250

Skyring GW, Chambers LA, Bauld J (1983). Sulfate reduction in sediments colonized by cyanobacteria, Spencer Gulf, South Australia. Aust J Mar Freshw Res 34:359-374

Stal LJ, Caumette P (1994). Microbial Mats: Structure, Development and Environmental Significance. Springer, Berlin.

Thamdrup B, Hansen JW, Jørgensen BB (1998). Temperature dependence of aerobic respiration in a coastal sediment. FEMS Microbiol Ecol 25:189-200

Ullman WJ, Aller RC (1982). Diffusion coefficients in nearshore marine sediments. Limnol Oceanogr 27(3):552-556

van Gemerden H (1993). Microbial mats: a joint venture. Mar Geol 113:3-25

Vogel S (1989). Life in moving fluids. Princeton University Press, New Jersey.

Webb WL, Newton M, Starr D (1974). Carbon dioxide exchange of *Alnus rubra*: a mathematical model. Oecologia 17:281-291

Wieland A, Kühl M (1999). Short term temperature effects on oxygen and sulfide cycling in a hypersaline cyanobacterial mat (Solar Lake, Egypt). Mar Ecol Prog Ser, in press

Chapter 4

Fine-scale measurement of diffusivity in a microbial mat with NMR imaging

Andrea Wieland[1], Dagmar van Dusschoten[2], Lars R. Damgaard[3], Dirk de Beer[1], Michael Kühl[4] and Henk Van As[2]

[1] Max-Planck-Institute for Marine Microbiology, Microsensor Research Group
Celsiusstr. 1, D-28359 Bremen, Germany
[2] Laboratory of Molecular Physics and Wageningen NMR Centre, Wageningen University
Dreijenlaan 3, NL-6703 HA Wageningen, Netherlands
[3] Department of Microbial Ecology, Institute of Biological Sciences, University of Aarhus,
B.540 Ny Munkegade, DK-8000 Aarhus C, Denmark
[4] Marine Biological Laboratory, University of Copenhagen
Strandpromenaden 5, DK-3000 Helsingør, Denmark

Manuscript in preparation

ABSTRACT

Non-invasive ^{1}H-NMR (Nuclear Magnetic Resonance) imaging was used to investigate the diffusive properties of microbial mats in two dimensions. Pulsed Field Gradient NMR was used to acquire images of the H_2O diffusion coefficient, D_s, and multi-echo imaging NMR was used to obtain images of the water density (intra- and extracellular water) in two structurally different microbial mats sampled from Solar Lake (Egypt). We found a pronounced lateral and vertical variability of both water density and water diffusion coefficient, correlated with the laminated and heterogeneous distribution of microbial cells and exopolymers within the mats. The average water density varied from 0.5 to 0.9, while the average water diffusion coefficient ranged from 0.4 to 0.9 relative to the values obtained in the water above the mat samples. The apparent water diffusivities estimated from NMR imaging compared well to apparent O_2 diffusivities measured with a diffusivity microsensor. Analysis of measured O_2 concentration profiles with a diffusion-reaction model showed that both the magnitude of calculated rates and the depth distribution of calculated O_2 consumption/production zones changed when the observed variations of diffusivity were taken into account. With NMR imaging, diffusivity can be determined at high spatial resolution, which can resolve inherent lateral and vertical heterogeneities found in most natural benthic systems.

INTRODUCTION

Diffusion is the predominant mode of solute mass transfer between bacteria and their surroundings, and is also the major mechanism of solute transport in impermeable sediments, biofilms and microbial mats (e.g. van Gemerden 1993). Knowledge about the diffusive properties is a key information for quantification of biogeochemical processes and their regulation in benthic microbial communities (Berner 1980; Boudreau 1997).

Due to their spatio-temporal resolution and minimal disturbance, microsensors are almost ideal tools for characterizing physico-chemical microenvironments and the steep gradients of solute concentration within biofilms and sediments (Revsbech and Jørgensen 1986; Amann and Kühl 1998). From measured concentration profiles, diffusive fluxes of solutes and the depth distribution and magnitude of process rates, i.e. net production-consumption of the diffusing chemical species, can be calculated via profile analysis based on diffusion-reaction models (e.g. Revsbech et al. 1986; Nielsen et al. 1990; Rasmussen and Jørgensen 1992; Epping and Jørgensen 1996; Berg et al. 1998).

However, a precise analysis of microsensor data requests fine-scale measurements of the apparent diffusivity, D_{app}, of the solute in the system (Revsbech et al. 1986; Revsbech 1989a; Glud et al. 1995). The presence of impermeable particles causes an increase of the diffusional pathlength by steric hindrance, referred to as the geometric tortuosity θ, resulting in a lower solute diffusion coefficient in the sediment, D_s, as compared with the free solution molecular diffusion coefficient, D_o, which is expressed by (Berner 1980):

$$D_s = D_o \, \theta^{-2} \qquad (1)$$

Furthermore, in sediments the porosity (ϕ) and thus the volume available for diffusion is reduced, and therefore:

$$D_{app} = \phi \, D_o \, \theta^{-2} \qquad (2)$$

Using inert tracers or biologically inactivated sediment samples, D_s can be determined with transient methods, e.g. by following the equilibration of the system after a momentaneous concentration change in the overlaying bulk liquid (e.g. Duursma and Bosch 1970). D_s can then be calculated from the time-dependent increase of the tracer concentration at different depths of the sample, as measured with e.g. microsensors (Revsbech et al. 1986; Cronenberg and Van den Heuvel 1991; Beuling 1998).

The apparent diffusivity, D_{app}, can either be calculated from D_s if the porosity is known, or directly be determined from measured steady state concentration profiles in the sediment and Fick`s first law of diffusion: $J = D_{app}\ dC/dx$. In steady state, the flux J is constant through all layers of the matrix, and changes in the slope (dC/dx) of the profile are caused by variations of D_{app}. Also for this approach, inert tracers or biologically inactivated samples must be used, and the sample has to be equilibrated in a diffusion chamber (Revsbech 1989a; Glud et al. 1995). The latter was recently overcome by the development of a novel microsensor for determination of D_{app}, which is based on the continuous detection of the diffusion of an inert tracer gas away from the sensor tip (Revsbech et al. 1998). However, even with this diffusivity microsensor, we can only address the diffusive properties of complex natural samples from a relative limited number of point measurements.

In translucent biofilms, confocal microscopy has been used for determining diffusivity with high spatial resolution (de Beer et al. 1997). This method is, however, not directly applicable in sediments and optically dense biofilms and microbial mats.

In the present study we used an alternative approach to determine D_s at a high spatial resolution in biologically active samples by using H_2O as a tracer in combination with non-invasive ^{1}H-NMR (Nuclear Magnetic Resonance) imaging. By this method, two-dimensional distributions of the water density and the diffusion coefficient of H_2O in stratified microbial mats were obtained for the first time.

Theoretical background of NMR imaging

The theory and basis of NMR measurements is shortly described here using a classical description, which ignores the more fundamental quantum mechanical description of NMR. NMR measurements are based on the angular moment or spin of certain nuclei, e.g. ^{1}H, ^{13}C. The rotation of the charged nucleus about its axis causes a magnetic dipole moment. When a sample containing these nuclei is placed in an external magnetic field, B_o, the magnetic dipoles align in the direction of B_o, i.e. the z-direction. The angular moment of ^{1}H can only achieve two possible stable orientations relative to B_o, one tending to be parallel (low energy level) and one counter-parallel to B_o. At room temperature and thermal equilibrium, slightly more nuclear spins align parallel to B_o, resulting in a macroscopic magnetization (M_z) of the sample parallel to the magnetic field.

The application of an intense and short radio frequency (r.f.) pulse perpendicular to B_0 (90° pulse) leads to a realignment of the spins in the x,y-plane perpendicular to B_0, if the frequency of the pulse corresponds to the energy difference between both spin orientations. This NMR resonance frequency, ν_0, is depending on and characteristic for a particular nucleus at a particular B_0. The magnetization in the x,y-plane oscillates with the frequency ν_0, thereby generating an oscillating magnetic field, which is detected by the same r.f. coil which generated the 90° pulse. The initial amplitude, A_0, of the NMR signal is a measure of the density of nuclei in the sample.

The amplitude of the NMR signal decreases as a function of time as the nuclear spins return to equilibrium. This process is characterized by two relaxation time constants, T_1 (spin-lattice relaxation time) and T_2 (spin-spin relaxation time). T_1 describes the return to the equilibrium state in the direction of B_0, whereas T_2 describes the decay of the transverse magnetization $M_{x,y}$ in the x,y-plane to zero. On top of the spin-spin relaxation, which is mainly caused by magnetic dipole-dipole interactions, field inhomogeneities accelerate the dephasing of the precessing spins in the x,y-plane and all initial phase coherence is lost. The dephasing due to field inhomogeneities can be eliminated by application of a 180° pulse, which inverts the phase of the spins. This results in a refocusing of all phases at two times the time between the 90° and the 180° pulse (TE), generating a spin-echo signal at TE. This spin-echo signal is reduced in amplitude (A(TE)) by spin-spin relaxation (T_2) and can be described by:

$$A(TE) = A_0 \exp(-TE/T_2). \quad (3)$$

A succession of spin-echoes during one relaxation process is produced by using e.g. a so-called Carr-Purcell-Meiboom-Gill (CPMG) or multiple spin-echo (MSE) sequence, where additional 180° pulses at intervals of TE after the first (at TE/2) 180° pulse are applied. The curve formed by the subsequent and decreasing spin-echo amplitudes at TE_n describes the T_2 relaxation decay (Farrar and Becker 1971; Morris 1986; Van As and van Dusschoten 1997).

Molecular diffusion, i.e. random translational motion of spin carrying molecules like H_2O, can be measured if additionally pulsed field gradients (PFG) are applied (Stejskal and Tanner 1965). After the 90° pulse, two subsequent magnetic field gradient pulses G (mT/m) of duration δ (ms) are applied with one or more additional 180° pulse(s) between both gradients. The first field gradient pulse enhances dephasing of the spins in the x,y-

plane during its duration. The direction of the dephasing is reversed by the 180° pulse(s). The second gradient pulse causes a rephasing which leads, in the absence of diffusion, to a complete phase refocusing with no extra echo signal loss, since the nuclei remain at the same position and therefore experience the same magnetic field strength during both gradients. Random displacement of spin carrying molecules by diffusion leads to an incomplete phase refocusing, resulting in an attenuation of the echo amplitude. The time between the onset of both magnetic field gradient pulses Δ (ms) is the time interval where the mean square displacement of the nuclei is monitored (Stejskal and Tanner 1965; Farrar and Becker 1971). The first spin-echo after the second gradient pulse can be followed by a train of 180° pulses, creating spin-echoes at TE_n of decaying amplitude, enabling the simultaneous determination of T_2 and diffusion at a set of echo times (van Dusschoten et al. 1996). This sequence is repeated with an increasing magnitude of the magnetic field gradients during one set of experiment. The (decay of the) signal amplitude at TE can be described by:

$$A(TE,b) = A_0 * \exp(-TE/T_2) * \exp(-b\,D) \quad (4)$$

with

$$b = \gamma^2 \delta^2 G^2 (\Delta - \delta/3)$$

where γ is the gyromagnetic ratio, a constant specific for each type of nucleus, which determines the resonance frequency in a given magnet field.

So far, only non-spatially resolved NMR was described, which in the case of microbial mats is insufficient due to the macroscopic heterogeneity in the mat. By applying the same pulsed field gradients in 3 different directions in combination with r.f. pulses with limited bandwidth (soft pulses), images of slices through the sample can be achieved. An image consists of N x N, here 128 x 128, picture elements, so-called pixels. All information which has been discussed above can be obtained on a pixel by pixel basis when NMR imaging is used after the pulsed field gradients and during the complete T_2 decay.

Slice selection through a sample is achieved by using a soft, shaped r.f. pulse in the presence of a magnetic field gradient, the so-called slice selection gradient. This slice selection gradient is applied along the direction perpendicular to the desired slice, e.g. along the z-direction. The soft, shaped r.f. pulse (90°) selectively excites only spins in a narrow frequency range. Therefore, only nuclei within a certain slice at the corresponding

magnetic field strength are excited. After the pulsed field gradients for the diffusion measurements are applied, the resulting NMR signal is acquired in the presence of a so-called read gradient. The direction of this read gradient (x-direction) is perpendicular to the direction of the slice selection gradient. Along the read gradient, nuclei experience different magnetic field strengths, resulting in different, position dependent resonance frequencies of the nuclei. Thus, each position in the read gradient direction is assigned to a unique frequency, which can be retrieved by Fourier Transformation. Spatial resolution in the y-direction is obtained by a stepwise incrementing gradient pulse applied perpendicular to the other magnetic gradients. This so-called phase-encoding gradient pulse causes a phase shift which increases along the y-axis. To obtain a complete N x N image of the selected slice after Fourier Transformation, the phase-encoding gradient has to be incremented N times (e.g. Morris 1986; Moonen et al. 1990). Subsequent application of 180° pulses in combination with read gradients results in a set of images with decreasing amplitude, governed by T_2.

As mentioned above, the pulsed field gradients for the diffusion measurements are incremented during one set of experiment. Thus, a 2D data set per pixel is obtained, containing both diffusion and relaxation information, which can be described by and analyzed with eq. 4 (van Dusschoten et al. 1996). A normal PFG MSE imaging experiment consists of 128 (= N) phase-encoding steps x 8 pulsed field gradients steps x 2-8 averaging steps. To reduce the measuring time, it is also possible to individually phase-encode the multiple echoes using a pulsed field gradient turbo spin echo sequence (PFG TSE) (Scheenen et al. 1998). The application of the PFG TSE reduces the measuring time 8 to 16 times, but T_2 and A_0 information is now mixed, and therefore only diffusion information is obtained, which can be described by:

$$A(b) = A_{TE} * \exp(-b\,D) \tag{5}$$

where A_{TE} is the signal amplitude of the spin-echo at time TE. To obtain 2D images of the H_2O diffusion constants in mat samples, i.e. D_s, we used either the PFG MSE sequence or the PFG TSE sequence. Additionally, 2D images of the amplitude A_0 were acquired each time by multi-echo imaging (Edzes et al. 1998) in a separate CPMG experiment.

MATERIAL AND METHODS

A SMIS (Surrey Medical Imaging System, Guildford, Surrey, UK) Imager was used for NMR experiments. The SMIS Imager is equipped with an electromagnet (Bruker, Karlsruhe) which generates a 0.47 T magnetic field, resulting in a ^{1}H resonance frequency of 20.35 MHz. A microscopy probe (Doty Scientific Inc., Columbia, South Carolina) containing a solenoidal radio frequency coil (length and diameter 45 mm), which is surrounded by a set of actively shielded gradients, was fitted in the 0.14 m air gap of the magnet. A Plexiglas core tube of ca. 2.6 cm inner diameter containing the mat sample was positioned in the probe bore, which had a diameter of 4.5 cm and was accessible from both ends. Home-written pulse programs written in SMIS language were used.

During one set of experiment, diffusion measurements were repeated 8 times at increasing G, using either the PFG CPMG (van Dusschoten et al. 1996) or the PFG TSE sequence (Scheenen et al. 1998). The magnetic field gradients were increased up to 500 mT/m. All measurements were performed at room temperature (24-25°C). The acquired sets of images were analyzed on a pixel by pixel basis. The 2D data set per pixel (as a function of time and G) obtained from the PFG CPMG experiment was analyzed with a 2D nonlinear least square (NLLS) fitting routine based on the Marquardt-Levenberg algorithm (Press et al. 1992). Using this 2D fitting routine, the data were fitted with eq. 4, assuming that molecules within one pixel element experienced a similar physical environment (see van Dusschoten et al. 1996). The set of images obtained from the PFG TSE experiment, were analyzed by fitting the data (in each pixel) to eq. 5, using a standard 1D NLLS fitting routine based on the Marquardt-Levenberg algorithm (Press et al. 1992). The fitting routines were programmed using IDL (Interactive Data Language, Research Systems Inc., Boulder, Colorado).

Images of the amplitude A_0 were obtained in separate CPMG experiments by multi-echo imaging (Edzes et al. 1998). As in the PFG CPMG experiment, the sequence was repeated 128 times to acquire complete 2D images (see Introduction). The signal intensity in each pixel in the successive echo images was fitted as a mono-exponential decay (eq. 3) with a NLLS fitting routine (see above), and real spin-density images (A_0) were obtained by extrapolation of the amplitude images to TE = 0.

The dimensions of the acquired images are given by the field of view, i.e. the dimension for each axis in the plane, and the slice thickness, which represents the plane thickness. All images consisted of 128 x 128 pixels with a field of view of 30 mm, resulting in a resolution of 234 μm per pixel. Further details concerning the recorded number of echoes (per sequence), TE, the repetition time TR, the slice thickness, and for the diffusion measurements δ and Δ are given in the figure legends. For the diffusion measurements, the pulsed field gradients were applied perpendicular to the mat surface, which is the direction in which diffusion is measured.

Values of D_s and water density were extracted from the data matrices obtained in the different NMR experiments. Only those values of D_s in the data matrix that were greater than zero, greater than their standard deviation, with an amplitude greater than the noise level, as estimated e.g. from the region of the Plexiglas tube where no water or proton signal was observed, and lower than the values obtained in the overlaying water were used. Data that did not fulfill these criteria were sorted out and subsequently set to zero (dark black zones). Similar criteria were used to sort the data of the water density. The mat surface of the April mat (see below) was not adjusted exactly horizontally during the NMR measurements, which was corrected during data analysis. Furthermore, to mimic the situation in the flow chamber during microsensor measurements, we created a minor flow in the overlaying water during the NMR experiment, by blowing gently air over the water surface with a Pasteur pipette connected to an air pump. The obtained data of D_s and water density in the mat were normalized to the values of stagnant water within the core tube, which is, for simplicity, in the following referred to as overlaying water. During the measurements in the November mat sample (see below), we did not create a flow in the overlaying water, and values of D_s and water density in the mat were normalized to the values in the overlaying water. The PFG NMR measurements resulted in a relative low signal to noise ratio (see Results). For data analysis most of these high noise signals were not considered, which resulted in a reduction of available data for the calculation of D_s.

Mat samples. Mat samples (approximately 20 cm x 12 cm x 3 cm) were collected in April 1997 and November 1997 in the shallow (0.3-0.5 m deep) eastern part of Solar Lake (Sinai, Egypt). The temperature and salinity were 28°C and 86‰ in April and 30°C and 83‰ in November. The mat samples were transported within a few hours after sampling to the

Interuniversity Institute in Eilat (Israel), where oxygen microsensor measurements were performed in a laboratory. The 2-3 mm thick gelatinous golden brownish surface layer of the mat sample taken in April was composed of diatoms (*Navicula* sp., *Nitzschia* sp.) and unicellular cyanobacteria belonging to the *Halothece* cluster (Garcia-Pichel et al. 1998). Below this surface layer, a ca. 0.5 mm thick green layer of filamentous cyanobacteria (mainly *Microcoleus chthonoplastes*) was found. In the November sample, a ca. 0.5-1 mm thick dark green cohesive surface layer composed of filamentous cyanobacteria (mainly *Microcoleus chthonoplastes*) was found at the mat surface.

After the microsensor measurements in Eilat, the mat samples were transferred to the MPI Bremen, where they were stored for 1-3 weeks in aerated brine in light, prior to the experiments at the EU large-scale NMR facility in Wageningen (Netherlands). During this time interval, the mat samples did not undergo a significant change in structure and macroscopic appearance as compared to the mat samples in Eilat.

Oxygen microsensor measurements. Mat subsamples were taken with Plexiglas core tubes with an inner diameter of 5.0-5.6 cm (April). The core tube was fixed in a flow chamber modified from Lorenzen et al. (1995). In November, a mat subsample (approximately 5 cm x 4 cm x 2 cm) was embedded in agar (1.5% in Solar Lake water) in a similar flow chamber. A constant flow of aerated Solar Lake water above the mat surface was generated by a submersible water pump (E-Heim, Germany), connected to the flow chamber. The mat subsamples in the flow chamber were illuminated with a fiber-optic halogen light source (Schott KL 1500). The downwelling surface irradiance, E_d (PAR), was quantified with an underwater quantum irradiance meter (LiCor, USA) by replacing the flow chamber by the underwater quantum sensor, which was submerged in Solar Lake water and placed at the same distance from the light source. Measurements in November were performed at room temperature (26°C) and 957 µmol photons m^{-2} s^{-1}, whereas in April E_d (PAR) was 626 µmol photons m^{-2} s^{-1} and the water temperature was adjusted to 30°C with a heat exchanging metal coil connected to a thermostat (Julabo).

Clark-type O_2 microelectrodes (Revsbech 1989b), with outer tip diameters of <10 µm and stirring sensitivities of <1.5%, were used to measure depth profiles of O_2. The O_2 microelectrodes, connected to fast responding picoamperemeters, were fixed in a motor driven micromanipulator (Oriel, Märzhäuser). By use of a dissection microscope (Zeiss),

the microsensors were positioned on the mat surface. The measuring signals were recorded on a strip chart recorder (Servogor) and on a computer data acquisition system (Labview, National Instruments). The O_2 microelectrodes were calibrated from readings in the aerated overlaying Solar Lake water (100% air saturation) and in the anoxic part of the mat (0% oxygen). Dissolved O_2 concentrations in aerated Solar Lake brine at experimental temperatures and salinities were calculated according to Sherwood et al. (1991).

Diffusivity microsensor measurements. The apparent diffusivity, i.e. ϕD_s, was measured in a Solar Lake mat with a diffusivity microsensor (Revsbech et al. 1998) using acetylene as the tracer gas. The diffusivity microsensor had an outer tip diameter of 60 μm. The Solar Lake mat was sampled in December 1998 and was stored aerated and illuminated prior to the diffusivity microsensor measurements. The mat sample had a similar structure and composition as the mat sample from November 1997 (see above). Diffusivity microsensor measurements were performed at room temperature (24°C) in a mat subsample, taken with a Plexiglas core tube of ca. 2.6 cm inner diameter. The mat subsample was covered by stagnant artificial seawater (95‰). The apparent diffusivity in the mat was measured with 250 μm vertical depth intervals. The microsensor was calibrated from signal readings in artificial seawater of experimental temperature and salinity and from readings in 40-60 μm glass beads in which the apparent diffusivity of oxygen had previously been established (Revsbech et al. 1998). It was assumed that relative changes of apparent diffusivity between different media was identical for oxygen and acetylene. The acetylene sensor is sensitive to H_2S, which was abundant below 1-2 mm depth in the mats (data not shown). The H_2S interference was minimized by using a high (100%) acetylene concentration in the diffusivity sensor reservoir and the measured data were corrected for the remaining H_2S interference by the following procedure: H_2S concentration profiles were measured in the Solar Lake mat with a H_2S microsensor (Jeroschewski et al. 1996) and a H_2S calibration was performed on the diffusivity sensor in stagnant water of the same temperature and salinity as in the mats. During data processing, the calculated H_2S-induced signal was subtracted from the total diffusivity sensor signal before the signal was transformed into diffusivity units.

Calculations. Measured O_2 concentration profiles were analyzed with a numerical procedure for the interpretation of steady state microprofiles (Berg et al. 1998). This procedure is based on a series of least square fits to measured concentration profiles, assuming an increasing number of production and consumption zones. The fits are compared by statistical F-testing, so that the simplest production-consumption profile results that reproduces the measured concentration profiles within the chosen statistical accuracy (Berg et al. 1998). The measured steady state O_2 concentration profiles were analyzed with this procedure by assuming a constant porosity of 0.9 (Jørgensen and Cohen 1977; Jørgensen et al. 1979) and a constant D_s, which was calculated by (Ullman and Aller 1982):

$$D_s = \phi^2 D_0 \quad (6)$$

where D_0 is the free solution molecular diffusion coefficient of O_2, which was taken from Broecker and Peng (1974) and corrected for salinity and temperature (Li and Gregory 1974). Profile analysis was also done with i) the D_s depth profiles obtained from the NMR measurements and a constant porosity of 0.9 (see above), and with ii) both the D_s profiles and the profiles of water density (A_0) measured in the NMR experiments. From the profile analysis, areal rates of net O_2 production and consumption in the mats were calculated by multiplying the calculated (volumetric) rates by the thickness of the reaction zone and summing the different rates of production and consumption. The total areal net O_2 production rate in the light incubated mats was calculated as the difference between the sum of net O_2 production and consumption.

RESULTS

NMR and diffusivity measurements

The NMR imaging experiments showed a pronounced heterogeneity of D_s and water density and, therefore, of diffusivity in the microbial mats (Figs. 1 and 3). Despite a relative low signal to noise ratio of the image of D_s in the November mat (Fig. 3, upper image), alternating strata of high and low D_s and water density were found with depth in both mats. As D_s and water density covaried, a similar stratification of low and high apparent diffusivity was found (Fig. 5).

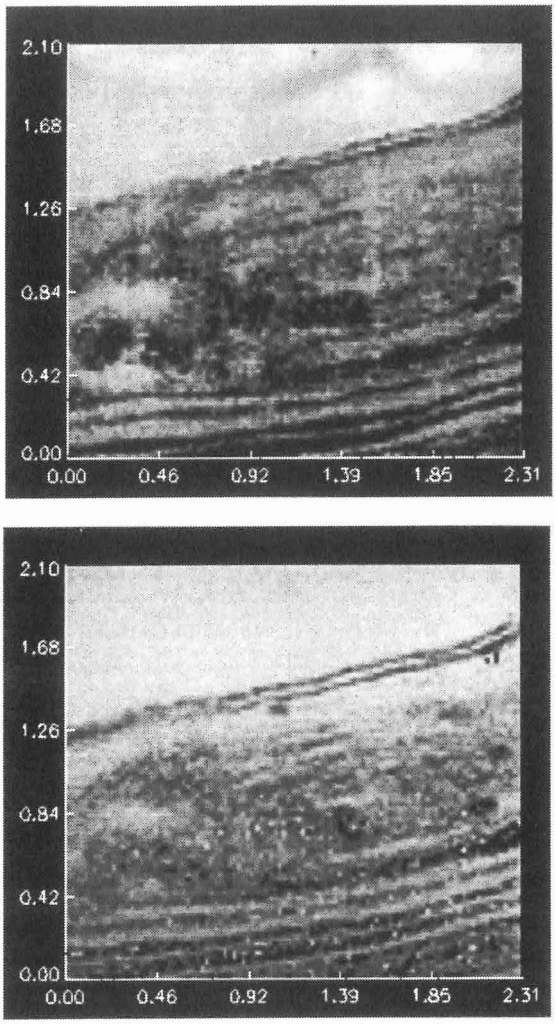

Figure 1. Image of the H_2O diffusion constants in the mat from April (upper image) measured with the PFG CPMG sequence. Parameters: Δ = 16.6 ms, δ = 3.5 ms, TE = 21 + n*6.6 ms (n = 0-15), TR = 3.5 s, 16 echoes, slice thickness = 2.5 mm. Image of the amplitude A_0 (water density, lower image) measured with the CPMG sequence. Parameters: TE = 21 + n*4.2 ms, TR = 9 s, 24 echoes, slice thickness = 2.5 mm. The framing scale indicates the corresponding size (cm) of the extracted and 3 times enlarged images. The water density and diffusion coefficients are proportional to the brightness of the pixels in the images.

In the gelatinous mat sampled in April, a broad zone of relative high water density and D_s was present in the upper 4 mm (Fig. 2, 5 A-B). In deeper mat layers the water density and D_s generally decreased (Fig. 5 A-B), while in some areas of the mat a pattern of alternating high and low values of water density and D_s were observed (Fig. 2 A-B). In some areas of the mat surface, a sharp transition between low and high values of water density and D_s occurred over the upper mm (Fig. 2 A-B). Average values of water density, D_s, and D_{app} in the April mat varied from 0.2-0.9 times the value in the overlaying water (Fig. 5 A-C).

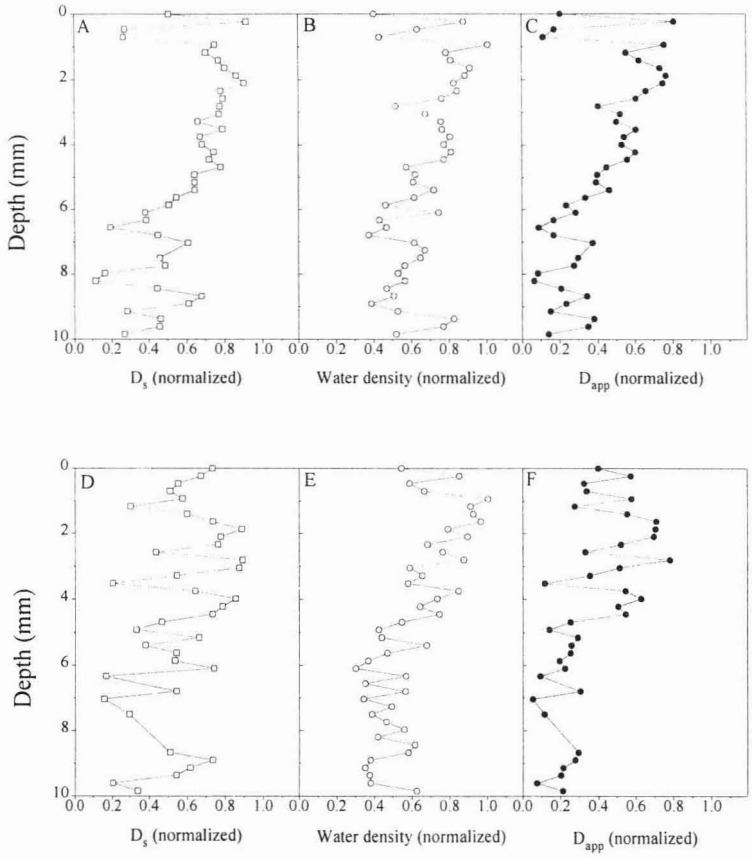

Figure 2. Depth profiles of the normalized D_s, water density and D_{app} at two different positions in the April mat. Upper panel shows the parameters at the first position (A-C), lower panel at the second position (D - F).

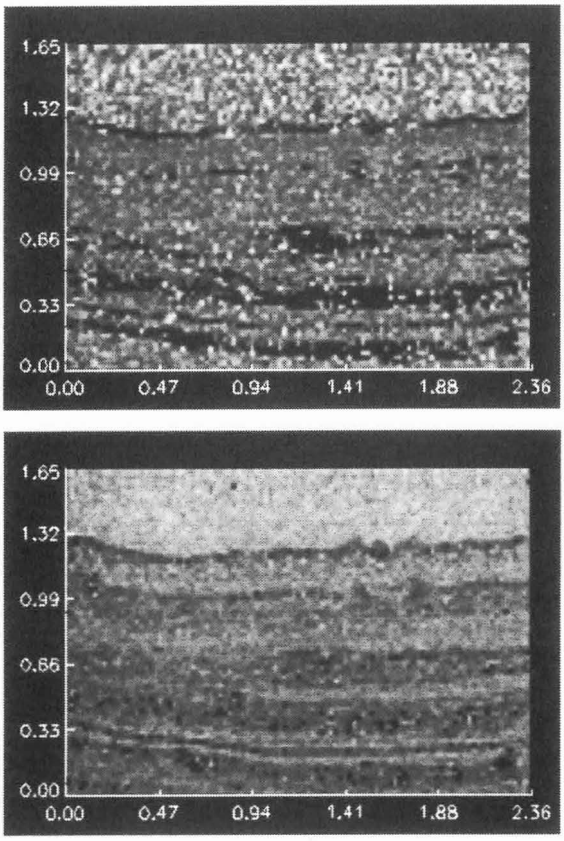

Figure 3. Image of the H_2O diffusion constants in the mat from November (upper image) measured with the PFG TSE sequence. Parameters: Δ = 7.9 ms, δ = 5.0 ms, TE = 15 + n*7.9 ms, TR = 1.5 s, 16 echoes, slice thickness = 2.2 mm. Image of the amplitude A_0 (water density, lower image) measured with the CPMG sequence. Parameters: TE = 15 + n*2.9 ms, TR = 7.5 s, 32 echoes, slice thickness = 2.2 mm. The framing scale indicates the corresponding size (in cm) of the extracted and 3 times enlarged images.

In the cohesive mat sampled in November, 1-2 mm thick bands of alternating high and low water density and D_s were present throughout the mat (Fig. 4, 5 D-E). The variability of water density, D_s, and, therefore, of diffusivity was less than in the April mat sample. Average values of water density, D_s, and D_{app} in the November mat varied from 0.4-0.9 times the value in the overlaying water (Fig. 5 D-F).

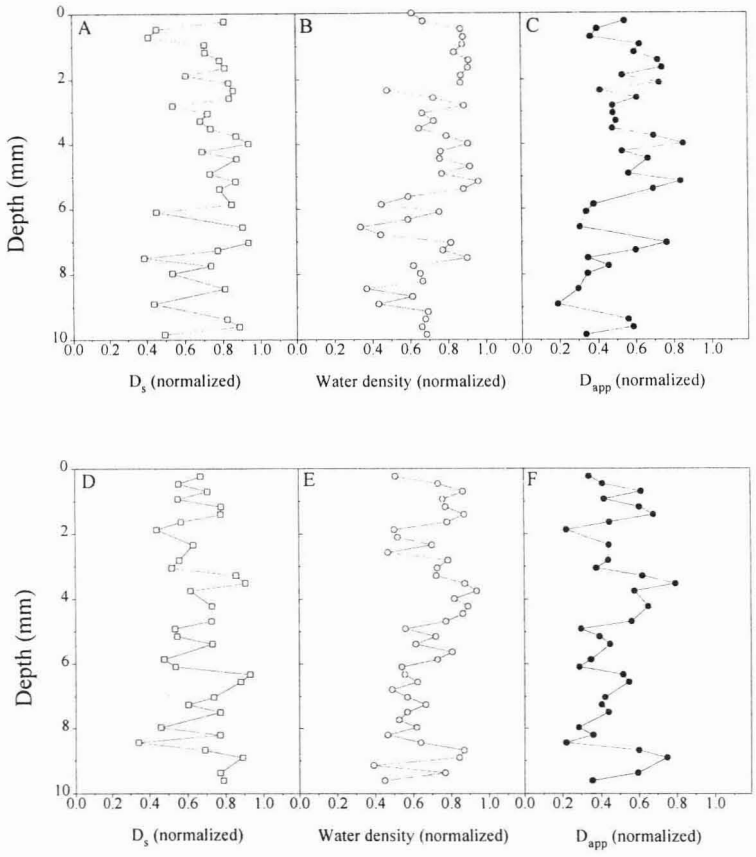

Figure 4. Depth profiles of the normalized D_s, water density and D_{app} at two different positions in the November mat. Upper panel shows the parameters at the first position (A-C), lower panel at the second position (D - F).

The apparent O_2 diffusivity was measured with a diffusivity microsensor in a Solar Lake mat sample from December 1998, which had a similar structure and composition as the November 1997 mat (Fig. 6A). In the uppermost ca. 1 mm of the mat, normalized O_2 diffusivity varied between 0.6 and 0.85 and then approached a relatively stable value of ca. 0.6 with increasing depths. Compared to these data obtained with the diffusivity microsensor, the diffusivity of H_2O, as determined from NMR measurements in the November mat (Fig. 6B), was lower in the upper mm and slightly higher 1-2 mm below the

mat surface. In deeper layers, both profiles varied approximately around the same range of normalized diffusivities.

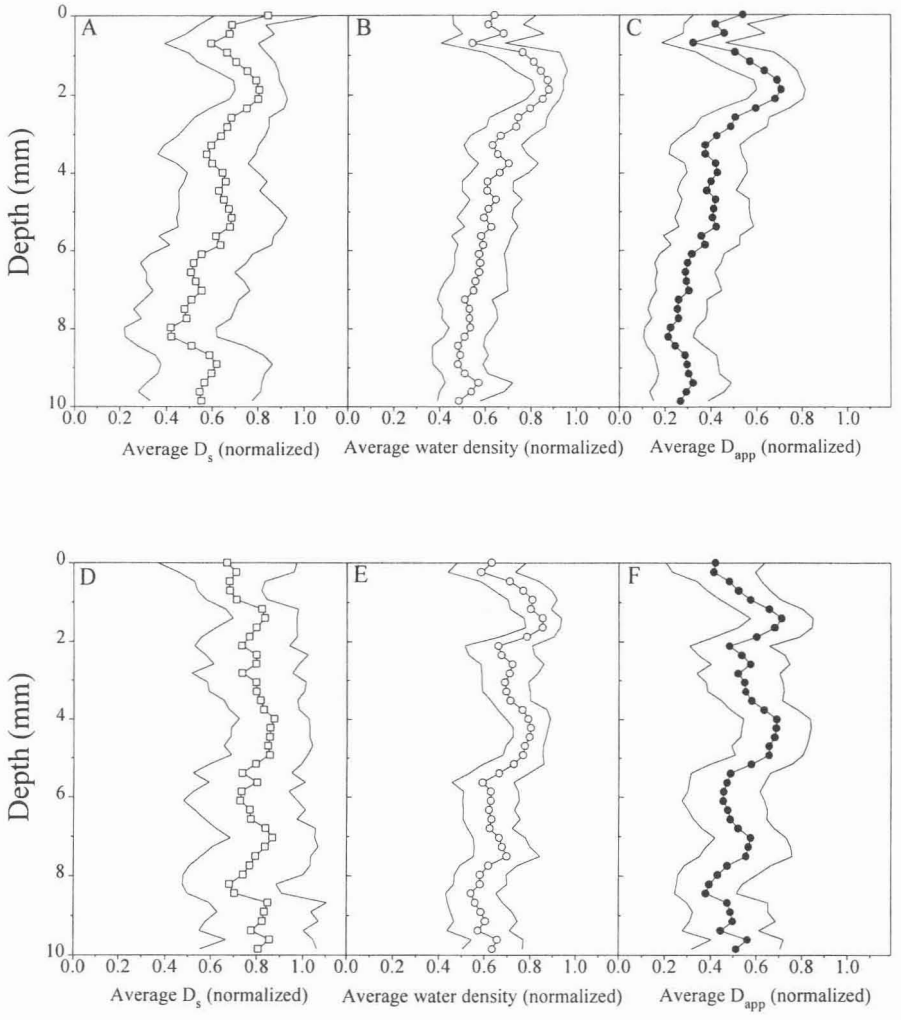

Figure 5. Depth profiles of the normalized average D_s (A: April mat, D: November mat), water density (B: April mat, E: November mat) and D_{app} (C: April mat, F: November mat) obtained from the different NMR experiments. The line graphs show the depth distribution of the standard deviation.

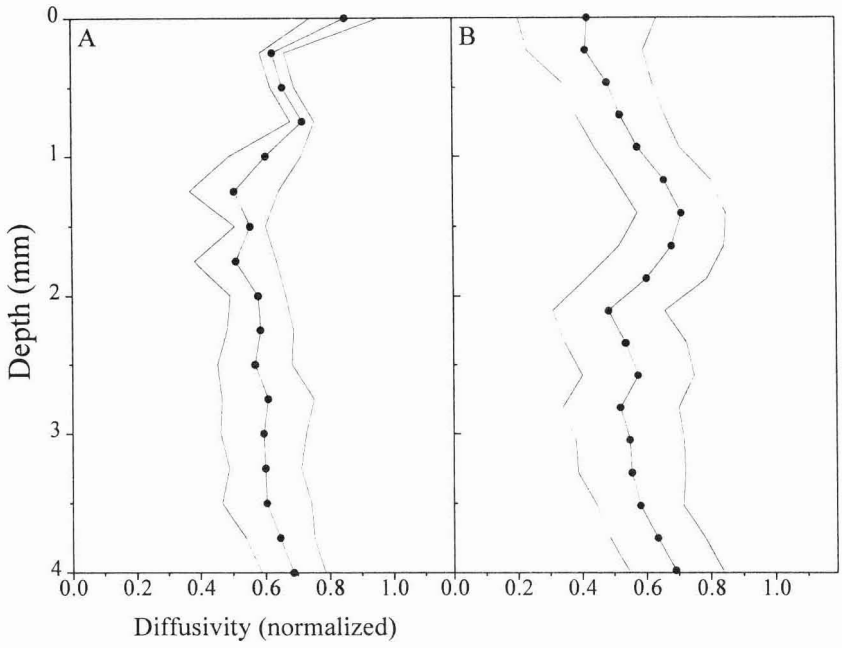

Figure 6. (A) Averaged (n = 3) and normalized depth profile of apparent O_2 diffusivity in a Solar Lake mat from December measured with a diffusivity microsensor. (B) Profile of the normalized average D_{app} from the NMR experiments in the November mat. The standard deviation is shown as line graphs.

Oxygen microprofiles

With a numerical procedure (Berg et al. 1998), the rates of net O_2 production/consumption within the mats were calculated from measured O_2 concentration profiles. In the light incubated mat from April, the oxic zone was 3.5 mm thick (Fig. 7). Beside a broad O_2 peak in the surface layer, a second O_2 peak at around 2.3-2.5 mm depth was observed. Assuming both a constant porosity and a constant D_s, two distinct zones of net O_2 production in the upper layer of the mat were calculated, with the highest rate located in the surface layer (Fig. 7A, dotted bars). A third zone of net O_2 production was calculated at the depth of the indicated second O_2 peak, which is separated from the other production zones by a zone of net O_2 consumption. A zone of high O_2 consumption was calculated at the lower boundary of the oxic zone, separated from the subsurface O_2 production zone, by a zone of low net O_2 consumption. Profile analysis using the average depth profile of D_s and D_{app} of H_2O,

resulted in a similar pattern and depth distribution of net O_2 production/consumption zones (data not shown).

Areal rates of O_2 production and consumption amounted to 0.35 nmol O_2 cm^{-2} s^{-1} and 0.12 nmol O_2 cm^{-2} s^{-1}, resulting in a total net production rate of 0.23 nmol O_2 cm^{-2} s^{-1}, if a constant diffusivity was assumed. If the variation of average D_{app} with depth (Fig. 5C) was taken into account in profile analysis, these rates became 0.24 nmol O_2 cm^{-2} s^{-1} and 0.08 nmol O_2 cm^{-2} s^{-1}, resulting in a total net production rate of 0.16 nmol O_2 cm^{-2} s^{-1}, which is 31% lower than the rate calculated assuming a constant diffusivity. Assuming a constant porosity of 0.9 and taking only the average D_s depth profile from the NMR measurement (Fig. 5A) into account, the calculated total areal net O_2 production rate was 0.7% higher than the rate calculated assuming a constant diffusivity.

The profile analysis was repeated with the D_s and D_{app} profile from two different positions in the mat (Fig. 2). The relatively homogeneous D_s profile in the April mat (Fig. 2A) resulted in a change of the pattern (depth distribution) of the calculated O_2 production/consumption zones (Fig. 7A) as compared with the one calculated by assuming constant diffusivities (dotted bars). This was also the case if the water density profile measured at approximately the same position (Fig. 2B) was included in profile analysis (Fig. 7B). Both analysis resulted in a decrease of the total net O_2 production rate, which amounted to 44% and 72%. We also repeated the analysis using the average of the D_s and D_{app} in the upper mm. The calculated depth distribution of the O_2 production/consumption zones from the analysis including the D_s profile was the same as the one calculated for constant diffusivities, whereas the calculated number of zones increased from 6 to 7 zones in the analysis with the D_{app} profile (data not shown). The total net O_2 production rate decreased by 36% and 53%. Using the more scattered profiles of D_s and D_{app} at the other position in the April mat (Fig. 2D, F), the same number of zones was calculated, but showed a different depth distribution and different rates as compared with the result obtained using constant diffusivities (Fig. 7C, D). The calculated total areal net O_2 production rates decreased by 30% and 52% as compared to the rate calculated assuming constant diffusivities.

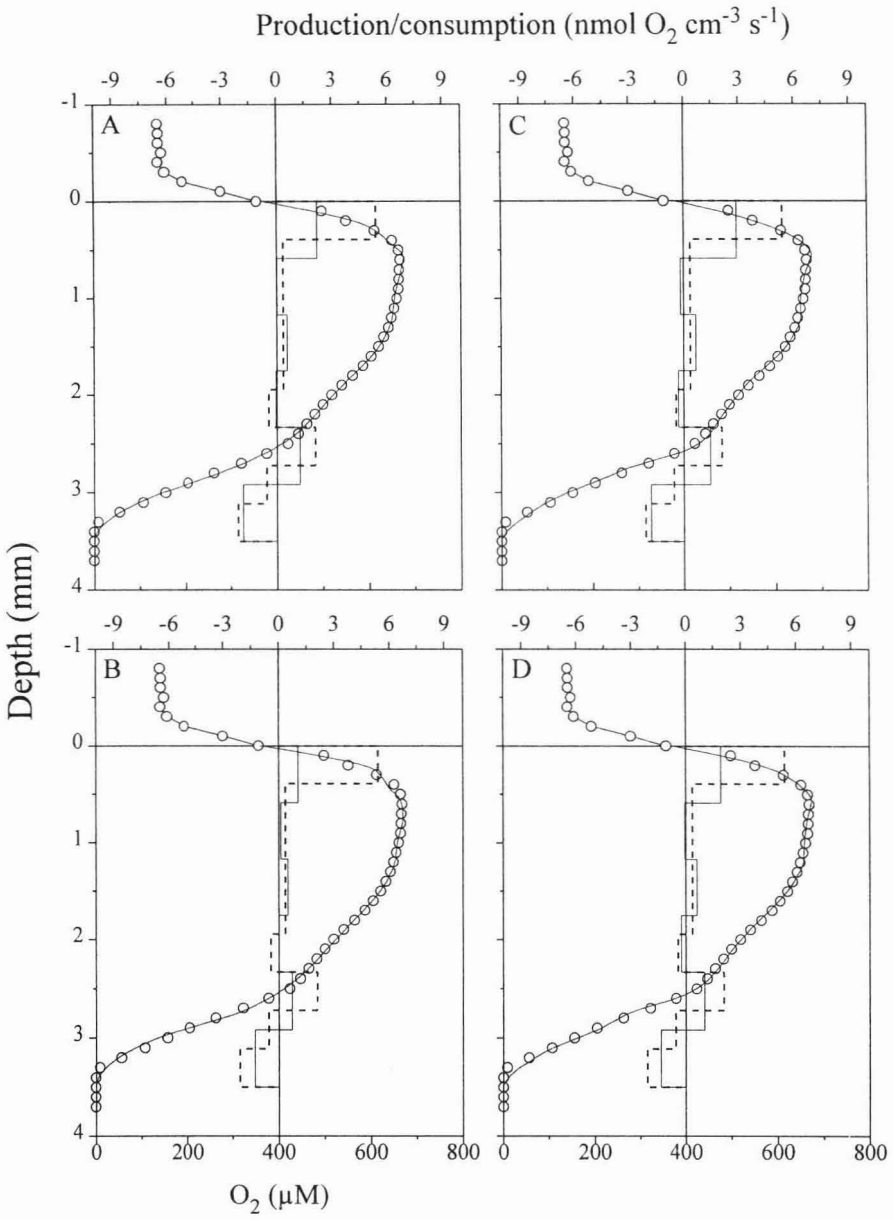

Figure 7. Calculated depth profile of O_2 production/consumption zones (bars) if (A) the D_s profile and (B) the D_{app} profile at the first position (Fig. 2A, C), and (C) the D_s profile and (D) the D_{app} profile at the second position (Fig. 2D, F) in the April mat was used for profile analysis (see text). The dotted bars indicate the calculated zones if a constant diffusivity is assumed. Open circles show the measured O_2 concentration profile. The line graphs indicate the fitted profiles calculated by the numerical procedure (Berg et al. 1998).

In the November mat, the oxic zone was only 1.8 mm thick, with one distinct O_2 peak in the surface layer (Fig. 8). Assuming a constant diffusivity for profile analysis, two net O_2 production zones in the surface layer, with the highest rate located in the upper ca. 0.3 mm, were calculated (Fig. 8A, dotted bars). Between these zones and the zone of net O_2 consumption at the lower boundary of the oxic zone, a zone of low O_2 production and a (broad) zone of low O_2 consumption were calculated. The calculated areal rates of net O_2 production and consumption amounted to 0.66 nmol O_2 cm^{-2} s^{-1} and 0.18 nmol O_2 cm^{-2} s^{-1}, resulting in a total net production rate of 0.48 nmol O_2 cm^{-2} s^{-1}. The pattern and depth distribution of the production/consumption zones did not change when the calculated average profiles of D_s and D_{app} from the NMR measurements were used for profile analysis (data not shown).

Using the average profile of D_{app} for oxygen profile analysis, the calculated areal rates of net O_2 production and consumption decreased to 0.40 nmol O_2 cm^{-2} s^{-1} and 0.13 nmol O_2 cm^{-2} s^{-1}, with a total net production rate of 0.27 nmol O_2 cm^{-2} s^{-1}, which corresponds to a decrease of 43%. From the analysis where only the average profile of D_s was taken into account, a 16% lower total net O_2 production rate was calculated as compared with the rate calculated assuming constant diffusivities.

The calculated depth distribution of O_2 production/consumption zones and the magnitude of the rates changed if the depth profile of D_s and D_{app} from two different positions (Fig. 4) were used for profile analysis. Since D_s and, therefore, also D_{app} at the mat surface could not be determined from the NMR measurements, the values from the next following depth were used for the mat surface in profile analysis. Both parameters from the first position (Fig. 4 A, C) resulted in a decrease of calculated zones, i.e. from 5 to 4 calculated zones, and the zone of low net O_2 production in the surface layer disappeared (Fig. 8A, B). The calculated total net O_2 production rate increased by 5% (D_s) and decreased by 24% (D_{app}) as compared to the rate calculated assuming constant diffusivities. Using the depth profiles of both parameters from the second position (Fig. 4 D, F), the calculated number of zones did not change, but the depth distribution of the zones (Fig. 8C, D). The most significant changes occurred in the surface layer, especially if D_{app} was used for profile analysis (Fig. 8D). Compared with the result using a constant diffusivity, the calculated total areal rate of net O_2 production decreased by 16% and 53%.

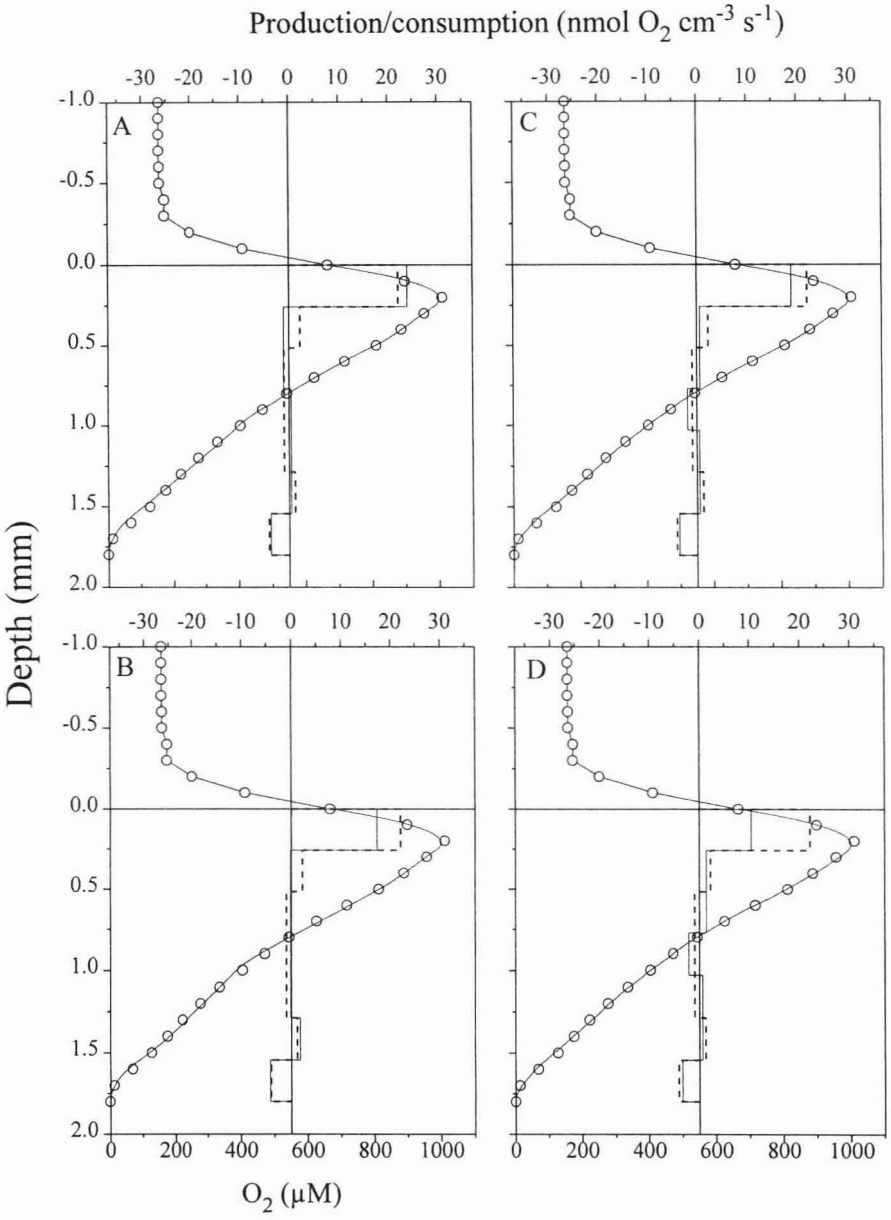

Figure 8. Calculated depth profile of O_2 production/consumption zones (bars) if (A) the D_s profile and (B) the D_{app} profile at the first position (Fig. 4A, C), and (C) the D_s profile and (D) the D_{app} profile at the second position (Fig. 4D, F) in the November mat was used for profile analysis (see text). The dotted bars indicate the calculated zones if a constant diffusivity is assumed. Open circles show the measured O_2 concentration profile. The line graphs indicate the fitted profiles calculated by the numerical procedure (Berg et al. 1998).

DISCUSSION

We present the first application of ^{1}H-NMR imaging to determine diffusion characteristics of microbial mats. Both the vertical depth distribution and an estimate of the lateral variability of the H_2O diffusion coefficients and water density within the mat could be obtained with this technique. In the following we discuss the current limitations of the technique together with the implications of our results for analysis of microprofiles.

Water density

The diffusion coefficients measured with pulsed field gradient NMR, correspond to the tortuosity corrected H_2O diffusion coefficient, i.e. D_s, since only the average displacement of the ensembles and not their magnitude is monitored (Beuling et al. 1998). To obtain information about the apparent diffusivities (D_{app}) in the mats, it is therefore necessary to additionally determine the porosity of the mat, preferable at the same high spatial resolution.

Porosity, i.e. the relative volume fraction of pore space in sediments, is determined as the ratio of the volume fraction of water and the sum of the volume fraction of water and solids (Buchanan 1984). We used the normalized mat water density determined in the CPMG experiments as an estimate of the mat porosity. The measured water density may include, however, not only extracellular, but also intracellular water, representing an aqueous phase that is not completely accessible for diffusive solute transport within mats. Furthermore, protons from e.g. fat and sugars can also contribute to the signal (Edzes et al. 1998), and the latter could cause a slight overestimation of the mat water density, especially in the upper layers of the mat with high microbial population densities. These factors could have led to an overestimation of the mat porosity. The error made by using the water density as an estimate of the porosity is difficult to estimate. We are well aware of the potential errors included in our estimate of the mat porosity. However, the product of the water density and the diffusion coefficient D_s represents the best possible estimate of the apparent diffusivity in the mat.

Water diffusion coefficients

Non spatially resolved pulsed field gradient NMR was applied by Beuling et al. (1998) to determine the diffusive properties of biofilms. These authors showed that the diffusion coefficients of water measured with pulsed field gradient NMR agreed with reported literature data, and that the water diffusion coefficients measured in alginate matrices with PFG NMR corresponded with literature data of normalized diffusion coefficients of e.g. O_2. It was also shown that in artificial biofilms the water diffusion coefficient decreased with increasing volume fraction of bacteria and that measured diffusion coefficients in natural biofilms compared well with those estimated from the physical biofilm characteristics by use of models.

We can, however, not exclude that the diffusion of solutes is differently affected in mats as compared with water. Whereas the effect of polymers on the diffusion of different solutes should be comparable, the permeability of cells for the solutes may vary. Cells are generally permeable for water, but if the short time period for diffusion labeling and the restricted and slow diffusion of water within bacterial cells is considered (see also Beuling et al. 1998), this diffusional flux of water through the cells may be of minor importance. It is assumed that diffusion of water is hindered or at least strongly reduced by the presence of bacterial cells, especially in the densely populated microbial mats. Although gases may passively pass the bacterial cell envelope by diffusion, there seem to exist significant differences between bacteria concerning the gas permeability (Beuling 1998). The permeability of bacteria is influenced by the structure/architecture of the bacterial cells and the diffusion coefficient of O_2 in immobilized and inactivated (gram-positive) bacteria permeable for O_2 was about 12% of the diffusion coefficient in water (Beuling 1998). We speculate that although a diffusive O_2 flux through cells might occur in microbial mats, this will be of minor importance due to the low diffusion coefficient in cells and O_2 diffusion may, therefore, be affected significantly by high densities of microbial cells.

NMR and microsensor diffusivity measurements

We obtained similar results with a diffusivity microsensor using an inert tracer gas and NMR imaging in comparable mats (Fig. 6). This indicates that the diffusion of water and gases seem to be similarly affected in microbial mats. The finding of rather low apparent diffusivities in microbial mats is in accordance with studies in an inactivated cultured

diatom biofilm, where an apparent O_2 diffusivity of 51% was determined (Revsbech 1989a).

The apparent diffusivity profiles determined with the microsensor and NMR imaging exhibited some differences in the upper 2 mm (Fig. 6). The diffusivity at the mat surface bears the highest uncertainty with both methods due to uncertainty in defining the surface. Also, if the principle of the diffusivity microsensor is considered (Revsbech et al. 1998), the diffusion of the tracer gas away from the sensor tip at the surface should be affected by the adjacent overlaying water. Thus, the diffusivity at the mat surface determined with the diffusivity microsensor was probably overestimated (Fig. 6A). Some difference could also arise due to the fact that we compare a non-invasive method with an invasive method.

The microsensor measures apparent diffusivities, i.e. gas diffusivity as a function of mat porosity and tortuosity (ϕD_s), whereas the apparent diffusivities of water were estimated as the product of the water density and D_s determined with NMR. Although some differences between both profiles may be explained by this estimation, apparent diffusivities in the depth interval from 2 to 4 mm were rather similar (Fig. 6), indicating that the error made by estimating the porosity from the normalized water density was not severe.

Oxygen, water density and diffusion coefficient in Solar Lake microbial mats

The structure and microbial composition of the April and the November mats differed significantly in the 1-3 mm thick surface layer, and this led also to pronounced differences of the O_2 distribution in the mats (Figs. 7, 8). Although measured at lower surface irradiances, O_2 penetrated deeper into the April mat as compared with the November mat. The O_2 concentration profile in the April mat showed the presence of a broad photosynthetic active zone. Photosynthesis in the layer dominated by filamentous cyanobacteria (*M. chthonoplastes*) below the surface layer of unicellular cyanobacteria and diatoms caused the subsurface peak of O_2 concentration and net O_2 production. An obvious prerequisite for this subsurface photosynthesis peak is a deep light penetration, probably facilitated by an accumulation of exopolymers in the gelatinous and partly translucent surface layer of the April mat.

The distinct O_2 peak in the November mat indicates intense photosynthesis only in the surface layer dominated by filamentous cyanobacteria. Whether the calculated zone of low net O_2 production at the lower boundary of the oxic zone was due to photosynthesis is

difficult to estimate, but could represent low photosynthetic activity in the previous years mat surface.

The seasonal changes of the cyanobacterial mats in the shallow part of Solar Lake, i.e. the dominance of filamentous cyanobacteria at the mat surface in winter and of unicellular cyanobacteria and diatoms in summer, were already described by Krumbein et al. (1977). These changes of the phototrophic community apparently have a significant effect on the O_2 distribution within the mats. A crucial parameter for this seasonality seem to be the sensitivity of filamentous cyanobacteria to photooxidative stress (Krumbein et al. 1977). Downward migration of filamentous cyanobacteria, primarily *M. chthonoplastes*, induced by UV and increases in visible light was reported in a Solar Lake mat (Bebout and Garcia-Pichel 1995). Furthermore, upward migration of filamentous cyanobacteria to the surface can also be induced in the summer mat by shading the mat (Krumbein et al. 1977). Thus, the depth zonation of the dominating cyanobacterium *M. chthonoplastes* in response to solar radiation and its seasonal changes could lead to an accumulation of exopolymer sheaths in the subsurface layer.

In both mats, an increase of the average water density below the surface layer was found (Fig. 5). The high water density in this layer could have been due to an enrichment of exopolysaccharides (exopolymers), which can contain significant amounts of water (Christensen and Characklis 1990; Decho 1994). Exopolymers may include e.g. sheaths and slimes produced by unicellular cyanobacteria and diatoms and, especially, the sheaths of filamentous cyanobacteria, like the sheathed bundles of *Microcoleus chthonoplastes*, which can reach a thickness of up to 15 µm (Jørgensen et al. 1983). The decrease of the water density in deeper parts of the mats indicates an increased compaction of the mat.

In the subsurface layer of high water density, the average H_2O diffusion coefficient D_s also showed a peak at approximately the same depth in both mats (Fig. 5). We speculate that an increased amount of (porous) exopolymers and probably also lower cell densities could have led to a less pronounced hindrance of diffusion in that layer. The variability of D_s at increasing depth was influenced by the distinct lamination pattern present in the mats due to overgrowth and preservation of photic layers from earlier years. It appears that the zone of high D_s/water density was not as broad in the November mat as compared with the April mat, indicating a more pronounced accumulation of exopolymers in the April mat.

Thus, the NMR data seem to relate well to the functional and structural properties of the mats.

Diffusion in microbial mats

In the uppermost active layers of dense and compact microbial mats, diffusion of solutes will mainly be affected by the polymer matrix and bacterial cells, which may act as diffusion barriers or, at least, impede the diffusion of solutes. As already suggested by Glud et al. (1995), the empirical relations used for sediments may not sufficiently describe the diffusional properties of microbial mats. Diffusion in microbial mats may rather be considered as diffusion in a cell-containing gel (see Westrin and Axelsson 1991). Nevertheless, some dilute biopolymer gels, i.e. natural gels with a low polymer volume fraction (e.g. alginate, agarose), resemble porous media, since they are heterogeneous and the open voids between the bundled polymer molecules may constitute a porous phase (Westrin 1991).

To predict the apparent diffusivity in a cell-containing gel, the polymer and the cell volume fraction, or at least their corresponding weight fraction, have to be determined and a model to estimate apparent diffusion coefficients in a polymer matrix and a model to estimate apparent diffusion coefficients as a function of the volume fraction of impermeable spheres (cells) have to be used (Westrin and Axelsson 1991). The use of physical characteristics (dry weight, ash content) to estimate the volume fraction of polymers and bacteria and the application of models to calculate their effect on the diffusion coefficient seem to yield good estimates for the apparent diffusivity in biofilms (Beuling 1998), but this procedure lacks spatial resolution. Deviations from a random distribution of individual impermeable spheres (cells), like large volume fractions, non-spherical shapes and irregular distribution, cause an additional decrease of the diffusion coefficient, which have to be accounted for by an estimation of the shape and spatial distribution of the cells (Beuling 1998). The observed variability of D_s and water density, especially in the upper part of the mats (Fig. 5), indicated a vertical and lateral heterogeneous distribution of exopolymers and microbial cell densities in the microbial mats. Due to this inhomogeneity and the deviation of the shape of some mat-inhabiting microorganisms from spheres and spheroids, like e.g. filamentous bacteria and bundles of the dominating *M. chthonoplastes*, the theoretical models used to estimate apparent

diffusivities in biofilms may not be sufficient to predict diffusion in microbial mats. More comparative experimental and theoretical studies are necessary to yield satisfactory models or empirical relations for diffusion in microbial mats. Thus, in such complex and heterogeneous matrices apparent diffusivities have to be determined experimentally with fine-scale techniques like NMR imaging or diffusivity microsensors.

Microprofile analysis

The diffusive properties of the mats obtained from the NMR measurements were used to estimate their effect on the analysis of measured O_2 concentration profiles and the calculation of net O_2 production rates. The obtained results demonstrate the potential of how solute diffusivities can affect profile analysis. Uncertainties of this approach are i) the estimates of D_{app} bear a potential error (see above), ii) some differences concerning the diffusivity of water and O_2 may occur in the microbial mats, and iii) the O_2 concentration profiles were measured at a certain position in the mats, and the diffusive properties of these positions may, therefore, have differed from the D_s and D_{app} profiles used for analysis of the O_2 concentration profiles. Since microsensor measurements are point measurements, we not only used the average D_s and average D_{app} profiles in the analysis, but also profiles of D_s and D_{app} selected from two different positions in the mats, representing extremes of variability as compared to the average profiles of these parameters. For the interpretation of the O_2 profiles, the laterally averaged D_{app} profile will result in an underestimation, whereas the distinct profiles of D_{app} extracted from different positions will overestimate the effect of vertical variability of D_{app} on profile analysis.

The obtained results clearly indicate the importance of considering the heterogeneity of solute diffusivity for the interpretation of measured concentration profiles. Maximal variations of more than 50% of calculated net O_2 production rates resulted when profile analysis was performed with the measured diffusivities and compared to the results when constant diffusivities were assumed. Furthermore, the solute diffusivity may not only affect the magnitude of calculated rates, but also the depth distribution of activity zones (Figs. 7, 8). In all analysis, the effect of D_{app} was much more pronounced as the effect of D_s, pointing to the necessity of fine-scale determination of both D_s and porosity, if the apparent diffusivity is not measured directly.

Summary/Conclusion

(PFG) NMR imaging is a powerful new tool to investigate the diffusional properties of heterogeneous systems like microbial mats and sediments. The Solar Lake microbial mats exhibited a strong lateral and vertical variability of water diffusion coefficient and water density due to the heterogeneous distribution of polymers and cell densities within the mats. The structure of the microbial mats exhibits seasonal changes, which influence the distribution of O_2 within the mats and led to differences of the diffusional properties of the upper mat layers. The profile of estimated apparent water diffusivities obtained with NMR imaging and of apparent O_2 diffusivities as measured with a diffusivity microsensor in a comparable mat, were rather similar, thus indicating that the diffusivity of gases and water was affected in the same way by the structure and composition of the microbial mats. The measured variability of the apparent diffusivities affected the outcome of measured O_2 concentration profile analysis significantly. It is thus important to take spatial heterogeneity of diffusive properties into account when interpreting solute concentration profiles measured with microsensors in natural microbial mats and sediments.

ACKNOWLEDGEMENTS

The NMR measurements were performed at the EU large-scale NMR facility in Wageningen (grant ERBFMGECT950066). This study was supported by the German Ministry for Research and Development (BMBF; Red Sea Program on Marine Sciences, Project E: Microbial activities in marine interfaces controlling sediment-water fluxes), and the Max-Planck Society. Gaby Eickert, Anja Eggers and Vera Hübner are thanked for the construction of the O_2 microsensors. The Interuniversity Institute in Eilat (Israel) is thanked for providing laboratory facilities. Yehuda Cohen is thanked for arranging the logistics of the Solar Lake field trip and his support in Israel. The Egyptian authorities are thanked for their allowance to work at Solar Lake. A.W. acknowledges the help from Bettina König with IDL and the fruitful discussions with Peter Berg.

REFERENCES

Amann R, Kühl M (1998). *In situ* methods for assessment of microorganisms and their activities. Curr Opin Microbiol 1:352-358

Bebout BM, Garcia-Pichel F (1995). UV B-induced vertical migrations of cyanobacteria in a microbial mat. Appl Environ Microbiol 61(12):4215-4222

Berg P, Risgaard-Petersen N, Rysgaard S (1998). Interpretation of measured concentration profiles in sediment pore water. Limnol Oceanogr 43(7):1500-1510

Berner RA (1980). Early diagenesis. Princeton University Press, Princeton.

Beuling EE (1998). Mass transfer properties of biofilms. Ph.D. thesis, University of Amsterdam (The Netherlands).

Beuling EE, van Dusschoten D, Lens P, van den Heuvel JC, Van As H, Ottengraf SPP (1998). Characterization of the diffusive properties of biofilms using pulsed field gradient-nuclear magnetic resonance. Biotechnol Bioeng 60(3):283-291

Boudreau BP (1997). Diagenetic models and their implementation. Springer, Berlin.

Broecker WS, Peng T-H (1974). Gas exchange rates between air and sea. Tellus 26:21-35

Buchanan JB (1984). Sediment analysis. In: Holme N, McIntire AD (Ed.) Methods for the study of marine benthos. Blackwell Scientific Publications, Oxford, p 41-65

Christensen BE, Characklis WG (1990). Physical and chemical properties of biofilms. In: Characklis WG, Marshall KC (Ed.) Biofilms. John Wiley and Sons, Inc., New York, p 93-130

Cronenberg CCH, Van den Heuvel JC (1991). Determination of glucose diffusion coefficients in biofilms with micro-electrodes. Biosens Bioelectron 6:255-262

de Beer D, Stoodley P, Lewandowski Z (1997). Measurement of local diffusion coefficients in biofilms by microinjection and confocal microscopy. Biotechnol Bioeng 53:151-158

Decho AW (1994). Exopolymers in microbial mats: Assessing their adaptive roles. In: Stal LJ, Caumette P (Ed.) Microbial Mats: Structure, Development and Environmental Significance. NATO ASI Series G Vol. 35. Springer, Berlin, p 215-219

Duursma EK, Bosch CJ (1970). Theoretical, experimental and field studies concerning diffusion of radioisotopes in sediments and suspended particles of the sea. Part B: Methods and experiments. Neth J Sea Res 4:395-469

Edzes HT, van Dusschoten D, Van As H (1998). Quantitative T_2 imaging of plant tissues by means of multi-echo MRI microscopy. Magn Reson Imaging 16(2):185-196

Epping EHG, Jørgensen BB (1996). Light-enhanced oxygen respiration in benthic phototrophic communities. Mar Ecol Prog Ser 139:193-203

Farrar TC, Becker ED (1971). Pulse and Fourier transform NMR. Academic Press, New York.

Garcia-Pichel F, Nübel U, Muyzer G (1998). The phylogeny of unicellular, extremely halotolerant cyanobacteria. Arch Microbiol 169:469-482

Glud RN, Jensen K, Revsbech NP (1995). Diffusivity in surficial sediments and benthic mats determined by use of a combined N_2O-O_2 microsensor. Geochim Cosmochim Acta 59(2):231-237

Jeroschewski P, Steuckart C, Kühl M (1996). An amperometric microsensor for the determination of H_2S in aquatic environments. Anal Chem 68:4351-4357

Jørgensen BB, Cohen Y (1977). Solar Lake (Sinai). 5. The sulfur cycle of the benthic cyanobacterial mats. Limnol Oceanogr 22(4):657-666

Jørgensen BB, Revsbech NP, Blackburn TH, Cohen Y (1979). Diurnal cycle of oxygen and sulfide microgradients and microbial photosynthesis in a cyanobacterial mat sediment. Appl Environ Microbiol 38(1):46-58

Jørgensen BB, Revsbech NP, Cohen Y (1983). Photosynthesis and structure of benthic microbial mats: Microelectrode and SEM studies of four cyanobacterial communities. Limnol Oceanogr 28(6):1075-1093

Krumbein WE, Cohen Y, Shilo M (1977). Solar Lake (Sinai). 4. Stromatolitic cyanobacterial mats. Limnol Oceanogr 22(4):635-656

Li Y-H, Gregory S (1974). Diffusion of ions in sea water and in deep-sea sediments. Geochim Cosmochim Acta 38:703-714

Lorenzen J, Glud RN, Revsbech NP (1995). Impact of microsensor-caused changes in diffusive boundary layer thickness on O_2 profiles and photosynthetic rates in benthic communities of microorganisms. Mar Ecol Prog Ser 119:237-241

Moonen CTW, van Zijl PCM, Frank JA, Le Bihan D, Becker ED (1990). Functional magnetic resonance imaging in medicine and physiology. Science 250:53-61

Morris PG (1986). Nuclear Magnetic Resonance imaging in medicine and biology. Clarendon Press, Oxford.

Nielsen LP, Christensen PB, Revsbech NP, Sørensen J (1990). Denitrification and oxygen respiration in biofilms studied with a microsensor for nitrous oxide and oxygen. Microb Ecol 19:63-72

Press WH, Teukolsky SA, Vetterling WT, Flannery BP (1992). Numerical recipes in C. Cambridge University Press, Cambridge.

Rasmussen H, Jørgensen BB (1992). Microelectrode studies of seasonal oxygen uptake in a coastal sediment: role of molecular diffusion. Mar Ecol Prog Ser 81:289-303

Revsbech NP (1989a). Diffusion characteristics of microbial communities determined by use of oxygen microsensors. J Microbiol Meth 9:111-122

Revsbech NP (1989b). An oxygen microelectrode with a guard cathode. Limnol Oceanogr 34:474-478

Revsbech NP, Jørgensen BB (1986). Microelectrodes: Their use in microbial ecology. Adv Microb Ecol 9:293-352

Revsbech NP, Madsen B, Jørgensen BB (1986). Oxygen production and consumption in sediments determined at high spatial resolution by computer simulation of oxygen microelectrode data. Limnol Oceanogr 31(2):293-304

Revsbech NP, Nielsen LP, Ramsing NB (1998). A novel microsensor for determination of apparent diffusivity in sediments. Limnol Oceanogr 43(5):986-992

Scheenen TWJ, van Dusschoten D, de Jager H, Van As H (1998). Fast spatially resolved displacement imaging in (bio)systems. In: Blümler P, Blümich B, Botto R, Fukushima E (Ed.) Spatially resolved magnetic resonance. Wiley-VCH, Weinheim, p 482-486

Sherwood JE, Stagnitti F, Kokkinn MJ, Williams WD (1991). Dissolved oxygen concentrations in hypersaline waters. Limnol Oceanogr 36(2):235-250

Stejskal EO, Tanner JE (1965). Spin diffusion measurements: Spin echoes in the presence of a time-dependent field gradient. J Chem Phys 42(288-292)

Ullman WJ, Aller RC (1982). Diffusion coefficients in nearshore marine sediments. Limnol Oceanogr 27(3):552-556

Van As H, van Dusschoten D (1997). NMR methods for imaging of transport processes in micro-porous systems. Geoderma 80:389-403

van Dusschoten D, Moonen CTW, de Jager PA, Van As H (1996). Unraveling diffusion constants in biological tissue by combining Carr-Purcell-Meiboom-Gill Imaging and Pulsed Field Gradient NMR. Magn Reson Med 36:907-913

van Gemerden H (1993). Microbial mats: a joint venture. Mar Geol 113:3-25

Westrin BA (1991). Diffusion measurements in gels: a methodological study. Ph.D. thesis, University of Lund (Sweden).

Westrin BA, Axelsson A (1991). Diffusion in gels containing immobilized cells: a critical review. Biotechnol Bioeng 38:439-446

Summary

In hypersaline environments such as Solar Lake, thick and finely laminated microbial mats develop since environmental conditions limit the survival of higher organisms. Due to their compacted microbial composition and due to the absence of bioturbation, microbial mats are ideal model systems to study biogeochemical processes and their regulation. Solar Lake mats probably belong to the most comprehensively studied of hypersaline environments, however, only little is known about the regulation of biogeochemical processes in these mats.

In this thesis, oxygen and sulfide cycling in hypersaline Solar Lake microbial mats was investigated with emphasis on regulatory effects of important environmental parameters like temperature and irradiance on the different processes involved.

The effect of temperature on oxygen and sulfide producing/consuming processes was investigated with microsensors under dark and light conditions (chapter 2). Oxygenic photosynthesis and oxygen consumption in the dark and in the aphotic zone of the light incubated mat exhibited a maximum close to the temperature of the natural habitat. Sulfide production and sulfide oxidation, however, increased further with temperature, leading to an increasing relative contribution of sulfide oxidation to oxygen consumption in the light incubated mat and to saturation of sulfide oxidation in the dark incubated mat at elevated temperatures. A minor temperature dependence of areal rates of dark oxygen consumption indicated diffusion limitation due to the mass transfer resistance imposed by the diffusive boundary layer. Sulfide production exceeded dark oxygen consumption rates at elevated temperatures, indicating an increasing importance of sulfate reduction for the mineralization of organic matter at elevated temperatures. Temperature did not only affect process rates, but also the depth zonation of different processes and caused a macroscopic change of the mat, possibly indirectly induced by the enhanced sulfide production. Thus, direct and indirect temperature effects determined the temperature response of the microbial community. The results of this study demonstrate that sulfide conversion processes became of increasing importance for oxygen turnover at elevated temperatures and that the close coupling of oxygen and sulfur cycling in Solar Lake mats is strongly regulated by temperature.

Since oxygenic photosynthesis is the driving force of hypersaline microbial mats, a detailed study on the regulatory effects of temperature and irradiance on photosynthesis and oxygen consumption was performed (chapter 3). In this study, areal rates of dark oxygen consumption increased almost linearly with temperature (15°C-45°C), but exhibited a relative low temperature dependence (Q_{10} = 1.3), again indicating that dark oxygen consumption in Solar Lake microbial mats is strongly controlled by the mass transfer constraints imposed by the diffusive boundary layer. Photosynthesis versus irradiance curves measured at three experimental temperatures indicated an adaptation of the phototrophic community to high irradiances and an optimum temperature of gross photosynthesis slightly above the *in situ* temperature. At moderate irradiances, temperature increased the percentage of photosynthetically produced oxygen which was consumed within the mat, resulting in an increased light requirement to turn the mat into a net autotrophic community at elevated temperatures, as estimated from the oxygen budget. Oxygen consumption in the photic zone of the mat contributed significantly to the total oxygen consumption of the microbial mat in the light and was coupled to photosynthesis. This coupling was enhanced by irradiance and temperature and led to an increased internal oxygen cycling in Solar Lake microbial mats. Based on these results, carbon cycling may also be characterized by a similar close coupling between autotrophs and heterotrophs, strongly regulated by temperature and irradiance.

Important for the quantification of biogeochemical processes in benthic ecosystems is the solute diffusivity. Non-invasive NMR imaging was used to determine the diffusive properties of two structurally different Solar Lake microbial mats, by measuring the two-dimensional distribution of the water density and the diffusion coefficient of water in the mats (chapter 4). A pronounced lateral and vertical variability of the water density and the water diffusion coefficient was found in the mats, influenced by the mat structure and heterogeneous distribution of microbial cells and exopolymers. Despite some differences in the uppermost layer, estimated apparent water diffusivities compared well with apparent oxygen diffusivities, measured with a diffusivity microsensor in a comparable mat. Thus, with NMR imaging it is possible to determine diffusivity at high spatial resolution and to resolve lateral and vertical heterogeneities. Analysis of measured oxygen concentration profiles with a diffusion-reaction model taking the observed diffusivity variations into

account, indicated the necessity to determine diffusive properties at high spatial resolution for the interpretation of measured solute concentration profiles in heterogeneous systems. The combination of NMR imaging for the determination of diffusive properties of benthic communities with two-dimensional methods for the detection of important solutes, like planar optodes, may provide a powerful tool to determine microbial activity in heterogeneous communities at high spatial resolution in two dimensions. This combination of methods could further resolve the effect of diffusive properties and heterogeneities on microbial activity in such communities.

List of publications

Contributions of (co-)authors to the manuscripts presented in this thesis

1. **Short term temperature effects on oxygen and sulfide cycling in a hypersaline cyanobacterial mat (Solar Lake, Egypt)**

   A. Wieland and M. Kühl

Concept by M. Kühl and A. Wieland, measurements by A. Wieland, writing of manuscript by A. Wieland with editorial help from M. Kühl.

2. **Irradiance and temperature regulation of oxygenic photosynthesis and O_2 consumption in a hypersaline cyanobacterial mat (Solar Lake, Egypt)**

   A. Wieland and M. Kühl

Concept by A. Wieland and M. Kühl, measurements by A. Wieland, writing of manuscript by A. Wieland with editorial help from M. Kühl

3. **Fine-scale measurement of diffusivity in a microbial mat with NMR imaging**

   A. Wieland, D. van Dusschoten, L. R. Damgaard, D. de Beer, M. Kühl and H. Van As

Concept by A. Wieland and D. de Beer, NMR measurements by D. van Dusschoten and H. Van As with assistance of A. Wieland and D. de Beer, oxygen microsensor measurements by A. Wieland, diffusivity microsensor measurements by L. R. Damgaard, writing of manuscript by A. Wieland with editorial help from co-authors.